Published for SISSA by Springer

Received: *April 10, 2018*
Revised: *September 3, 2018*
Accepted: *January 31, 2019*
Published: *March 5, 2019*

Search for $\mathrm{t\bar{t}H}$ production in the $\mathrm{H} \to \mathrm{b\bar{b}}$ decay channel with leptonic $\mathrm{t\bar{t}}$ decays in proton-proton collisions at $\sqrt{s} = 13\,\text{TeV}$

The CMS collaboration

E-mail: cms-publication-committee-chair@cern.ch

Abstract: A search is presented for the associated production of a standard model Higgs boson with a top quark-antiquark pair ($\mathrm{t\bar{t}H}$), in which the Higgs boson decays into a b quark-antiquark pair, in proton-proton collisions at a centre-of-mass energy $\sqrt{s} = 13\,\text{TeV}$. The data correspond to an integrated luminosity of $35.9\,\text{fb}^{-1}$ recorded with the CMS detector at the CERN LHC. Candidate $\mathrm{t\bar{t}H}$ events are selected that contain either one or two electrons or muons from the $\mathrm{t\bar{t}}$ decays and are categorised according to the number of jets. Multivariate techniques are employed to further classify the events and eventually discriminate between signal and background. The results are characterised by an observed $\mathrm{t\bar{t}H}$ signal strength relative to the standard model cross section, $\mu = \sigma/\sigma_{\text{SM}}$, under the assumption of a Higgs boson mass of 125 GeV. A combined fit of multivariate discriminant distributions in all categories results in an observed (expected) upper limit on μ of 1.5 (0.9) at 95% confidence level, and a best fit value of $0.72 \pm 0.24(\text{stat}) \pm 0.38(\text{syst})$, corresponding to an observed (expected) signal significance of 1.6 (2.2) standard deviations above the background-only hypothesis.

Keywords: Hadron-Hadron scattering (experiments), Higgs physics, Top physics

ArXiv ePrint: 1804.03682

https://doi.org/10.1007/JHEP03(2019)026

JHEP03(2019)026

Contents

1 Introduction 1

2 The CMS detector 3

3 Simulation of signal and background 4

4 Object and event reconstruction 5

5 Analysis strategy and event classification 7

6 Systematic uncertainties 12

7 Results 15

8 Summary 23

A BDT and DNN input variables and configuration 26

B Pre-fit discriminant shapes (single-lepton channel) 30

C Post-fit discriminant shapes (single-lepton channel) 34

The CMS collaboration 43

JHEP03(2019)026

1 Introduction

The observation [1–3] of a Higgs boson with a mass of approximately 125 GeV [4, 5] at the CERN LHC marked the starting point of a broad experimental programme to determine the properties of the newly discovered particle. Decays into $\gamma\gamma$, ZZ, WW, and $\tau\tau$ final states have been observed, and there is evidence for the direct decay of the particle to the bottom quark-antiquark ($\mathrm{b\bar{b}}$) final state [6–10]. The measured rates for various production and decay channels are consistent with the standard model (SM) expectations [11, 12], and the hypothesis of a spin-0 particle is favoured over other hypotheses [13, 14].

In the SM, the Higgs boson couples to fermions with a Yukawa-type interaction, with a coupling strength proportional to the fermion mass. Probing the coupling of the Higgs boson to the heaviest known fermion, the top quark, is therefore very important for testing the SM and for constraining various models of physics beyond the SM (BSM), some of which predict a different coupling strength than the SM. Indirect constraints on the coupling between the top quark and the Higgs boson are available from processes including virtual top quark loops, for example Higgs boson production through gluon-gluon fusion [11, 12],

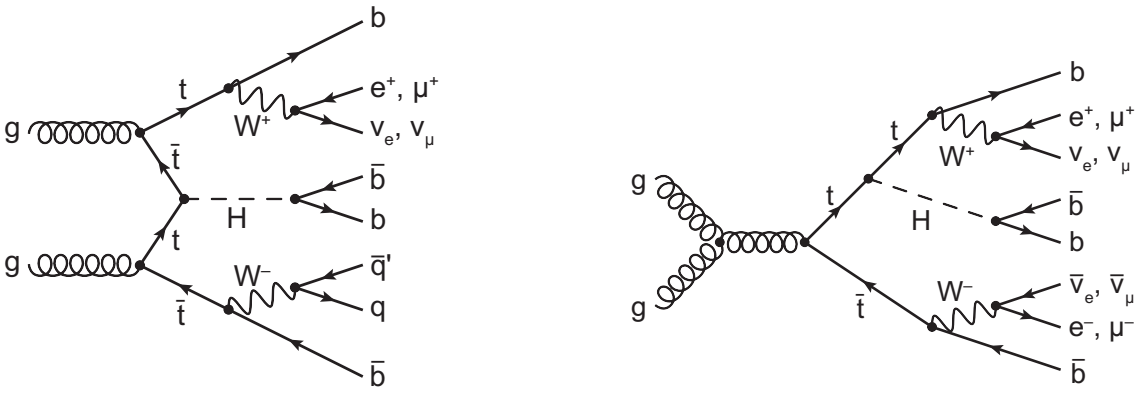

Figure 1. Representative leading-order Feynman diagrams for $t\bar{t}H$ production, including the subsequent decay of the Higgs boson into a b quark-antiquark pair, and the decay of the top quark-antiquark pair into final states with either one (single-lepton channel, left) or two (dilepton channel, right) electrons or muons.

as well as from production of four top quarks [15]. On the other hand, the associated production of a Higgs boson and a top quark-antiquark pair ($t\bar{t}H$ production) as illustrated by the Feynman diagrams in figure 1 is a direct probe of the Higgs boson coupling to fermions with weak isospin $+1/2$. The Higgs boson decay into $b\bar{b}$, also shown in figure 1, is experimentally attractive as a final state because it features the largest branching fraction of 0.58 ± 0.02 for a 125 GeV Higgs boson [16].

Several BSM physics scenarios predict a significantly enhanced production rate of events with $t\bar{t}H$ final states, while not modifying the branching fractions of Higgs boson decays by a measurable amount [17–26]. In this context, a measurement of the $t\bar{t}H$ production cross section has the potential to distinguish the SM Higgs mechanism of generating fermion masses from alternative ones.

Various dedicated searches for $t\bar{t}H$ production have been conducted during Run 1 of the LHC. The CMS Collaboration searches employed proton-proton (pp) collision data corresponding to an integrated luminosity of $5\,\text{fb}^{-1}$ at a centre-of-mass energy of $\sqrt{s} = 7\,\text{TeV}$ and $19.5\,\text{fb}^{-1}$ at $\sqrt{s} = 8\,\text{TeV}$. These searches have been performed by studying Higgs boson decays to b quarks, photons, and leptons using multivariate analysis (MVA) techniques, showing a mild excess of the observed $t\bar{t}H$ cross section relative to the SM expectation of $\mu = \sigma/\sigma_{\text{SM}} = 2.8 \pm 1.0$ [27]. A similar excess of $\mu = 2.1^{+1.4}_{-1.2}$ was observed in a search for $t\bar{t}H$ production in multilepton final states by the ATLAS Collaboration using data at $\sqrt{s} = 8\,\text{TeV}$, corresponding to an integrated luminosity of $20.3\,\text{fb}^{-1}$ [28]. The searches in the $H \to b\bar{b}$ decay channel were performed with several analysis techniques [27, 29, 30], yielding a most stringent observed (expected) upper limit on μ of 3.4 (2.2) at the 95% confidence level (CL).

The increased centre-of-mass energy of $\sqrt{s} = 13\,\text{TeV}$ results in a $t\bar{t}H$ production cross section 3.9 times larger than at $\sqrt{s} = 8\,\text{TeV}$ based on next-to-leading-order (NLO) calculations; while the cross section for the most important background, $t\bar{t}$ production, is increased by a factor of 3.3 [31], resulting in a more favourable signal-to-background ratio. The CMS Collaboration has performed searches in the all-jets [32] and multilepton [33]

JHEP03(2019)026

final states with 35.9 fb^{-1} of data, achieving evidence for $\text{t}\bar{\text{t}}\text{H}$ production with an observed (expected) significance of 3.2 (2.8) standard deviations in the latter case. Recently, the ATLAS Collaboration reported observed (expected) evidence for $\text{t}\bar{\text{t}}\text{H}$ production with a significance of 4.2 (3.8) standard deviations, based on an integrated luminosity of 36.1 fb^{-1} and combining several Higgs boson decay channels [34]; in the $\text{H} \to \text{b}\bar{\text{b}}$ channel alone, an observed (expected) upper limit on μ of 2.0 (1.2) at 95% CL and a best fit value of $\mu = 0.84^{+0.64}_{-0.61}$ were obtained [35].

In this paper, a search for $\text{t}\bar{\text{t}}\text{H}$ production in the $\text{H} \to \text{b}\bar{\text{b}}$ final state is presented that has been performed using 35.9 fb^{-1} of data recorded with the CMS detector at $\sqrt{s} = 13$ TeV in 2016. In the SM, the top quark is expected to decay into a W boson and a b quark almost exclusively. Hence different $\text{t}\bar{\text{t}}$ decay modes can be identified according to the subsequent decays of the W bosons. The event selection is based on the decay topology of $\text{t}\bar{\text{t}}\text{H}$ events in which the Higgs boson decays into $\text{b}\bar{\text{b}}$ and the $\text{t}\bar{\text{t}}$ decay involves at least one lepton, resulting in either $\ell\nu\,\text{q}\bar{\text{q}}'\,\text{b}\bar{\text{b}}$ (single-lepton) or $\ell^+\nu\,\ell^-\bar{\nu}\,\text{b}\bar{\text{b}}$ (dilepton) $\text{t}\bar{\text{t}}$ final states, where $\ell = \text{e}, \mu$ arising either from the prompt decay of a W boson or from leptonic τ decays. Analysis methods established in Run 1 [27, 29] have been significantly improved, and novel methods have been added. In particular, two multivariate techniques — namely boosted decision trees (BDTs) and the matrix element method (MEM) [36–40] — that utilise event information differently in order to discriminate signal from background events have been employed in combination. Since the two methods aim at separating signal from different background processes, their combined usage helps to obtain a better sensitivity. In addition, a new multivariate technique based on deep neural networks (DNNs) has been employed to separate signal from background events. The best fit value of the signal strength modifier μ is obtained from a combined profile likelihood fit of the classifier output distributions to the data, correlating processes and their uncertainties where appropriate.

This document is structured as follows. The CMS detector is described in section 2. In section 3, the simulated signal and background samples are described. The basic selection of analysis objects and events is discussed in section 4. The general analysis strategy and background estimation methods are introduced in section 5. The effect of systematic uncertainties is studied in section 6. Results of the analysis are presented in section 7, followed by a summary in section 8.

2 The CMS detector

The central feature of the CMS apparatus is a superconducting solenoid of 6 m internal diameter, providing a magnetic field of 3.8 T. Within the solenoid volume are a silicon pixel and strip tracker, a lead tungstate crystal electromagnetic calorimeter, and a brass and scintillator hadron calorimeter, each composed of a barrel and two endcap sections. Forward calorimeters extend the pseudorapidity (η) coverage provided by the barrel and endcap detectors. Muons are detected in gas-ionisation chambers embedded in the steel magnetic flux-return yoke outside the solenoid. A more detailed description of the CMS detector, together with a definition of the coordinate system used and the relevant kinematic variables, can be found in ref. [41]. Events of interest are selected using a two-tiered

JHEP03(2019)026

trigger system [42]. The first level, composed of custom hardware processors, uses information from the calorimeters and muon detectors to select events, while the second level selects events by running a version of the full event reconstruction software optimised for fast processing on a farm of computer processors.

3 Simulation of signal and background

Several Monte Carlo event generators, interfaced with a detailed detector simulation, are used to model experimental effects, such as reconstruction and selection efficiencies, as well as detector resolutions. The CMS detector response is simulated using GEANT4 (v.9.4) [43].

For the simulation of the $t\bar{t}H$ signal sample, the NLO event generator POWHEG (v.2) [44–47] is used. Standard model backgrounds are simulated using POWHEG (v.2), PYTHIA (v.8.200) [48], or MADGRAPH5_aMC@NLO (v.2.2.2) [49], depending on the process. The value of the Higgs boson mass is assumed to be 125 GeV, while the top quark mass value is set to 172.5 GeV. The proton structure is described by the parton distribution functions (PDF) NNPDF3.0 [50].

The main background contribution originates from $t\bar{t}$ production, the production of W and Z/γ^* bosons with additional jets (referred to as W+jets and Z+jets, or commonly as V+jets), single top quark production (tW and t-channel production), diboson (WW, WZ, and ZZ) processes, and $t\bar{t}$ production in association with a W or Z boson (referred to as $t\bar{t}$+W and $t\bar{t}$+Z, or commonly as $t\bar{t}$+V). Both the $t\bar{t}$ and the single top quark processes in the t- and tW-channels are simulated with POWHEG [51, 52]. The s-channel single top quark processes, as well as V+jets and $t\bar{t}$+V processes are simulated at NLO with MADGRAPH5_aMC@NLO, where for the V+jets processes the matching of matrix-element (ME) jets to parton showers (PS) is performed using the FXFX [53] prescription. The PYTHIA event generator is used to simulate diboson events.

Parton showering and hadronisation are simulated with PYTHIA (v.8.200) for all signal and background processes. The PYTHIA CUETP8M2T4 [54] tune is used to characterise the underlying event in the $t\bar{t}H$ signal and $t\bar{t}$ and single top quark background processes, while the CUETP8M1 [55] tune is used for all other background processes.

For comparison with the observed distributions, the events in the simulated samples are normalised to the same integrated luminosity of the data sample, according to their predicted cross sections. These are taken from theoretical calculations at next-to-next-to-leading order (NNLO, for V+jets production), approximate NNLO (single top quark tW channel [56]), and NLO (single top quark t- and s-channels [57, 58], $t\bar{t}$+V production [59], and diboson production [60]). The $t\bar{t}H$ cross section of 507^{+35}_{-50} fb and Higgs boson branching fractions used in the analysis also correspond to NLO accuracy [16]. The $t\bar{t}$ simulated sample is normalised to the full NNLO calculation with resummation to next-to-next-to-leading-logarithmic accuracy [61–67], assuming a top quark mass value of 172.5 GeV and using the NNPDF3.0 PDF set. This sample is further separated into the following processes based on the flavour of additional jets that do not originate from the top quark decays in the event: $t\bar{t}$+$b\bar{b}$, defined at generator level as the events in which two additional b jets are generated within the acceptance requirements (see section 4), each of which originates from

JHEP03(2019)026

one or more B hadrons; $t\bar{t}$+b, for which only one additional b jet within the acceptance originates from a single B hadron; $t\bar{t}$+2b, which corresponds to events with two additional B hadrons that are close enough in direction to produce a single b jet; $t\bar{t}$+$c\bar{c}$, for which events have at least one additional c jet within the acceptance and no additional b jets; $t\bar{t}$ + light flavour jets ($t\bar{t}$+lf), which corresponds to events that do not belong to any of the above processes. The $t\bar{t}$+$b\bar{b}$, $t\bar{t}$+b, $t\bar{t}$+2b, and $t\bar{t}$+$c\bar{c}$ processes are collectively referred to as $t\bar{t}$+hf in the following. This categorisation is important because the subsamples originate from different physics processes and have different systematic uncertainties.

Effects from additional pp interactions in the same bunch crossings (pileup) are modelled by adding simulated minimum-bias events (generated with PYTHIA v.8.212, tune CUETP8M1) to all simulated processes. The pileup multiplicity distribution in simulation is reweighted to reflect the luminosity profile of the observed pp collisions. Correction factors described in section 4 are applied to the simulation where necessary to improve the description of the data.

4 Object and event reconstruction

The event selection is optimised to identify events from the production of a Higgs boson in association with $t\bar{t}$ events, where the Higgs boson decays into $b\bar{b}$. Two $t\bar{t}$ decay modes are considered: the single-lepton mode ($t\bar{t} \to \ell\nu\, q\bar{q}'\, b\bar{b}$), where one W boson decays into a charged lepton and a neutrino, and the dilepton mode ($t\bar{t} \to \ell^+\nu\, \ell^-\bar{\nu}\, b\bar{b}$), where both W bosons decay into a charged lepton and a neutrino. These signatures imply the presence of isolated leptons (ℓ = e, μ), missing transverse momentum due to the neutrinos from W boson decays, and highly energetic jets originating from the final-state quarks. Jets originating from the hadronisation of b quarks are identified through b tagging techniques [68].

Online, events in the single-lepton channel were selected by single-lepton triggers which require the presence of one electron (muon) with a transverse momentum (p_T) threshold of $p_T > 27(24)$ GeV. Events in the dilepton channel were selected either by the single-lepton trigger (retaining events with an additional lepton) or by dilepton triggers that require the presence of two electrons or muons. The same-flavour dilepton triggers required two electrons with $p_T > 23$ and 12 GeV, or two muons with $p_T > 17$ and 8 GeV, respectively. The different-flavour dilepton triggers required either a muon with $p_T > 23$ GeV and an electron with $p_T > 12$ GeV, or an electron with $p_T > 23$ GeV and a muon with $p_T > 8$ GeV.

Events are reconstructed using a particle-flow (PF) technique [69], which combines information from all subdetectors to enhance the reconstruction performance by identifying individual particle candidates in pp collisions. An interaction vertex [70] is required within 24 cm of the detector centre along the beam line direction, and within 2 cm of the beam line in the transverse plane. Among all such vertices, the reconstructed vertex with the largest value of summed physics-object p_T^2 is taken to be the primary pp interaction vertex. The physics objects are the jets, clustered using a jet finding algorithm [71, 72] with the tracks assigned to the vertex as inputs, and the associated missing transverse momentum, taken as the negative vector sum of the p_T of those jets. All other interaction vertices are

JHEP03(2019)026

considered as pileup vertices. Charged tracks identified as hadrons from pileup vertices are omitted in the subsequent event reconstruction.

The electron and muon candidates are required to be sufficiently isolated from nearby jet activity as follows. For each electron (muon) candidate, a cone of $\Delta R = 0.3\,(0.4)$ is constructed around the direction of the track at the event vertex, where ΔR is defined as $\sqrt{(\Delta\eta)^2 + (\Delta\phi)^2}$, and $\Delta\eta$ and $\Delta\phi$ are the distances in the pseudorapidity and azimuthal angle. Excluding the contribution from the lepton candidate, the scalar p_{T} sum of all particle candidates inside the cone consistent with arising from the chosen primary event vertex is calculated. The neutral component from pileup interactions is subtracted event-by-event, based on the average transverse energy deposited by neutral particles in the event in the case of electrons, and half the transverse momentum carried by charged particles identified to come from pileup vertices in the case of muons. A relative isolation discriminant I_{rel} is defined as the ratio of this sum to the p_{T} of the lepton candidate. Electron candidates are selected if they have values of $I_{\mathrm{rel}} < 0.06$, while muons are selected if they fulfil the requirement $I_{\mathrm{rel}} < 0.15$ in the single-lepton channel and $I_{\mathrm{rel}} < 0.25$ in the dilepton channel. In addition, electrons from identified photon conversions are rejected [73]. To further increase the purity of muons originating from the primary interaction and to suppress misidentified muons or muons from decay-in-flight processes, additional quality criteria, such as a minimal number of hits associated with the muon track, are required in both the silicon tracker and the muon system [74].

For the single-lepton channel, events are selected containing exactly one energetic, isolated lepton (e or μ), which is required to have $p_{\mathrm{T}} > 30(26)$ GeV in the case of the electron (muon), and $|\eta| < 2.1$. Electron candidates in the transition region between the barrel and endcap calorimeters, $1.4442 < |\eta| < 1.5560$, are excluded. The flavour of the lepton must match the flavour of the trigger that accepted the event (e.g. if an electron is identified, the single-electron trigger must have accepted the event). For the dilepton channel, events are required to have a pair of oppositely charged energetic leptons ($\mathrm{e^+e^-}$, $\mu^{\pm}\mathrm{e}^{\mp}$, $\mu^+\mu^-$). The lepton with the highest p_{T} out of the pair is required to have $p_{\mathrm{T}} > 25\,\mathrm{GeV}$, and the other lepton $p_{\mathrm{T}} > 15\,\mathrm{GeV}$; both leptons are required to fulfil the requirement $|\eta| < 2.4$, excluding electrons in the transition region. The flavours of the lepton pair must match the flavour of the trigger that accepted the event. The events are unambiguously classified as $\mathrm{e^+e^-}$, $\mu^{\pm}\mathrm{e}^{\mp}$, or $\mu^+\mu^-$, depending on the type of the selected lepton pair, and there is no overlap with the other channels under study. The invariant mass of the selected lepton pair, $m_{\ell\ell}$, is required to be larger than 20 GeV to suppress events from heavy-flavour resonance decays and low-mass Drell-Yan processes. In the same-flavour channels, events are also rejected if $76 < m_{\ell\ell} < 106\,\mathrm{GeV}$, thereby suppressing further contribution from Z+jets events. In both the single- and dilepton channel, events with additional isolated leptons with $p_{\mathrm{T}} > 15\,\mathrm{GeV}$ and $|\eta| < 2.4$ are excluded from further analysis.

The missing transverse momentum vector $\vec{p}_{\mathrm{T}}^{\,\mathrm{miss}}$ is defined as the projection of the negative vector sum of the momenta of all reconstructed PF objects in an event on the plane perpendicular to the beams. Its magnitude is referred to as $p_{\mathrm{T}}^{\mathrm{miss}}$. Events are required to fulfil $p_{\mathrm{T}}^{\mathrm{miss}} > 20\,\mathrm{GeV}$ in the single-lepton and $p_{\mathrm{T}}^{\mathrm{miss}} > 40\,\mathrm{GeV}$ in the dilepton same-flavour channels to further suppress background contribution.

JHEP03(2019)026

Jets are reconstructed from the PF particle candidates using the anti-k_T clustering algorithm [71] with a distance parameter of 0.4, as implemented in FastJet [72]. Charged hadrons that are associated to pileup vertices are discarded from the clustering. The jet energy is corrected for the remaining neutral-hadron pileup component in a manner similar to that used to find the energy within the lepton isolation cone [75]. Jet energy corrections are also applied as a function of jet p_T and η [76] to data and simulation. All reconstructed jets in the single-lepton channel and the two jets leading in p_T in the dilepton channel are required to satisfy $|\eta| < 2.4$ and $p_T > 30\,\text{GeV}$. Other jets in the dilepton channel are selected if $p_T > 20\,\text{GeV}$. Events are selected if they contain at least four jets in the single-lepton channel or at least two jets in the dilepton channel.

Jets originating from the hadronisation of b quarks are identified using a combined secondary vertex algorithm (CSVv2) [68], which provides a b tagging discriminant by combining identified secondary vertices and track-based lifetime information. A discriminant value is chosen such that the probability of tagging jets originating from light-flavour quarks (u, d, or s) or gluons is about 1%, and the corresponding efficiency for tagging jets from b (c) quarks is ≈65% (10%). The shape of the CSVv2 discriminant distribution in simulation is corrected by scale factors to better describe the data. This correction is derived separately for light-flavour and b jets with a tag-and-probe approach. Control samples enriched in events with a Z boson and exactly two jets where a b jet veto is applied are used to obtain the correction for light-flavour jets. The correction for b jets is estimated using a sample enriched in $\mathrm{t\bar{t}}$ events with no additional jets [68]. For c jets, the data-to-simulation scale factor is set to unity with an uncertainty twice the one of the correction for b jets. Events are required to have at least two (one) b-tagged jets in the single-lepton (dilepton) channels.

Event yields observed in data and predicted by the simulation after this selection (referred to as baseline selection in the following) are listed in table 1 for the single-lepton and dilepton channels. The corresponding jet and b-tagged jet multiplicity distributions are shown in figures 2 and 3, respectively. The $\mathrm{t\bar{t}H}$ signal includes $\mathrm{H} \to \mathrm{b\bar{b}}$ and all other Higgs boson decay modes. Background contributions from QCD multijet production, estimated using a low-p_T^{miss} control region in data, have been found to be negligible in this analysis.

5 Analysis strategy and event classification

In both the single-lepton and dilepton channels, events with at least four jets of which at least three are b-tagged are selected among those passing the baseline selection described in section 4. These events are then further divided into categories with varying signal purity and different background composition. In each category, combinations of several multivariate discriminants are optimised to separate signal from background. The signal is extracted in a simultaneous template fit of the discriminant output obtained from the simulation to the data across all the categories, correlating processes and their uncertainties where appropriate. In this way, the different background composition in the different categories helps to constrain the uncertainties of the different processes and increases the overall sensitivity of the search.

JHEP03(2019)026

Process	SL channel	DL channel
$t\bar{t}$+lf	$463\,658 \pm 174$	$241\,032 \pm 99$
$t\bar{t}$+c$\bar{c}$	$76\,012 \pm 70$	$24\,550 \pm 32$
$t\bar{t}$+b	$22\,416 \pm 38$	$5\,979 \pm 16$
$t\bar{t}$+2b	$9\,052 \pm 24$	$1\,785 \pm 9$
$t\bar{t}$+b$\bar{b}$	$10\,897 \pm 27$	$1\,840 \pm 9$
Single t	$25\,215 \pm 166$	$12\,206 \pm 125$
V+jets	$12\,309 \pm 58$	$5\,684 \pm 209$
$t\bar{t}$+V	$2\,457 \pm 12$	$2\,570 \pm 23$
Diboson	449 ± 14	430 ± 15
Total bkg.	$622\,466 \pm 263$	$296\,077 \pm 266$
$t\bar{t}$H	$1\,232 \pm 2$	314.0 ± 0.9
Data	610 556	283 942

Table 1. Event yields observed in data and predicted by the simulation after the baseline selection requirements in the single-lepton (SL) and dilepton (DL) channels. The $t\bar{t}H$ signal includes $H \to b\bar{b}$ and all other Higgs boson decay modes. The quoted uncertainties are statistical only.

Several methods that classify events as signal- or background-like were explored to achieve optimal sensitivity: DNNs and BDTs, combined with a MEM. In the DNN approach, the jet multiplicity and the DNN classification output, described below, are used for the event categorisation ("jet-process categories"). In the BDT approach, events are divided into categories based on their jet and b-tagged jet multiplicity ("jet-tag categories"). The approach that provided the best expected sensitivity in each channel, evaluated on fits to simulated data, was chosen for obtaining the final result from data. Therefore, in the single-lepton channel the DNN approach is used, while in the dilepton channel a BDT+MEM classification is chosen. The methods and the corresponding categorisation are illustrated in figure 4 and described in the following.

In the single-lepton channel, events are separated depending on the jet multiplicity into three categories with (4 jets, ≥ 3 b tags), (5 jets, ≥ 3 b tags), and (≥ 6 jets, ≥ 3 b tags). Dedicated multi-classification DNNs [77] are trained in each jet multiplicity category to separate signal and each of the five $t\bar{t}$+jets background processes $t\bar{t}$+b$\bar{b}$, $t\bar{t}$+2b, $t\bar{t}$+b, $t\bar{t}$+c$\bar{c}$, or $t\bar{t}$+lf.

The DNN training is performed using simulated $t\bar{t}H$ and $t\bar{t}$+jets events as signal and background, respectively. The overall set of events is split into a training set (30%), an independent set (20%) for validation and optimisation of the DNN configuration (hyper parameters), such as the number of nodes per layer, and a set that is reserved for the fit to the data (50%). The hyper parameters and input variables are detailed in appendix A.

The training is conducted in two stages. In the first stage, a DNN is trained to predict which of the reconstructed physics objects originate from the expected underlying hard

JHEP03(2019)026

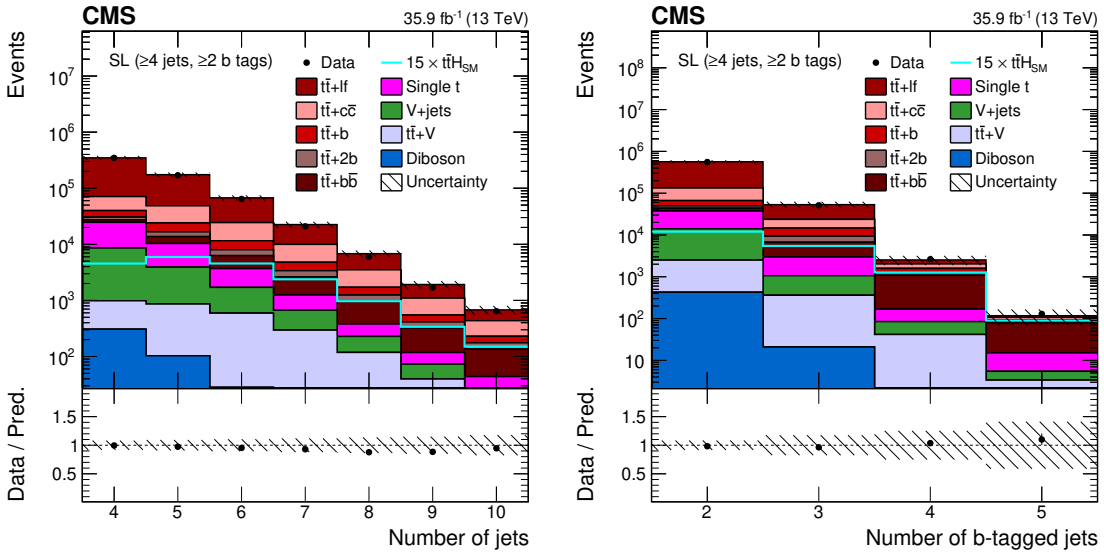

Figure 2. Jet (left) and b-tagged jet (right) multiplicity in the single-lepton (SL) channel after the baseline selection. The expected background contributions (filled histograms) are stacked, and the expected signal distribution (line), which includes $H \to b\bar{b}$ and all other Higgs boson decay modes, is superimposed. Each contribution is normalised to an integrated luminosity of $35.9\,\text{fb}^{-1}$, and the signal distribution is additionally scaled by a factor of 15 for better visibility. The hatched uncertainty bands correspond to the total statistical and systematic uncertainties (excluding uncertainties that affect only the normalisation of the distribution) added in quadrature. The distributions observed in data (markers) are overlayed. The last bin includes overflow events. The lower plots show the ratio of the data to the background prediction.

process, such as for example the b quark jet from the decay of a top quark. In the second stage, the initial network is extended by adding hidden layers, which take as input the variables and the output values of the first stage, and the resulting network is trained to predict the physics process of an event. The values obtained in the output nodes of the second stage are normalised to unity using a "softmax" function [77], and, as a result, can be interpreted as probabilities describing the likelihood of the event being a $t\bar{t}H$ signal or one of the five $t\bar{t}$+jets background processes. Events are divided into subcategories of the most probable process according to this DNN classification. Thus, there are in total 18 jet-process categories in the single-lepton channel. In each of the jet-process categories, the DNN classifier output distribution of the node that matches the process category is used as the final discriminant.

The DNNs utilise input variables related to kinematic properties of individual objects, event shape, and the jet CSVv2 b tagging discriminant, and additionally the MEM discriminant output, described in the following.

The MEM discriminant is constructed as the ratio of the probability density values for the signal ($t\bar{t}H$) and background ($t\bar{t}$+$b\bar{b}$) hypotheses, following the algorithm described in ref. [29]. Each event is assigned a probability density value computed from the four-momenta of the reconstructed particles, which is based on the leading order scattering amplitudes for the $t\bar{t}H$ and $t\bar{t}$+$b\bar{b}$ processes and integrated over the particle-level quanti-

JHEP03(2019)026

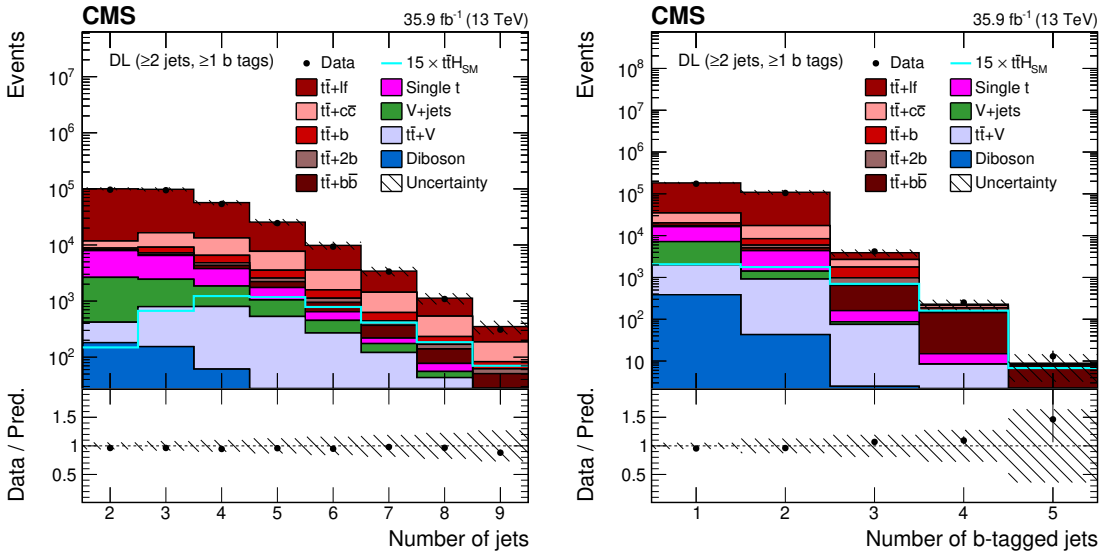

Figure 3. Jet (left) and b-tagged jet (right) multiplicity in the dilepton (DL) channel after the baseline selection. The expected background contributions (filled histograms) are stacked, and the expected signal distribution (line), which includes $H \to b\bar{b}$ and all other Higgs boson decay modes, is superimposed. Each contribution is normalised to an integrated luminosity of 35.9 fb^{-1}, and the signal distribution is additionally scaled by a factor of 15 for better visibility. The hatched uncertainty bands correspond to the total statistical and systematic uncertainties (excluding uncertainties that affect only the normalisation of the distribution) added in quadrature. The distributions observed in data (markers) are overlayed. The last bin includes overflow events. The lower plots show the ratio of the data to the background prediction.

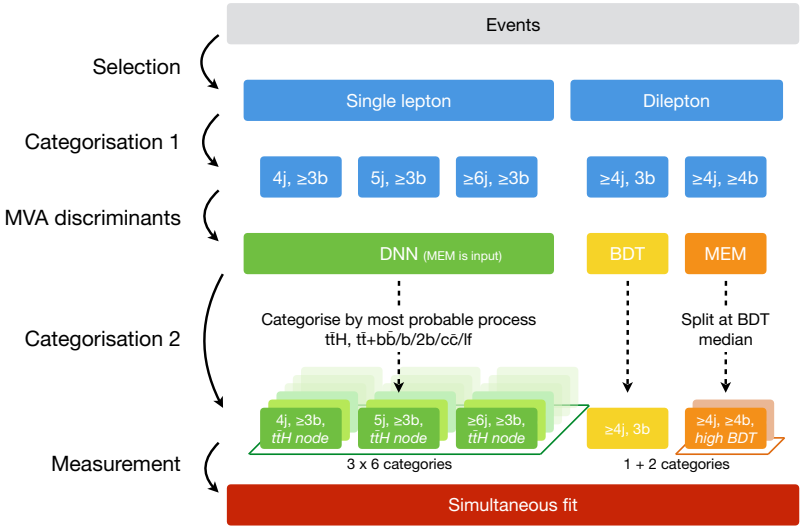

Figure 4. Illustration of the analysis strategy.

JHEP03(2019)026

ties that are either unknown or poorly measured. The probability density functions are constructed at leading order, assuming gluon-gluon fusion production both for signal and background processes as it represents the majority of the event rate. In each event, the four jets that are most likely to originate from b quarks are considered explicitly as candidates for the b quarks from the decay of the Higgs boson and the top quarks. All permutations of jets, regardless of their b tagging discriminant, are considered when associating the b-quark-like jets to the top quark or Higgs boson decays in the matrix element. The four b-like jets are selected using a likelihood ratio criterion as follows. The likelihoods are computed under either the hypothesis that four jets or that two jets in the event originate from b quarks, based on the expected b tagging discriminant probability densities from simulation. The used ratio is computed as the four-b-jets likelihood, normalised to the sum of the four- and the two-b-jets likelihoods. When computing the MEM in the single-lepton channel, up to four additional light jets, ordered in p_{T}, are permuted over as candidates for the light quarks from the hadronic decay of the W boson.

In the dilepton channel, events are separated into two jet-tag categories with (≥ 4 jets, 3 b tags) and (≥ 4 jets, ≥ 4 b tags). In each jet-tag category, a dedicated BDT is trained to separate signal from background processes. The BDTs utilise input variables related to kinematic properties of individual objects, event shape, and the jet CSVv2 b tagging discriminant, similar as the DNNs, but no MEM information. The training is performed using simulated $\mathrm{t\bar{t}H}$ and $\mathrm{t\bar{t}}$+jets events as signal and background, respectively, which are weighted to achieve equal yields of signal and background events. In order to avoid a biased performance estimate, the events are separated in half for training and validation. The specific BDT boosting method used is the stochastic gradient boost [36, 78], available as part of the TMVA package [38]. The choice of the BDT architecture and the input variables was optimised with a procedure based on the particle swarm algorithm [79, 80], selecting the configuration and set of variables that yields the highest discrimination power. They are detailed in appendix A.

In the (≥ 4 jets, 3 b tags) category, the BDT output distribution is used as the final discriminant. The (≥ 4 jets, ≥ 4 b tags) category is further divided into two subcategories, one with small values of the BDT output (background-like) and one with large output values (signal-like). The division is taken at the median of the BDT output distribution for simulated signal events. In each subcategory, the MEM discriminant output is used as the final discriminant. The high BDT output subcategory is expected to be enhanced with signal events and residual $\mathrm{t\bar{t}}$+$\mathrm{b\bar{b}}$ background events, and the MEM discriminant achieves by construction particularly powerful additional separation against the $\mathrm{t\bar{t}}$+$\mathrm{b\bar{b}}$ background contributions. The choice of the median contributes to a robust result by ensuring a sufficient number of events in each subcategory. Including the low b tag multiplicity and the low BDT output subcategories into the fit constrains the background contributions and systematic uncertainties for each of the different event topologies. Thus, there are in total three categories in the dilepton channel.

In summary, in the single-lepton channel events are subdivided into 18 jet-process categories and the DNN output distribution of the most probable process is used as the final discriminant. In the dilepton channel events are subdivided into three jet-tag categories and either the BDT or MEM output distribution is used as the final discriminant.

JHEP03(2019)026

6 Systematic uncertainties

In table 2, all sources of systematic uncertainties considered in the analysis are listed. They affect either the rate of the signal or background processes, or the discriminant shape, or both. In the last case, the rate and shape effects are treated as entirely correlated and are varied simultaneously. The uncertainties are taken into account via nuisance parameters in the final fit procedure described in section 7, where the effects from the same source are treated as fully correlated among the different categories. The impact of the uncertainties on the final result is discussed in section 7.

The uncertainty in the integrated luminosity estimate is 2.5% [81]. The trigger efficiency in the single-lepton channel and the electron and muon identification efficiency uncertainties are estimated by comparing variations in measured efficiency between data and simulation using a high-purity sample of Z boson decays. In the dilepton channel, the trigger efficiency is measured in data with a method based on triggers that are uncorrelated with those used in the analysis, in particular based on $p_{\mathrm{T}}^{\mathrm{miss}}$ requirements. These uncertainties are found to be small, typically below 1–2%. Effects of the uncertainty in the distribution of the number of pileup interactions are evaluated by varying the total inelastic cross section used to predict the number of pileup interactions in the simulated events by ±4.6% from its nominal value [82]. The uncertainty due to the limited knowledge of the jet energy scale (resolution) is determined by variations of the energy scale (resolution) correction of all jets in the signal and background predictions by one standard deviation. In the case of the jet energy scale uncertainty, these variations are divided into 26 sources, which include uncertainties owing to the extrapolation between samples of different jet-flavour composition and the presence of pileup collisions in the derivation of the corrections [76]. The effect of each source is evaluated individually. The uncertainty of the CSVv2 b tagging scale factors is evaluated by applying alternative scale factors based on varying the following systematic effects [68] by one standard deviation, separately for the different jet flavours: the contamination of background processes in the control samples, the jet energy scale uncertainty — which is correlated with the overall jet energy scale uncertainty — and the statistical uncertainty in the scale factor evaluation. The impact of the statistical uncertainty is parameterised as the sum of two contributions: one term with linear dependence on the b tagging discriminant value, allowing an overall tilt of the discriminant distribution, and another term with quadratic dependence, allowing an overall shift of the discriminant distribution.

Theoretical uncertainties of the cross sections used to predict the rates of various processes are propagated to the yield estimates. All rates are estimated using cross sections with at least NLO accuracy, which have uncertainties arising primarily from PDFs and the choice of factorisation and renormalisation scales (both in the ME and the PS). The cross section uncertainties are each separated into their PDF and scale components (renorm./fact. scales) and are correlated where appropriate between processes. For example, the PDF uncertainties for background processes originating primarily from gluon-gluon initial states are treated as 100% correlated. The PDF uncertainty of the $\mathrm{t\bar{t}H}$ signal production is treated separately from the background processes.

The $\mathrm{t\bar{t}+b\bar{b}}$ process, and to lesser extent the $\mathrm{t\bar{t}+2b}$, $\mathrm{t\bar{t}+b}$, and $\mathrm{t\bar{t}+c\bar{c}}$ production, represent important sources of irreducible background. Neither previous measurements of

JHEP03(2019)026

Source	Type	Remarks
Integrated luminosity	rate	Signal and all backgrounds
Lepton identification/isolation	shape	Signal and all backgrounds
Trigger efficiency	shape	Signal and all backgrounds
Pileup	shape	Signal and all backgrounds
Jet energy scale	shape	Signal and all backgrounds
Jet energy resolution	shape	Signal and all backgrounds
b tag hf fraction	shape	Signal and all backgrounds
b tag hf stats (linear)	shape	Signal and all backgrounds
b tag hf stats (quadratic)	shape	Signal and all backgrounds
b tag lf fraction	shape	Signal and all backgrounds
b tag lf stats (linear)	shape	Signal and all backgrounds
b tag lf stats (quadratic)	shape	Signal and all backgrounds
b tag charm (linear)	shape	Signal and all backgrounds
b tag charm (quadratic)	shape	Signal and all backgrounds
Renorm./fact. scales ($t\bar{t}H$)	rate	Scale uncertainty of NLO $t\bar{t}H$ prediction
Renorm./fact. scales ($t\bar{t}$)	rate	Scale uncertainty of NNLO $t\bar{t}$ prediction
Renorm./fact. scales ($t\bar{t}$+hf)	rate	Additional 50% rate uncertainty of $t\bar{t}$+hf predictions
Renorm./fact. scales (t)	rate	Scale uncertainty of NLO single t prediction
Renorm./fact. scales (V)	rate	Scale uncertainty of NNLO W and Z prediction
Renorm./fact. scales (VV)	rate	Scale uncertainty of NLO diboson prediction
PDF (gg)	rate	PDF uncertainty for gg initiated processes except $t\bar{t}H$
PDF (gg $t\bar{t}H$)	rate	PDF uncertainty for $t\bar{t}H$
PDF ($q\bar{q}$)	rate	PDF uncertainty of $q\bar{q}$ initiated processes ($t\bar{t}$+W,W,Z)
PDF (qg)	rate	PDF uncertainty of qg initiated processes (single t)
μ_R scale ($t\bar{t}$)	shape	Renormalisation scale uncertainty of the $t\bar{t}$ ME generator (POWHEG), same for additional jet flavours
μ_F scale ($t\bar{t}$)	shape	Factorisation scale uncertainty of the $t\bar{t}$ ME generator (POWHEG), same for additional jet flavours
PS scale: ISR ($t\bar{t}$)	rate	Initial state radiation uncertainty of the PS (for $t\bar{t}$ events), jet multiplicity dependent rate uncertainty, independent for additional jet flavours
PS scale: FSR ($t\bar{t}$)	rate	Final state radiation uncertainty (for $t\bar{t}$ events), jet multiplicity dependent rate uncertainty, independent for additional jet flavours
ME-PS matching ($t\bar{t}$)	rate	NLO ME to PS matching, *hdamp* [54] (for $t\bar{t}$ events), jet multiplicity dependent rate uncertainty, independent for additional jet flavours
Underlying event ($t\bar{t}$)	rate	Underlying event (for $t\bar{t}$ events), jet multiplicity dependent rate uncertainty, independent for additional jet flavours
NNPDF3.0NLO ($t\bar{t}H$, $t\bar{t}$)	shape	Based on the NNPDF replicas, same for $t\bar{t}H$ and additional jet flavours
Bin-by-bin event count	shape	Statistical uncertainty of the signal and background prediction due to the limited sample size

Table 2. Systematic uncertainties considered in the analysis, their corresponding type (affecting rate or shape of the distributions), and additional remarks.

JHEP03(2019)026

$t\bar{t}$+hf production [83–86] nor higher-order theoretical calculations can currently constrain the normalisation of these contributions to better than 35% accuracy [87, 88]. The shape of the final discriminant distributions as well as important input variable distributions of the sum of the $t\bar{t}+b\bar{b}$, $t\bar{t}$+2b, and $t\bar{t}$+b processes obtained with the nominal $t\bar{t}$ simulation were compared to those obtained from a 4-flavour scheme SHERPA (v.2.2.2) [89] $t\bar{t}+b\bar{b}$ simulation combined with OPENLOOPS (v.1.3.1) [90]. The shapes agree within the statistical precision. Therefore, an additional 50% rate uncertainty is assigned to each of the $t\bar{t}$+hf processes to account also for differences in the phase space with respect to ref. [86]. Moreover, the robustness of the fit model was verified using simulated toy data, which were sampled from the templates of the fit model. The background templates were modified in the following ways to sample the toy data: increasing the normalisation of the $t\bar{t}+b\bar{b}$ background template by 30% in accordance with the results in ref. [86] or replacing the sum of the templates of the $t\bar{t}+b\bar{b}$, $t\bar{t}$+2b, and $t\bar{t}$+b processes obtained with the nominal $t\bar{t}$ simulation by those obtained from the 4-flavour scheme SHERPA plus OPENLOOPS mentioned above. In each case, a fit of the nominal model to the toy data is performed as described in section 7, including the full set of systematic uncertainties. The injected signal is recovered within a few percent, well within the uncertainties assigned to these processes.

The uncertainty arising from the missing higher-order terms in the simulation with POWHEG of the $t\bar{t}$+jets process at the ME level is assessed by varying the renormalisation and factorisation scales in the simulation up and down by factors of two with respect to the nominal values, using event weights obtained directly from the generator. At the PS level, the corresponding uncertainty is estimated by varying the parameters controlling the amount of initial- and final-state radiation independently by factors of 0.5 and 2 [91]. These sources of uncertainties are treated as uncorrelated. The uncertainty originating from the scheme used to match the ME level calculation to the PS simulation is derived by comparing the reference $t\bar{t}$+jets simulation with two samples with varied *hdamp* parameter [54], which controls the ME and PS matching and effectively regulates the high-p_{T} radiation. The effect on the final discriminators owing to uncertainties in the underlying event tune of the $t\bar{t}$+jets event generator are estimated using simulations with varied parameters with respect to those used to derive the CUETP8M2T4 tune in the default setup. The event count in the additional samples required to estimate the modelling uncertainties was small and induced changes to the discriminant distributions comparable in size to the statistical fluctuations of the additional samples. For this reason, the uncertainties were estimated conservatively as the changes in the rates of the different $t\bar{t}$ subprocesses independently for different jet multiplicities. If the statistical uncertainty owing to the size of the simulated samples was larger than the rate change, the former was assigned as uncertainty. The derived rate uncertainties were then correlated between jet multiplicities to account for migration effects and are treated as uncorrelated among the $t\bar{t}$ subprocesses. Possible shape variations of the final discriminant distributions due to the PDF uncertainty have been estimated by evaluating the PDF replicas provided with the NNPDF set [50]. The impact of the mismodelling of the top quark p_{T} spectrum in the $t\bar{t}$ simulation [92] was found to be negligible.

The impact of statistical fluctuations in the signal and background prediction due to the limited number of simulated events is accounted for using the Barlow-Beeston approach described in refs. [93, 94].

JHEP03(2019)026

	pre-fit (post-fit) yields					
Process	$t\bar{t}H$ node	$t\bar{t}+b\bar{b}$ node	$t\bar{t}+2b$ node	$t\bar{t}+b$ node	$t\bar{t}+c\bar{c}$ node	$t\bar{t}+lf$ node
$t\bar{t}+lf$	1249 (962)	727 (572)	1401 (1090)	1035 (823)	2909 (2296)	8463 (6829)
$t\bar{t}+c\bar{c}$	298 (458)	232 (359)	428 (678)	251 (400)	686 (1068)	1022 (1652)
$t\bar{t}+b$	253 (356)	215 (311)	370 (530)	326 (484)	308 (437)	469 (683)
$t\bar{t}+2b$	124 (96)	77 (62)	317 (254)	90 (73)	100 (79)	134 (108)
$t\bar{t}+b\bar{b}$	139 (137)	191 (192)	149 (140)	105 (103)	119 (114)	133 (128)
Single t	96 (96)	117 (109)	167 (162)	93 (96)	231 (232)	304 (307)
V+jets	37 (37)	76 (74)	48 (46)	27 (27)	97 (89)	69 (69)
$t\bar{t}+V$	13 (13)	6 (6)	12 (11)	6 (6)	10 (10)	16 (16)
Diboson	4 (4)	5 (5)	0.9 (0.8)	0.6 (0.7)	2 (2)	4 (4)
Total bkg.	2213 (2158)	1645 (1688)	2892 (2911)	1935 (2012)	4462 (4328)	10614 (9795)
± tot unc.	±508 (±58)	±415 (±53)	±588 (±89)	±402 (±67)	±1051 (±120)	±2359 (±270)
$t\bar{t}H$	27 (21)	9 (7)	16 (12)	7 (5)	9 (7)	16 (13)
± tot unc.	±4 (±3)	±1 (±1)	±2 (±2)	±1 (±1)	±1 (±1)	±2 (±2)
Data	2125	1793	2896	2027	4366	9693

Table 3. Observed and expected event yields per jet-process category (node) in the single-lepton channel with 4 jets and at least 3 b tags, prior to the fit to data (after the fit to data). The quoted uncertainties denote the total statistical and systematic components.

7 Results

The numbers of events selected in the jet-process categories of the single-lepton channel and in the jet-tag categories of the dilepton channel, before and after the fit of the signal strength modifier and the nuisance parameters, are listed in tables 3–6. The final discriminants in some example categories in the single-lepton channel and the three dilepton categories before and after the fit to data are displayed in figures 5–6 and figures 7–8, respectively. All final discriminants in the single-lepton channel before and after the fit to data are displayed in appendices B and C.

The signal strength modifier $\mu = \sigma/\sigma_{\mathrm{SM}}$ of the $t\bar{t}H$ production cross section is determined in a simultaneous binned maximum likelihood fit to the data across all analysis categories. The fit procedure takes into account systematic uncertainties that modify the shape and normalisation of the final discriminant distributions, as described in section 6. The best fit values of the nuisance parameters are within 1 standard deviation of the prior uncertainty for more than 95% of the total number of nuisance parameters. The best fit values of the 20 parameters ranked highest in impact are presented in figure 9. As expected, the fit constrains the nuisance parameters related to the conservatively assigned 50% prior uncertainties on the $t\bar{t}$+hf cross section to 40–60% of the prior. A few other nuisance parameters that are related to jet energy scale and b tagging uncertainties are constrained up to a factor of 50%. These constraints are not due to conservatively assigned prior uncertainties but are attributed to the fact that events are selected according to different, large multiplicities of jets and b-tagged jets, thus increasing the sensitivity of the

JHEP03(2019)026

	pre-fit (post-fit) yields											
Process	$t\bar{t}H$ node		$t\bar{t}+b\bar{b}$ node		$t\bar{t}+2b$ node		$t\bar{t}+b$ node		$t\bar{t}+c\bar{c}$ node		$t\bar{t}+lf$ node	
$t\bar{t}+lf$	785	(570)	647	(467)	830	(604)	683	(525)	1148	(848)	4903	(3697)
$t\bar{t}+c\bar{c}$	336	(455)	341	(469)	445	(633)	264	(382)	552	(756)	1207	(1726)
$t\bar{t}+b$	257	(351)	290	(399)	355	(494)	321	(477)	219	(301)	494	(692)
$t\bar{t}+2b$	136	(104)	128	(99)	324	(253)	89	(73)	85	(65)	184	(143)
$t\bar{t}+b\bar{b}$	266	(251)	410	(397)	224	(207)	150	(143)	144	(132)	228	(212)
Single t	62	(63)	82	(84)	98	(96)	45	(58)	114	(113)	189	(193)
V+jets	25	(23)	54	(53)	34	(31)	11	(12)	46	(41)	54	(51)
$t\bar{t}+V$	20	(20)	14	(13)	17	(16)	7	(7)	11	(10)	25	(24)
Diboson	1	(1)	3	(3)	0.4	(0.4)	—	(—)	0.6	(0.4)	3	(3)
Total bkg.	1889	(1838)	1969	(1985)	2326	(2332)	1570	(1676)	2320	(2268)	7287	(6742)
± tot unc.	±459	(±57)	±485	(±70)	±489	(±71)	±334	(±47)	±597	(±79)	±1655	(±219)
$t\bar{t}H$	53	(41)	21	(17)	20	(15)	8	(6)	11	(8)	28	(22)
± tot unc.	±7	(±6)	±3	(±3)	±2	(±2)	±1	(±1)	±1	(±1)	±3	(±3)
Data	1848		2040		2299		1690		2302		6918	

Table 4. Observed and expected event yields per jet-process category (node) in the single-lepton channel with 5 jets and at least 3 b tags, prior to the fit to data (after the fit to data). The quoted uncertainties denote the total statistical and systematic uncertainty.

	pre-fit (post-fit) yields											
Process	$t\bar{t}H$ node		$t\bar{t}+b\bar{b}$ node		$t\bar{t}+2b$ node		$t\bar{t}+b$ node		$t\bar{t}+c\bar{c}$ node		$t\bar{t}+lf$ node	
$t\bar{t}+lf$	1982	(1381)	1280	(897)	852	(595)	916	(661)	243	(172)	50	(36)
$t\bar{t}+c\bar{c}$	1150	(1415)	998	(1230)	636	(805)	444	(567)	115	(147)	16	(19)
$t\bar{t}+b$	549	(705)	575	(746)	314	(409)	253	(338)	28	(35)	4	(5)
$t\bar{t}+2b$	306	(233)	282	(215)	372	(293)	78	(62)	10	(8)	1	(0.8)
$t\bar{t}+b\bar{b}$	834	(769)	1156	(1082)	299	(266)	145	(129)	17	(15)	3	(2)
Single t	110	(116)	146	(145)	92	(82)	53	(53)	4	(4)	3	(3)
V+jets	38	(37)	78	(76)	34	(30)	10	(9)	7	(6)	0.6	(0.6)
$t\bar{t}+V$	80	(75)	58	(54)	31	(28)	11	(11)	4	(4)	0.4	(0.4)
Diboson	0.9	(0.9)	0.5	(0.5)	0.4	(0.4)	0.4	(0.4)	—	(—)	—	(—)
Total bkg.	5049	(4733)	4575	(4447)	2629	(2509)	1911	(1831)	429	(392)	77	(67)
± tot unc.	±1216	(±186)	±1156	(±142)	±603	(±80)	±422	(±65)	±107	(±14)	±18	(±3)
$t\bar{t}H$	142	(108)	53	(40)	24	(18)	10	(7)	2.1	(1.5)	0.30	(0.23)
± tot unc.	±19	(±15)	±8	(±6)	±3	(±2)	±1	(±1)	±0.2	(±0.2)	±0.03	(±0.03)
Data	4822		4400		2484		1852		422		76	

Table 5. Observed and expected event yields per jet-process category (node) in the single-lepton channel with at least 6 jets and at least 3 b tags, prior to the fit to data (after the fit to data). The quoted uncertainties denote the total statistical and systematic uncertainty.

JHEP03(2019)026

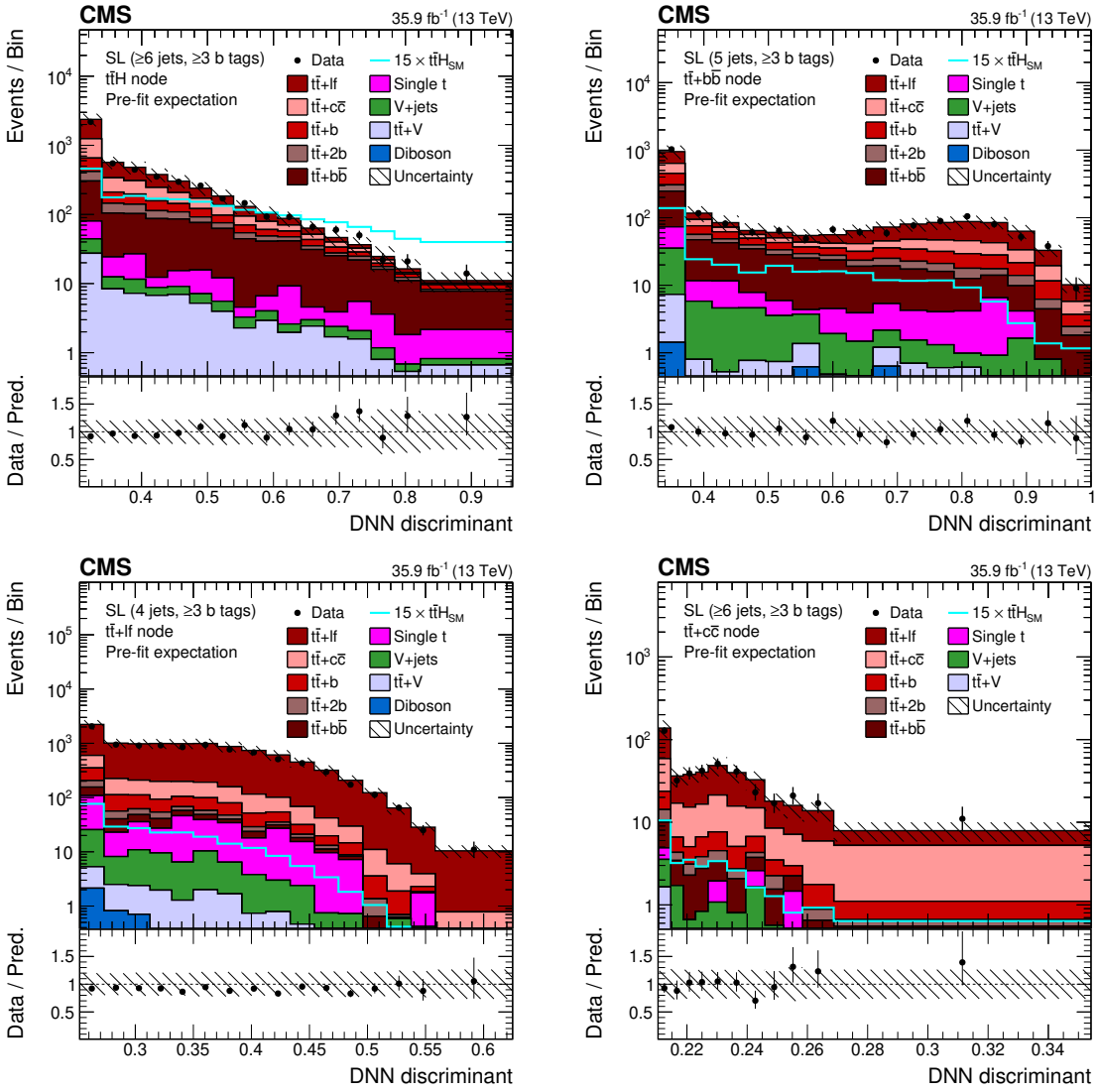

Figure 5. Final discriminant shapes in the single-lepton (SL) channel before the fit to data: DNN discriminant in the jet-process categories with ≥6 jets-t$\bar{\text{t}}$H (upper left); 5 jets-t$\bar{\text{t}}$+b$\bar{\text{b}}$ (upper right); 4 jets-t$\bar{\text{t}}$+lf (lower left); and ≥6 jets-t$\bar{\text{t}}$+c$\bar{\text{c}}$ (lower right). The expected background contributions (filled histograms) are stacked, and the expected signal distribution (line), which includes H → b$\bar{\text{b}}$ and all other Higgs boson decay modes, is superimposed. Each contribution is normalised to an integrated luminosity of 35.9 fb^{-1}, and the signal distribution is additionally scaled by a factor of 15 for better visibility. The hatched uncertainty bands include the total uncertainty of the fit model. The distributions observed in data (markers) are overlayed. The first and the last bins include underflow and overflow events, respectively. The lower plots show the ratio of the data to the background prediction.

JHEP03(2019)026

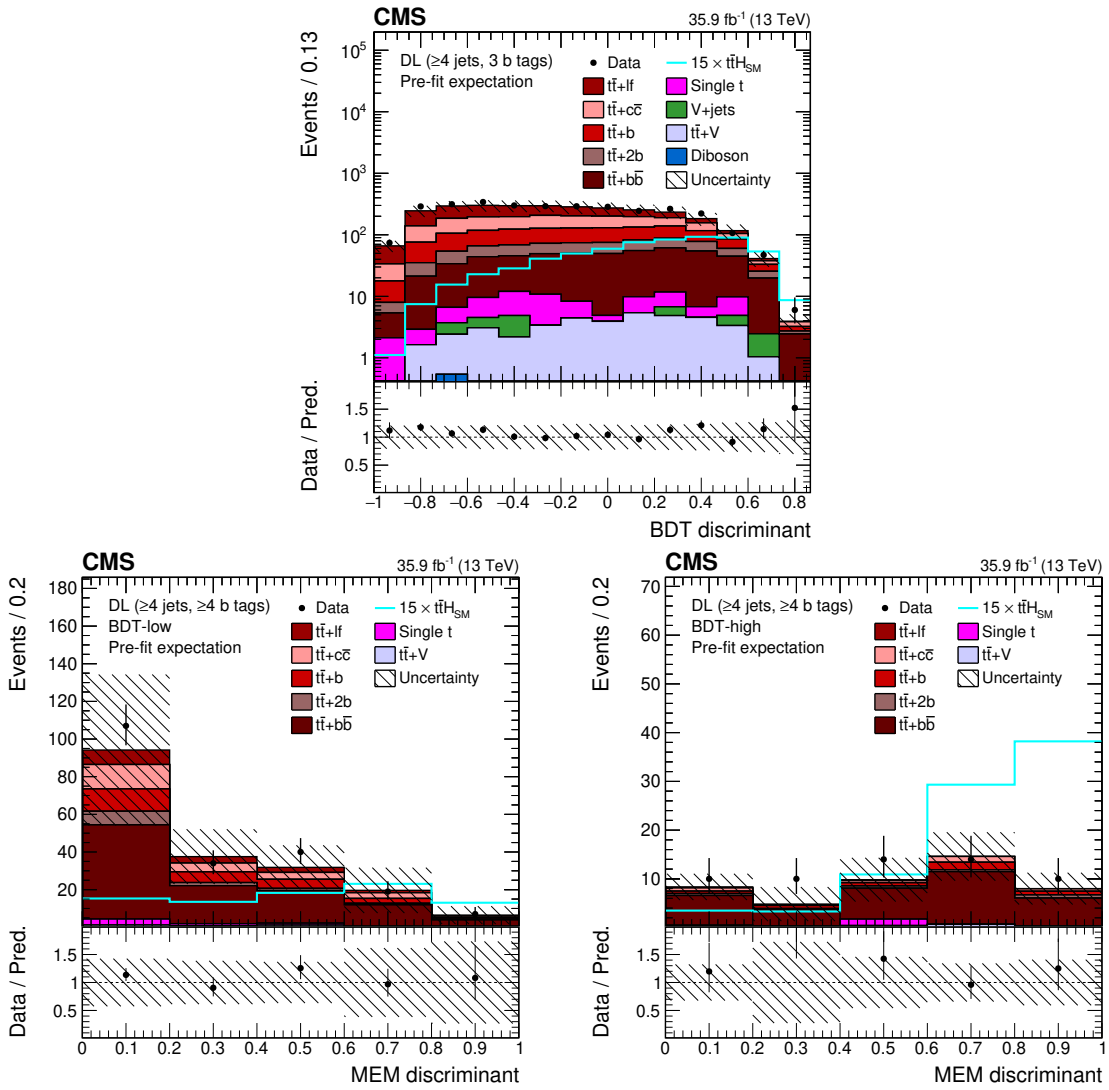

Figure 6. Final discriminant shapes in the dilepton (DL) channel before the fit to data: BDT discriminant in the analysis category with (≥ 4 jets, 3 b tags) (upper row) and MEM discriminant in the analysis categories with (≥ 4 jets, ≥ 4 b tags) (lower row) with low (left) and high (right) BDT output. The expected background contributions (filled histograms) are stacked, and the expected signal distribution (line), which includes $\mathrm{H} \to \mathrm{b\bar{b}}$ and all other Higgs boson decay modes, is superimposed. Each contribution is normalised to an integrated luminosity of 35.9 fb^{-1}, and the signal distribution is additionally scaled by a factor of 15 for better visibility. The hatched uncertainty bands include the total uncertainty of the fit model. The distributions observed in data (markers) are overlayed. The first and the last bins include underflow and overflow events, respectively. The lower plots show the ratio of the data to the background prediction.

JHEP03(2019)026

Process	pre-fit (post-fit) yields					
	≥ 4 jets, 3 b tags		≥ 4 jets, ≥ 4 b tags			
			BDT-low		BDT-high	
$t\bar{t}$+lf	845	(637)	16	(11)	0.7	(0.5)
$t\bar{t}$+c$\bar{c}$	712	(966)	25	(31)	3	(4)
$t\bar{t}$+b	546	(747)	26	(35)	4	(6)
$t\bar{t}$+2b	252	(196)	11	(8)	2	(1)
$t\bar{t}$+b$\bar{b}$	439	(415)	103	(109)	33	(32)
Single t	47	(51)	5	(3)	1	(2)
V+jets	10	(8)	—	(—)	—	(—)
$t\bar{t}$+V	40	(38)	4	(4)	2	(2)
Diboson	0.9	(0.7)	—	(—)	—	(—)
Total bkg.	2893	(3058)	190	(201)	46	(48)
$\pm$ tot unc.	$\pm$705	($\pm$98)	$\pm$67	($\pm$10)	$\pm$17	($\pm$3)
$t\bar{t}$H	42	(32)	6	(5)	6	(5)
$\pm$ tot unc.	$\pm$6	($\pm$5)	$\pm$1	($\pm$1)	$\pm$1	($\pm$1)
Data	3077		207		58	

Table 6. Observed and expected event yields per jet-tag category in the dilepton channel, prior to the fit to data (after the fit to data). The quoted uncertainties denote the total statistical and systematic uncertainty.

analysis to changes of the jet energy scale and b tagging efficiency, e.g. by their effect on the event yield per analysis category. Furthermore, the impact on μ of the most relevant sources of uncertainty is shown in figure 9, which is computed as the difference of the nominal best fit value of μ and the best fit value obtained when fixing the nuisance parameter under scrutiny to its best fit value plus/minus its post-fit uncertainty. In particular, the 20 parameters with the highest impact are shown, excluding nuisance parameters describing the statistical uncertainties due to the size of the simulated samples. The nuisance parameters with the highest impact are related to the uncertainty in the $t\bar{t}$+hf and signal cross sections, as well as in the b tagging scale factors.

The obtained best fit value of μ is $0.72 \pm 0.24\,(\text{stat}) \pm 0.38\,(\text{syst})$ with a total uncertainty of ± 0.45. This corresponds to an observed (expected) significance of 1.6 (2.2) standard deviations above the background-only hypothesis. The observed and predicted event yields in all the bins of the final discriminants, ordered by the pre-fit expected signal-to-background ratio (S/B) are shown in figure 10 (left). The best fit values in each analysis channel separately and in the combination are listed in table 7 and displayed in figure 10 (right).

The contributions of the statistical and various systematic uncertainties to the uncertainty in μ are listed in table 8. The statistical uncertainty is evaluated by fixing all nuisance parameters to their post-fit values. The impact of the systematic uncertainties is evaluated

JHEP03(2019)026

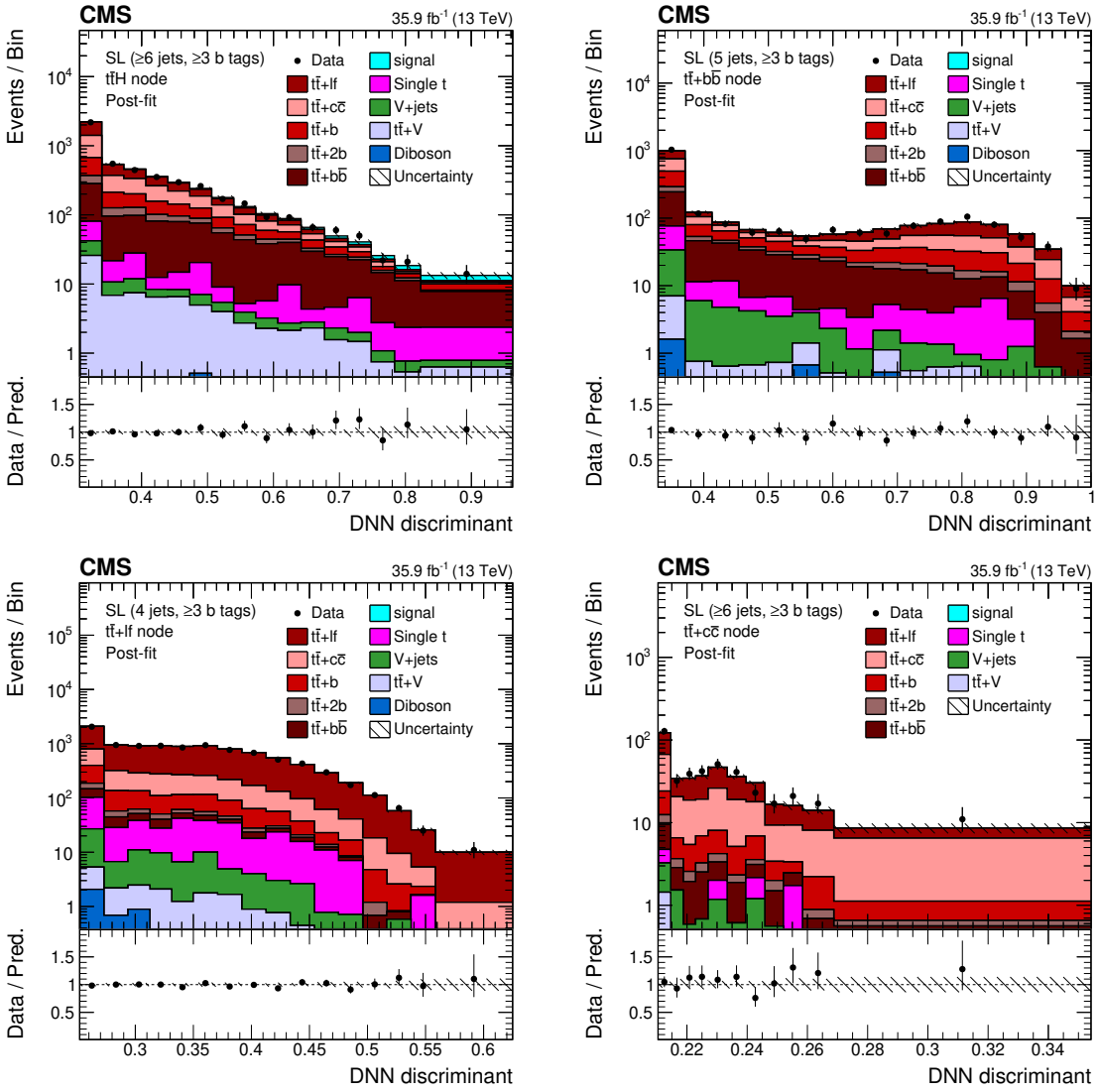

Figure 7. Final discriminant shapes in the single-lepton (SL) channel after the fit to data: DNN discriminant in the jet-process categories with ≥6 jets-t$\bar{\text{t}}$H (upper left); 5 jets-t$\bar{\text{t}}$+b$\bar{\text{b}}$ (upper right); 4 jets-t$\bar{\text{t}}$+lf (lower left); and ≥6 jets-t$\bar{\text{t}}$+c$\bar{\text{c}}$ (lower right). The hatched uncertainty bands include the total uncertainty after the fit to data. The distributions observed in data (markers) are overlayed. The first and the last bins include underflow and overflow events, respectively. The lower plots show the ratio of the data to the post-fit background plus signal distribution.

by repeating the fit fixing only the nuisance parameters related to the uncertainty under scrutiny to their post-fit values and subtracting the obtained uncertainty in quadrature from the total uncertainty of the fit where no parameters are fixed. The total uncertainty of the full fit (0.45) is different from the quadratic sum of the listed contributions because of correlations between the nuisance parameters.

The total uncertainty of 0.45 is dominated by contributions from systematic effects, while the statistical component is 0.24. The largest contributions originate from the theo-

JHEP03(2019)026

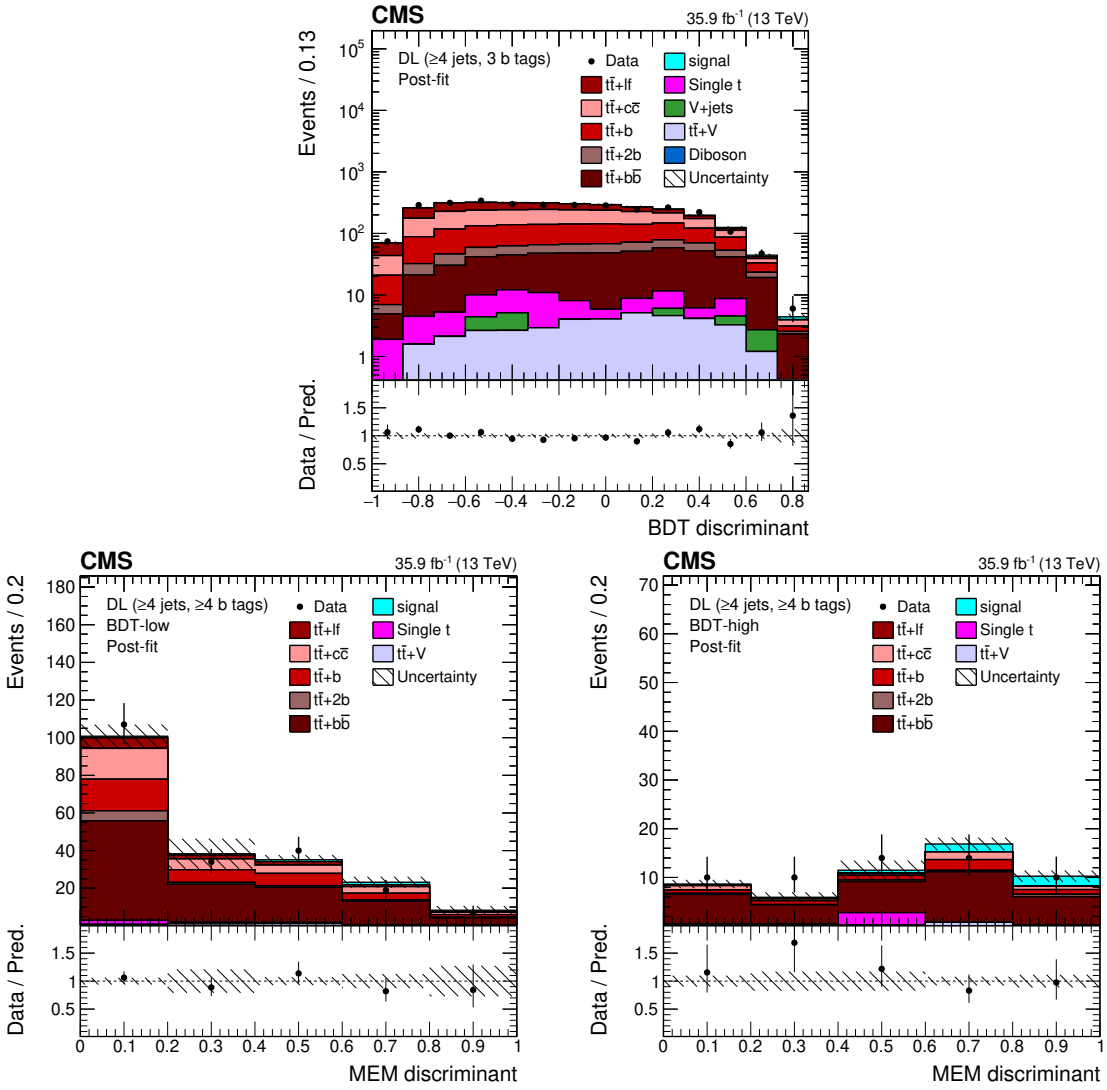

Figure 8. Final discriminant shapes in the dilepton (DL) channel after the fit to data: BDT discriminant in the analysis category with (≥ 4 jets, 3 b tags) (upper row) and MEM discriminant in the analysis categories with (≥ 4 jets, ≥ 4 b tags) (lower row) with low (left) and high (right) BDT output. The hatched uncertainty bands include the total uncertainty after the fit to data. The distributions observed in data (markers) are overlayed. The first and the last bins include underflow and overflow events, respectively. The lower plots show the ratio of the data to the post-fit background plus signal distribution.

JHEP03(2019)026

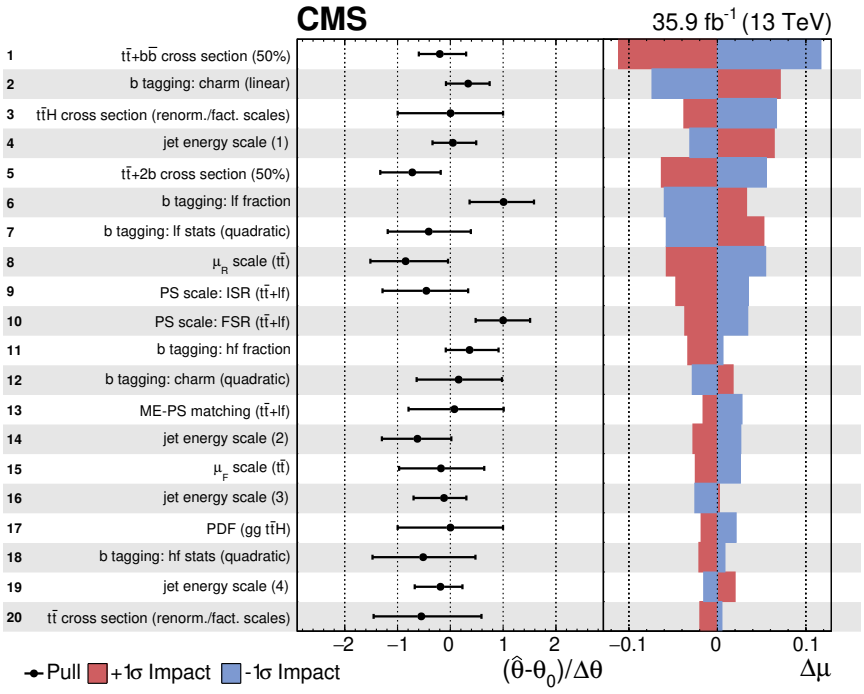

Figure 9. Post-fit pull and impact on the signal strength μ of the nuisance parameters included in the fit, ordered by their impact. Only the 20 highest ranked parameters are shown, not including nuisance parameters describing the uncertainty due to the size of the simulated samples. The four highest-ranked nuisance parameters related to the jet energy scale uncertainty sources are shown as indicated in parentheses. The pulls of the nuisance parameters (black markers) are computed relative to their pre-fit values θ_0 and uncertainties $\Delta\theta$. The impact $\Delta\mu$ is computed as the difference of the nominal best fit value of μ and the best fit value obtained when fixing the nuisance parameter under scrutiny to its best fit value $\hat{\theta}$ plus/minus its post-fit uncertainty (coloured areas).

Channel	95% CL upper limit		Best-fit μ
	observed	expected	$\pm$tot ($\pm$stat $\pm$ syst)
Single-lepton	1.75	$1.03^{+0.44}_{-0.29}$	$0.84^{+0.52}_{-0.50}$ $\left(^{+0.27}_{-0.26}\ ^{+0.44}_{-0.43}\right)$
Dilepton	2.34	$2.48^{+1.17}_{-0.76}$	$-0.24^{+1.21}_{-1.12}$ $\left(^{+0.63}_{-0.60}\ ^{+1.04}_{-0.95}\right)$
Combined	1.51	$0.92^{+0.39}_{-0.26}$	$0.72^{+0.45}_{-0.45}$ $\left(^{+0.24}_{-0.24}\ ^{+0.38}_{-0.38}\right)$

Table 7. Best fit value of the signal strength modifier μ and the observed and median expected 95% CL upper limits in the single-lepton and the dilepton channels as well as the combined results. The one standard deviation confidence intervals of the expected limit and the best fit value are also quoted, split into the statistical and systematic components in the latter case.

JHEP03(2019)026

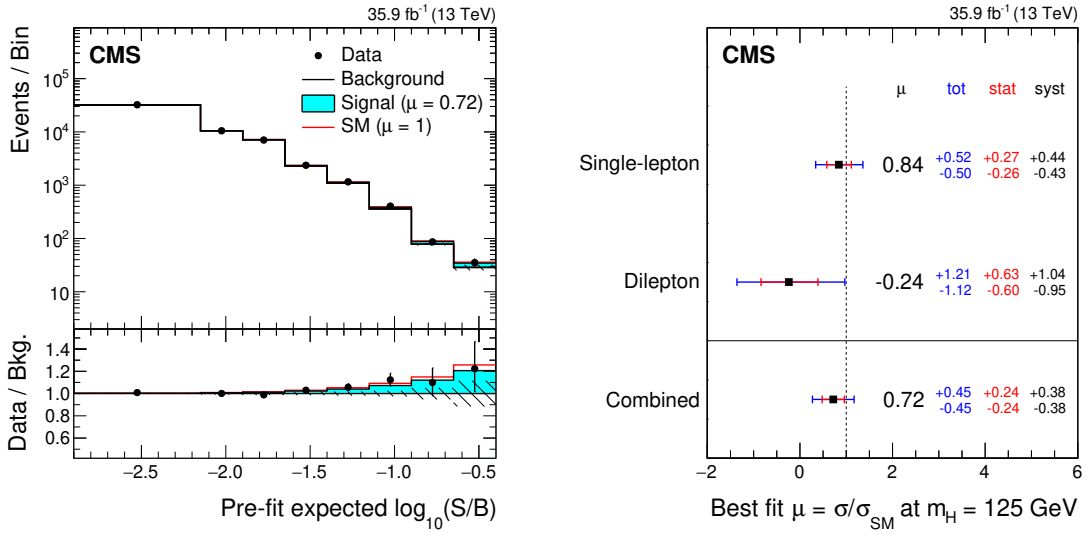

Figure 10. Bins of the final discriminants as used in the fit (left), reordered by the pre-fit expected signal-to-background ratio (S/B). Each of the shown bins includes multiple bins of the final discriminants with similar S/B. The fitted signal (cyan) is compared to the expectation for the SM Higgs boson $\mu = 1$ (red). Best fit values of the signal strength modifiers μ (right) with their 68% expected confidence intervals (outer error bar), also split into their statistical (inner error bar) and systematic components.

retical uncertainties amounting to $+0.28/-0.29$, where the $t\bar{t}$+hf modelling uncertainties have a major contribution. Experimental uncertainties amount to $+0.15/-0.16$, dominated by the b tagging related uncertainties. Systematic uncertainties due to the size of the various simulated samples used to model the background and signal templates are at the same order and amount to $+0.14/-0.15$.

An upper limit on μ under the background-only hypothesis is also determined, using a modified frequentist CL_S procedure [95, 96] with the asymptotic method [97]. When combining all categories and channels, an observed (expected) upper limit at 95% CL on μ of 1.5 (0.9) is obtained. The observed and expected upper limits in each channel and in the combination are listed in table 7 and visualised in figure 11.

In addition, the statistical analysis has been performed using the jet-process categorisation and DNN output in both channels and their combination, as well as using the jet-tag categorisation and the BDT or MEM in both channels. The results obtained in each channel and the combination are compatible within 1.7 standard deviations or better, evaluated using a jackknife procedure [98]. This serves as an important cross check and validation of the complex analysis methods.

8 Summary

A search for the associated production of a Higgs boson and a top quark-antiquark pair ($t\bar{t}H$) is performed using pp collision data recorded with the CMS detector at a centre-of-mass energy of 13 TeV in 2016, corresponding to an integrated luminosity of 35.9 fb^{-1}. Candidate events are selected in final states compatible with the Higgs boson decaying into

JHEP03(2019)026

Uncertainty source	$\pm\Delta\mu$ (observed)	$\pm\Delta\mu$ (expected)
Total experimental	+0.15/−0.16	+0.19/−0.17
b tagging	+0.11/−0.14	+0.12/−0.11
jet energy scale and resolution	+0.06/−0.07	+0.13/−0.11
Total theory	+0.28/−0.29	+0.32/−0.29
$t\bar{t}$+hf cross section and parton shower	+0.24/−0.28	+0.28/−0.28
Size of the simulated samples	+0.14/−0.15	+0.16/−0.16
Total systematic	+0.38/−0.38	+0.45/−0.42
Statistical	+0.24/−0.24	+0.27/−0.27
Total	+0.45/−0.45	+0.53/−0.49

Table 8. Contributions of different sources of uncertainties to the result for the fit to the data (observed) and to the expectation from simulation (expected). The quoted uncertainties $\Delta\mu$ in μ are obtained by fixing the listed sources of uncertainties to their post-fit values in the fit and subtracting the obtained result in quadrature from the result of the full fit. The statistical uncertainty is evaluated by fixing all nuisance parameters to their post-fit values. The quadratic sum of the contributions is different from the total uncertainty because of correlations between the nuisance parameters.

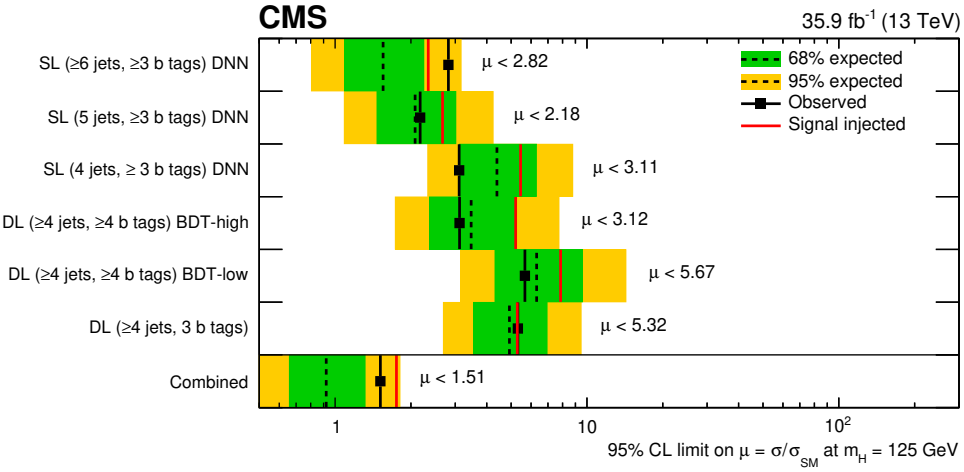

Figure 11. Median expected (dashed line) and observed (markers) 95% CL upper limits on μ. The inner (green) band and the outer (yellow) band indicate the regions containing 68 and 95%, respectively, of the distribution of limits expected under the background-only hypothesis. Also shown is the limit that is expected in case a SM $t\bar{t}H$ signal ($\mu = 1$) is present in the data (solid red line).

JHEP03(2019)026

a b quark-antiquark pair and the single-lepton and dilepton decay channels of the $t\bar{t}$ system. Selected events are split into mutually exclusive categories according to their $t\bar{t}$ decay channel and jet content. In each category a powerful discriminant is constructed to separate the $t\bar{t}H$ signal from the dominant $t\bar{t}$+jets background, based on several multivariate analysis techniques (boosted decision trees, matrix element method, and deep neural networks). An observed (expected) upper limit on the $t\bar{t}H$ production cross section μ relative to the SM expectations of 1.5 (0.9) at 95% confidence level is obtained. The best fit value of μ is $0.72 \pm 0.24\,(\text{stat}) \pm 0.38\,(\text{syst})$. These results correspond to an observed (expected) significance of 1.6 (2.2) standard deviations above the background-only hypothesis.

Acknowledgments

We congratulate our colleagues in the CERN accelerator departments for the excellent performance of the LHC and thank the technical and administrative staffs at CERN and at other CMS institutes for their contributions to the success of the CMS effort. In addition, we gratefully acknowledge the computing centres and personnel of the Worldwide LHC Computing Grid for delivering so effectively the computing infrastructure essential to our analyses. Finally, we acknowledge the enduring support for the construction and operation of the LHC and the CMS detector provided by the following funding agencies: the Austrian Federal Ministry of Science, Research and Economy and the Austrian Science Fund; the Belgian Fonds de la Recherche Scientifique, and Fonds voor Wetenschappelijk Onderzoek; the Brazilian Funding Agencies (CNPq, CAPES, FAPERJ, and FAPESP); the Bulgarian Ministry of Education and Science; CERN; the Chinese Academy of Sciences, Ministry of Science and Technology, and National Natural Science Foundation of China; the Colombian Funding Agency (COLCIENCIAS); the Croatian Ministry of Science, Education and Sport, and the Croatian Science Foundation; the Research Promotion Foundation, Cyprus; the Secretariat for Higher Education, Science, Technology and Innovation, Ecuador; the Ministry of Education and Research, Estonian Research Council via IUT23-4 and IUT23-6 and European Regional Development Fund, Estonia; the Academy of Finland, Finnish Ministry of Education and Culture, and Helsinki Institute of Physics; the Institut National de Physique Nucléaire et de Physique des Particules / CNRS, and Commissariat à l'Énergie Atomique et aux Énergies Alternatives / CEA, France; the Bundesministerium für Bildung und Forschung, Deutsche Forschungsgemeinschaft, and Helmholtz-Gemeinschaft Deutscher Forschungszentren, Germany; the General Secretariat for Research and Technology, Greece; the National Research, Development and Innovation Fund, Hungary; the Department of Atomic Energy and the Department of Science and Technology, India; the Institute for Studies in Theoretical Physics and Mathematics, Iran; the Science Foundation, Ireland; the Istituto Nazionale di Fisica Nucleare, Italy; the Ministry of Science, ICT and Future Planning, and National Research Foundation (NRF), Republic of Korea; the Lithuanian Academy of Sciences; the Ministry of Education, and University of Malaya (Malaysia); the Mexican Funding Agencies (BUAP, CINVESTAV, CONACYT, LNS, SEP, and UASLP-FAI); the Ministry of Business, Innovation and Employment, New Zealand; the Pakistan Atomic Energy Commission; the Ministry of Science and Higher Education

JHEP03(2019)026

and the National Science Centre, Poland; the Fundação para a Ciência e a Tecnologia, Portugal; JINR, Dubna; the Ministry of Education and Science of the Russian Federation, the Federal Agency of Atomic Energy of the Russian Federation, Russian Academy of Sciences and the Russian Foundation for Basic Research; the Ministry of Education, Science and Technological Development of Serbia; the Secretaría de Estado de Investigación, Desarrollo e Innovación, Programa Consolider-Ingenio 2010, Plan Estatal de Investigación Científica y Técnica y de Innovación 2013-2016, Plan de Ciencia, Tecnología e Innovación 2013-2017 del Principado de Asturias and Fondo Europeo de Desarrollo Regional, Spain; the Swiss Funding Agencies (ETH Board, ETH Zurich, PSI, SNF, UniZH, Canton Zurich, and SER); the Ministry of Science and Technology, Taipei; the Thailand Center of Excellence in Physics, the Institute for the Promotion of Teaching Science and Technology of Thailand, Special Task Force for Activating Research and the National Science and Technology Development Agency of Thailand; the Scientific and Technical Research Council of Turkey, and Turkish Atomic Energy Authority; the National Academy of Sciences of Ukraine, and State Fund for Fundamental Researches, Ukraine; the Science and Technology Facilities Council, U.K.; the US Department of Energy, and the US National Science Foundation.

Individuals have received support from the Marie-Curie programme and the European Research Council and Horizon 2020 Grant, contract No. 675440 (European Union); the Leventis Foundation; the A. P. Sloan Foundation; the Alexander von Humboldt Foundation; the Belgian Federal Science Policy Office; the Fonds pour la Formation à la Recherche dans l'Industrie et dans l'Agriculture (FRIA-Belgium); the Agentschap voor Innovatie door Wetenschap en Technologie (IWT-Belgium); the F.R.S.-FNRS and FWO (Belgium) under the "Excellence of Science — EOS" — be.h project n. 30820817; the Ministry of Education, Youth and Sports (MEYS) of the Czech Republic; the Lendület ("Momentum") Programme and the János Bolyai Research Scholarship of the Hungarian Academy of Sciences, the New National Excellence Program ÚNKP, the NKFIA research grants 123842, 123959, 124845, 124850 and 125105 (Hungary); the Council of Scientific and Industrial Research, India; the HOMING PLUS programme of the Foundation for Polish Science, cofinanced from European Union, Regional Development Fund, the Mobility Plus programme of the Ministry of Science and Higher Education, the National Science Center (Poland), contracts Harmonia 2014/14/M/ST2/00428, Opus 2014/13/B/ST2/02543, 2014/15/B/ST2/03998, and 2015/19/B/ST2/02861, Sonata-bis 2012/07/E/ST2/01406; the National Priorities Research Program by Qatar National Research Fund; the Programa de Excelencia María de Maeztu and the Programa Severo Ochoa del Principado de Asturias; the Thalis and Aristeia programmes cofinanced by EU-ESF and the Greek NSRF; the Rachadapisek Sompot Fund for Postdoctoral Fellowship, Chulalongkorn University and the Chulalongkorn Academic into Its 2nd Century Project Advancement Project (Thailand); the Welch Foundation, contract C-1845; and the Weston Havens Foundation (U.S.A.).

A BDT and DNN input variables and configuration

All input variables used in the DNNs and BDTs are listed in tables 9–11.

JHEP03(2019)026

Variable	Definition	SL (4 jets, ≥ 3 b tags)	SL (5 jets, ≥ 3 b tags)	SL (≥ 6 jets, ≥ 3 b tags)	DL (≥ 4 jets, 3 b tags)	DL (≥ 4 jets, ≥ 4 b tags)
p_{T}(jet 1)	p_{T} of the highest-p_{T} jet	+	+	-	-	-
η(jet 1)	η of the highest-p_{T} jet	-	+	+	-	-
d(jet 1)	b tagging discriminant of the highest-p_{T} jet	+	+	+	-	-
p_{T}(jet 2)	p_{T} of the second highest-p_{T} jet	-	+	-	-	-
η(jet 2)	η of the second highest-p_{T} jet	+	+	+	-	-
d(jet 2)	b tagging discriminant of the second highest-p_{T} jet	+	+	+	-	-
p_{T}(jet 3)	p_{T} of the third highest-p_{T} jet	-	+	-	-	-
η(jet 3)	η of the third highest-p_{T} jet	+	+	+	-	-
d(jet 3)	b tagging discriminant of the third highest-p_{T} jet	+	+	+	-	-
p_{T}(jet 4)	p_{T} of the fourth highest-p_{T} jet	+	+	-	-	-
η(jet 4)	η of the fourth highest-p_{T} jet	+	+	+	-	-
d(jet 4)	b tagging discriminant of the fourth highest-p_{T} jet	+	-	+	-	-
p_{T}(lep 1)	p_{T} of the highest-p_{T} lepton	-	+	+	-	-
η(lep 1)	η of the highest-p_{T} lepton	+	-	+	-	-
$d_{\mathrm{j}}^{\mathrm{avg}}$	average b tagging discriminant value of all jets	+	+	+	-	-
$d_{\mathrm{b}}^{\mathrm{avg}}$	average b tagging discriminant value of b-tagged jets	+	+	+	+	+
$d_{\text{non-b}}^{\mathrm{avg}}$	average b tagging discriminant value of non-b-tagged jets	-	-	-	+	+
$\frac{1}{N_{\mathrm{b}}}\sum_{b}^{N_{\mathrm{b}}}\left(d-d_{\mathrm{b}}^{\mathrm{avg}}\right)^2$	squared difference between the b tagging discriminant value of a b-tagged jet and the average b tagging discriminant values of all b-tagged jets, summed over all b-tagged jets	+	+	+	-	-
$d_{\mathrm{j}}^{\mathrm{max}}$	maximal b tagging discriminant value of all jets	+	+	+	-	-
$d_{\mathrm{b}}^{\mathrm{max}}$	maximal b tagging discriminant value of b-tagged jets	+	+	+	-	-
$d_{\mathrm{j}}^{\mathrm{min}}$	minimal b tagging discriminant value of all jets	+	+	+	-	-
$d_{\mathrm{j}}^{\mathrm{min}}$	minimal b tagging discriminant value of b-tagged jets	+	+	+	-	-
d_2	second highest b tagging discriminant value of all jets	+	+	+	-	-

Table 9. Input variables used in the DNNs or BDTs in the different categories of the single-lepton and dilepton channels. Variables used in a specific multivariate method and analysis category are denoted by a "+" and unused variables by a "−". (Continued in tables 10 and 11.)

JHEP03(2019)026

Variable	Definition	SL ($4\,\text{jets}, \geq 3\,\text{b tags}$)	SL ($5\,\text{jets}, \geq 3\,\text{b tags}$)	SL ($\geq 6\,\text{jets}, \geq 3\,\text{b tags}$)	DL ($\geq 4\,\text{jets}, 3\,\text{b tags}$)	DL ($\geq 4\,\text{jets}, \geq 4\,\text{b tags}$)
$N_{\text{b}}(\text{tight})$	number of b-tagged jets at a working point with a 0.1% probability of tagging gluon and light-flavour jets	+	+	+	-	-
BLR	likelihood ratio discriminating between 4 b quark jets and 2 b quark jets events	+	+	+	-	-
$\text{BLR}^{\text{trans}}$	transformed BLR defined as $\ln[\text{BLR}/(1.0-\text{BLR})]$	+	+	+	-	-
$\Delta R_{\text{j,j}}^{\text{min}}$	ΔR between the two closest jets	+	+	+	-	-
$\Delta R_{\text{b,b}}^{\text{min}}$	ΔR between the two closest b-tagged jets	+	+	+	-	-
$\Delta R_{\text{j,j}}^{\text{max}}$	ΔR between the two jets furthest apart	-	+	-	-	-
$\Delta R_{\text{b,b}}^{\text{max}}$	ΔR between the two b-tagged jets furthest apart	-	-	+	-	-
$\Delta\eta_{\text{j,j}}^{\text{max}}$	$\Delta\eta$ between the two jets furthest apart in η	-	-	-	-	+
$\Delta\eta_{\text{b,b}}^{\text{max}}$	$\Delta\eta$ between the two b-tagged jets furthest apart in η	-	-	-	+	+
$\Delta\eta_{\text{b,b}}^{\text{avg}}$	average $\Delta\eta$ between b-tagged jets	-	-	+	-	-
$\Delta R_{\text{b,b}}^{\text{avg}}$	average ΔR between b-tagged jets	-	+	+	-	-
$\Delta R_{\text{j,b}}^{\text{avg}}$	average ΔR between jets of which at least one is b-tagged	-	-	-	+	-
$\Delta R_{\text{lep,j}}^{\text{min}\Delta R}$	ΔR between lepton and closest jet	+	+	-	-	-
$\Delta R_{\text{lep,b}}^{\text{min}\Delta R}$	ΔR between lepton and closest b-tagged jet	-	+	+	-	-
$m_{\text{lep,b}}^{\text{min}\Delta R}$	mass of lepton and closest b-tagged jet	+	+	+	-	-
$m_{\text{b,b}}^{\text{min}\Delta R}$	mass of closest b-tagged jets	+	+	+	-	+
$m_{\text{j,b}}^{\text{min}\Delta R}$	mass of closest jets of which at least one is b-tagged	-	-	-	+	-
$m_{\text{b,b}}^{\text{max mass}}$	maximal mass of pairs of b-tagged jets	-	-	-	+	+
$p_{\text{T}\,\text{b,b}}^{\text{min}\Delta R}$	combined p_{T} of closest b-tagged jets	-	-	-	+	-
$p_{\text{T}\,\text{j,b}}^{\text{min}\Delta R}$	combined p_{T} of closest jets of which at least one is b-tagged	-	-	-	-	+
$m_{\text{j}}^{\text{avg}}$	average mass of all jets	+	+	+	-	-
$(m^2)_{\text{b}}^{\text{avg}}$	average squared mass of all b-tagged jets	+	-	+	-	-
$m_{\text{b,b}}^{\text{closest to 125}}$	mass of pair of b-tagged jets closest to 125 GeV	-	+	+	-	-
$N^{\text{j,b}}$	number of pairs of jets (with at least one b-tagged jet) with an invariant mass within 110–140 GeV	-	-	-	+	+
MEM	matrix element method discriminant	+	+	+	-	-

Table 10. Continued from table 9 and continued in table 11.

JHEP03(2019)026

Variable	Definition	SL (4 jets, ≥ 3 b tags)	SL (5 jets, ≥ 3 b tags)	SL (≥ 6 jets, ≥ 3 b tags)	DL (≥ 4 jets, 3 b tags)	DL (≥ 4 jets, ≥ 4 b tags)
$H_{\mathrm{T}}^{\mathrm{j}}$	scalar sum of jet p_{T}	-	+	-	+	-
$H_{\mathrm{T}}^{\mathrm{b}}$	scalar sum of b-tagged jet p_{T}	+	+	+	-	-
A^{j}	$\frac{3}{2}\lambda_3$ where λ_i are the eigenvalues of the momentum tensor built with jets [99]	-	+	+	-	-
A^{b}	$\frac{3}{2}\lambda_3$ where λ_i are the eigenvalues of the momentum tensor built with b-tagged jets [99]	+	+	+	-	-
C^{j}	$H_{\mathrm{T}}^{\mathrm{j}}$ divided by the sum of the energies of all jets	-	-	+	-	-
C^{b}	$H_{\mathrm{T}}^{\mathrm{b}}$ divided by the sum of the energies of all b-tagged jets	-	-	+	-	+
S^{j}	$\frac{3}{2}(\lambda_2+\lambda_3)$ where λ_i are the eigenvalues of the momentum tensor built with jets [99]	+	+	+	-	-
S^{b}	$\frac{3}{2}(\lambda_2+\lambda_3)$ where λ_i are the eigenvalues of the momentum tensor built with b-tagged jets [99]	-	+	+	-	-
$S_{\mathrm{T}}^{\mathrm{j}}$	$\frac{2\lambda_2}{\lambda_2+\lambda_1}$ where λ_i are the eigenvalues of the momentum tensor built with jets [99]	+	+	+	-	-
$S_{\mathrm{T}}^{\mathrm{b}}$	$\frac{2\lambda_2}{\lambda_2+\lambda_1}$ where λ_i are the eigenvalues of the momentum tensor built with b-tagged jets [99]	+	+	+	-	-
I^{b}	a measure of how spherical or linear in $r-\phi$ space b-tagged jets are in the event	-	-	-	+	-
H_2	second Fox-Wolfram moment [100]	-	+	-	-	-
H_3	third Fox-Wolfram moment [100]	+	+	-	-	-
H_3^{b}	third Fox-Wolfram moment calculated with b-tagged jets [100]	-	-	-	-	+
R_3	ratio of Fox-Wolfram moments H_3/H_0 [100]	-	-	-	+	-
H_4	fourth Fox-Wolfram moment [100]	+	-	+	-	-

Table 11. Continued from table 10.

JHEP03(2019)026

Category	N_{trees}	shrinkage	bagging fraction	N_{cuts}	depth
(≥ 4 jets, 3 b tags)	955	0.022	0.42	30	2
(≥ 4 jets, ≥ 4 b tags)	638	0.006	0.41	42	2

Table 12. Configuration of the BDTs used in the dilepton channel.

The BDTs employed in the dilepton channel were trained using the stochastic gradient boost method [36, 78], available as part of the TMVA package [38]. The number of trees (N_{trees}), the learning rate (shrinkage), the fraction of events used for the training of an individual tree (bagging fraction), the granularity of the cuts at each node splitting (N_{cuts}), and the number of node splittings per tree (depth) are listed in table 12.

The DNNs used in the single-lepton channel comprise two layers with 100 nodes each in each of the two network stages. Overtraining is suppressed by random node dropout with a probability of 30% and an L2 weight normalisation factor of 10^{-5}. All networks are optimised using the ADAM optimiser with a learning rate of 10^{-4}, and the ELU activation function is used to add non-linearity to the response of the network [77].

B Pre-fit discriminant shapes (single-lepton channel)

JHEP03(2019)026

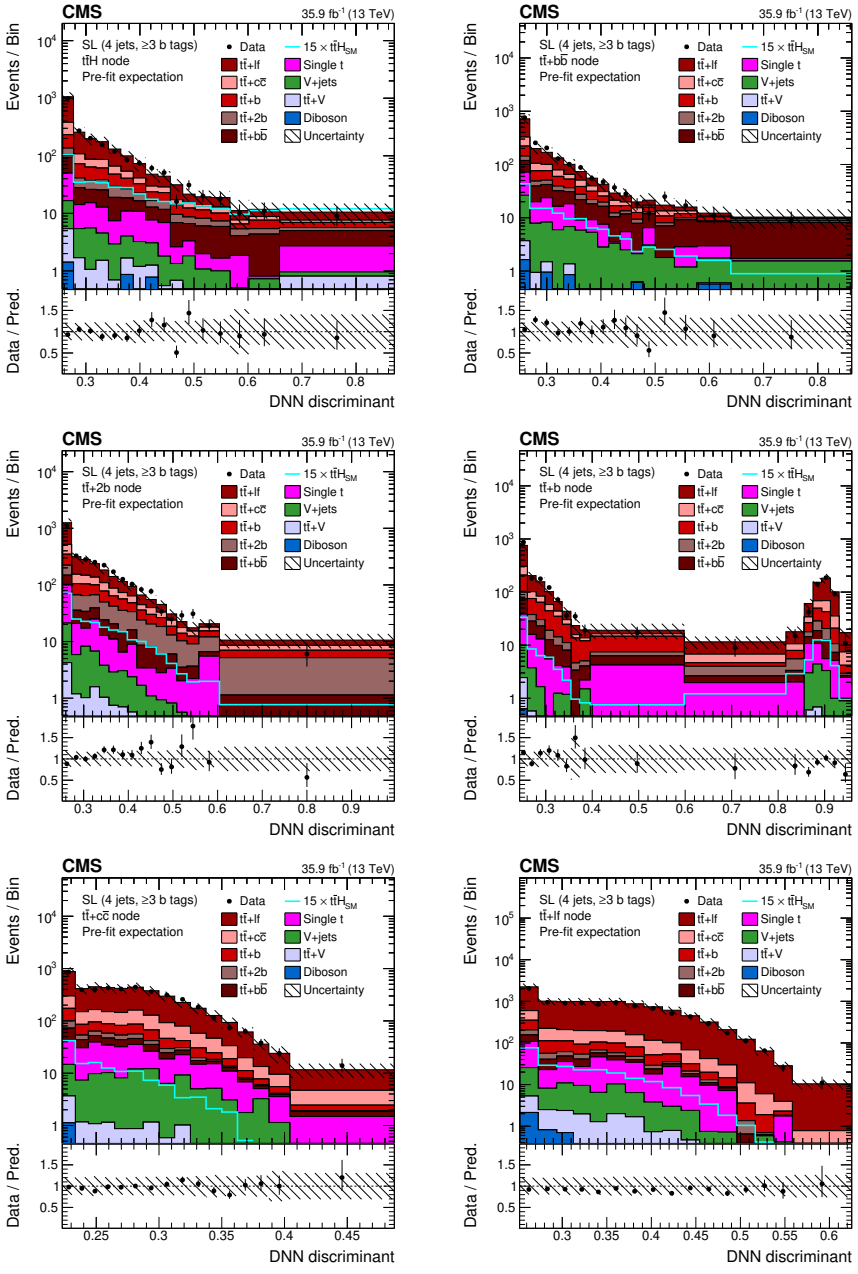

Figure 12. Final discriminant (DNN) shapes in the single-lepton (SL) channel before the fit to data, in the jet-process categories with (4 jets, ≥ 3 b tags) and (from upper left to lower right) $\mathrm{t\bar{t}H}$, $\mathrm{t\bar{t}+b\bar{b}}$, $\mathrm{t\bar{t}+2b}$, $\mathrm{t\bar{t}+b}$, $\mathrm{t\bar{t}+c\bar{c}}$, and $\mathrm{t\bar{t}+lf}$. The expected background contributions (filled histograms) are stacked, and the expected signal distribution (line), which includes $\mathrm{H} \to \mathrm{b\bar{b}}$ and all other Higgs boson decay modes, is superimposed. Each contribution is normalised to an integrated luminosity of 35.9 fb^{-1}, and the signal distribution is additionally scaled by a factor of 15 for better visibility. The hatched uncertainty bands include the total uncertainty of the fit model. The first and the last bins include underflow and overflow events, respectively. The lower plots show the ratio of the data to the background prediction.

JHEP03(2019)026

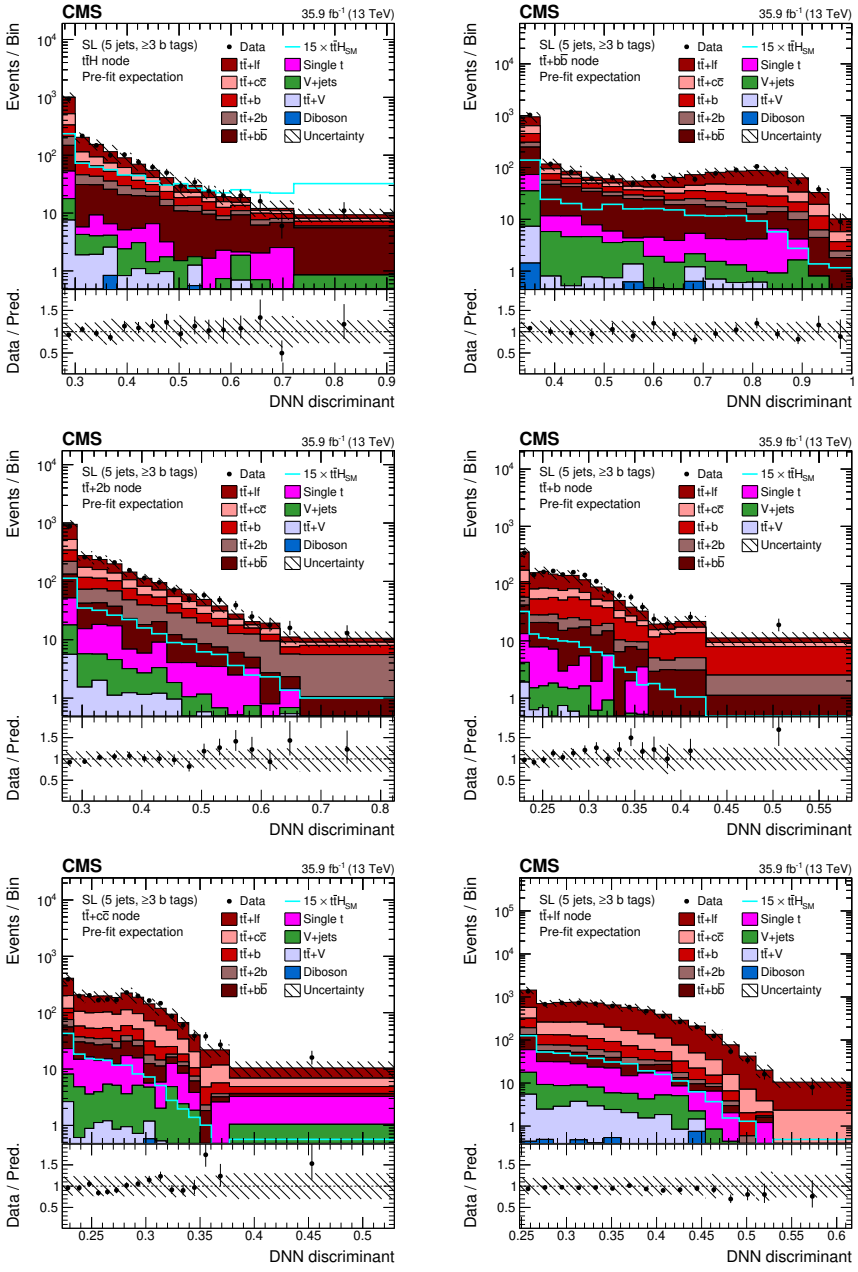

Figure 13. Final discriminant (DNN) shapes in the single-lepton (SL) channel before the fit to data, in the jet-process categories with ($5\,\text{jets}, \geq 3\,\text{b}$ tags) and (from upper left to lower right) $\mathrm{t\bar{t}H}$, $\mathrm{t\bar{t}+b\bar{b}}$, $\mathrm{t\bar{t}+2b}$, $\mathrm{t\bar{t}+b}$, $\mathrm{t\bar{t}+c\bar{c}}$, and $\mathrm{t\bar{t}+lf}$. The expected background contributions (filled histograms) are stacked, and the expected signal distribution (line), which includes $\mathrm{H} \to \mathrm{b\bar{b}}$ and all other Higgs boson decay modes, is superimposed. Each contribution is normalised to an integrated luminosity of $35.9\,\text{fb}^{-1}$, and the signal distribution is additionally scaled by a factor of 15 for better visibility. The hatched uncertainty bands include the total uncertainty of the fit model. The first and the last bins include underflow and overflow events, respectively. The lower plots show the ratio of the data to the background prediction.

JHEP03(2019)026

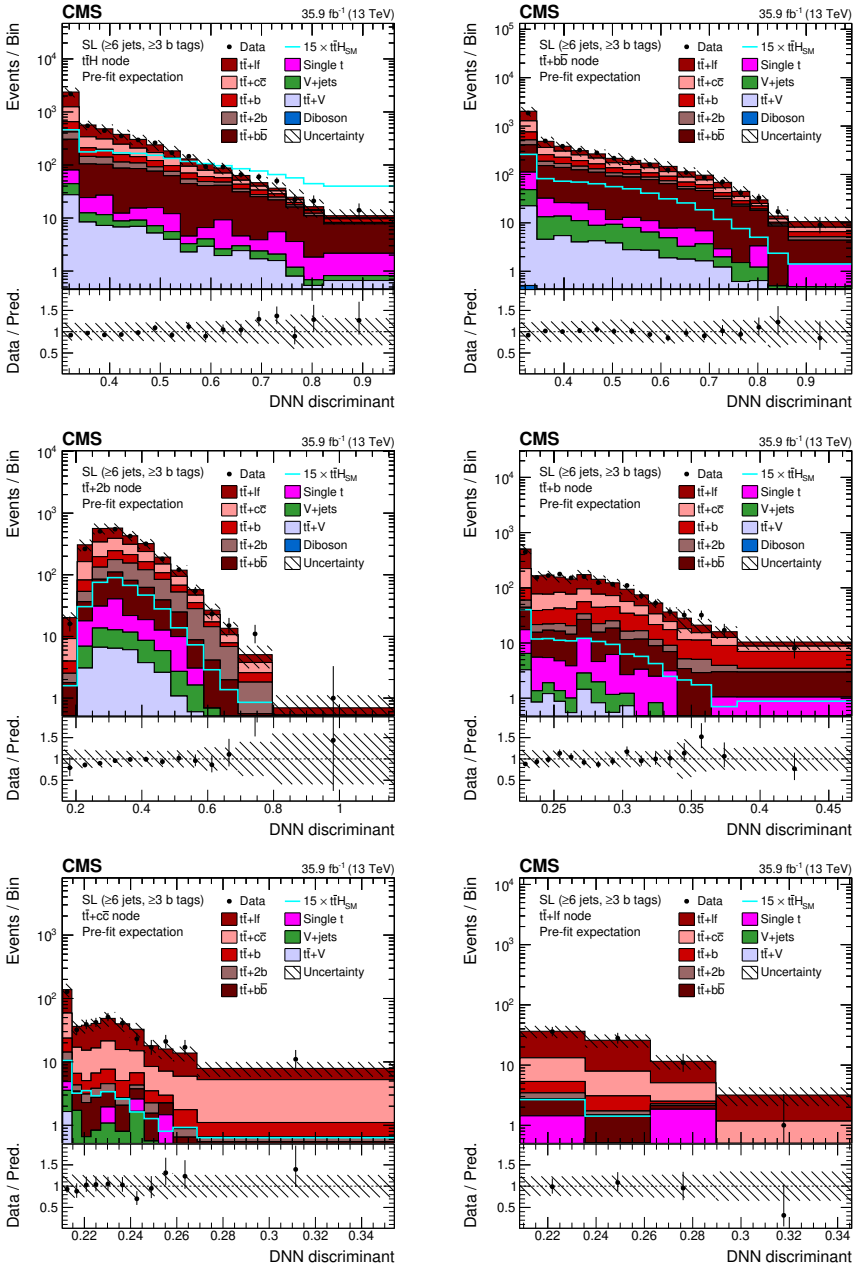

Figure 14. Final discriminant (DNN) shapes in the single-lepton (SL) channel before the fit to data, in the jet-process categories with (≥ 6 jets, ≥ 3 b tags) and (from upper left to lower right) $\mathrm{t\bar{t}H}$, $\mathrm{t\bar{t}+b\bar{b}}$, $\mathrm{t\bar{t}+2b}$, $\mathrm{t\bar{t}+b}$, $\mathrm{t\bar{t}+c\bar{c}}$, and $\mathrm{t\bar{t}+lf}$. The expected background contributions (filled histograms) are stacked, and the expected signal distribution (line), which includes $\mathrm{H \to b\bar{b}}$ and all other Higgs boson decay modes, is superimposed. Each contribution is normalised to an integrated luminosity of $35.9\,\mathrm{fb}^{-1}$, and the signal distribution is additionally scaled by a factor of 15 for better visibility. The hatched uncertainty bands include the total uncertainty of the fit model. The first and the last bins include underflow and overflow events, respectively. The lower plots show the ratio of the data to the background prediction.

JHEP03(2019)026

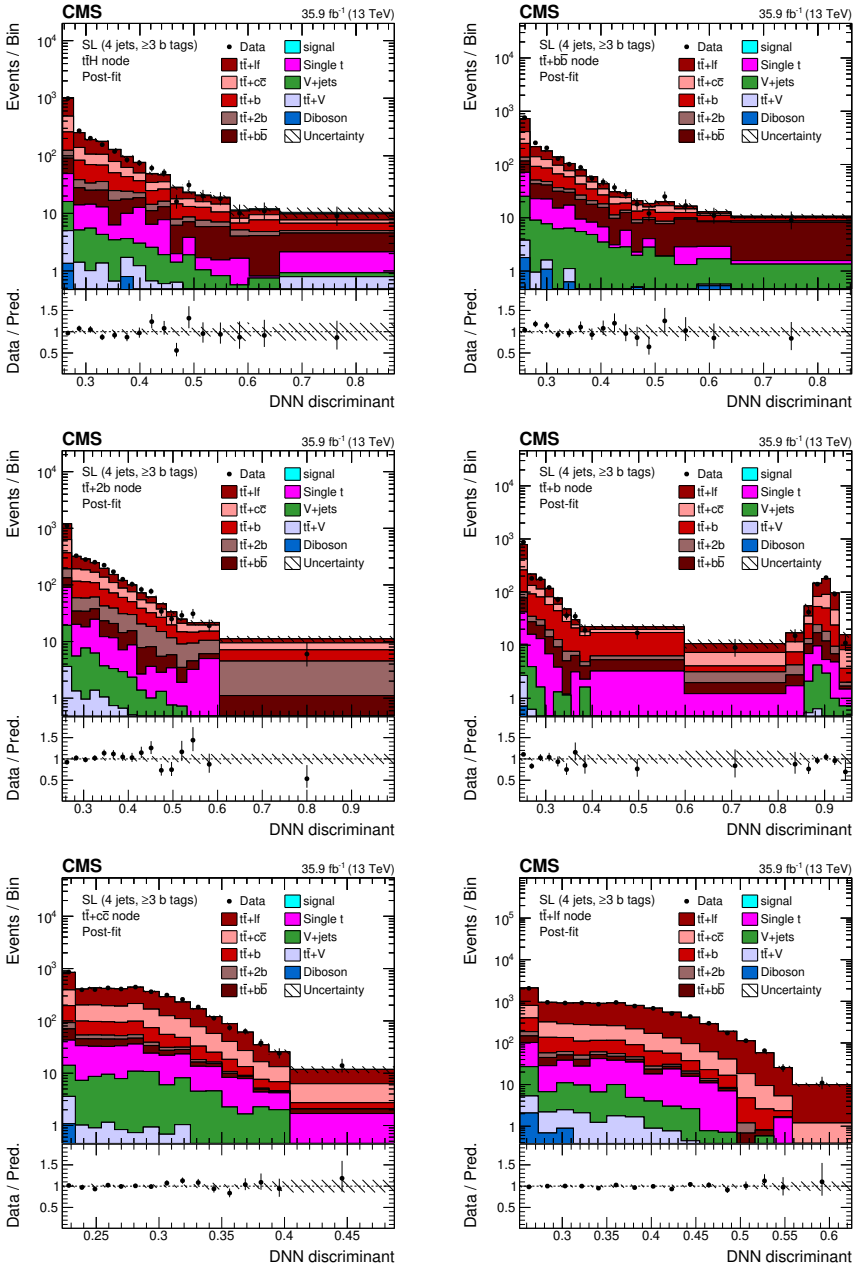

Figure 15. Final discriminant (DNN) shapes in the single-lepton (SL) channel after the fit to data, in the jet-process categories with (4 jets, ≥ 3 b tags) and (from upper left to lower right) $\mathrm{t\bar{t}H}$, $\mathrm{t\bar{t}+b\bar{b}}$, $\mathrm{t\bar{t}+2b}$, $\mathrm{t\bar{t}+b}$, $\mathrm{t\bar{t}+c\bar{c}}$, and $\mathrm{t\bar{t}+lf}$. The error bands include the total uncertainty after the fit to data. The first and the last bins include underflow and overflow events, respectively. The lower plots show the ratio of the data to the post-fit background plus signal distribution.

C Post-fit discriminant shapes (single-lepton channel)

JHEP03(2019)026

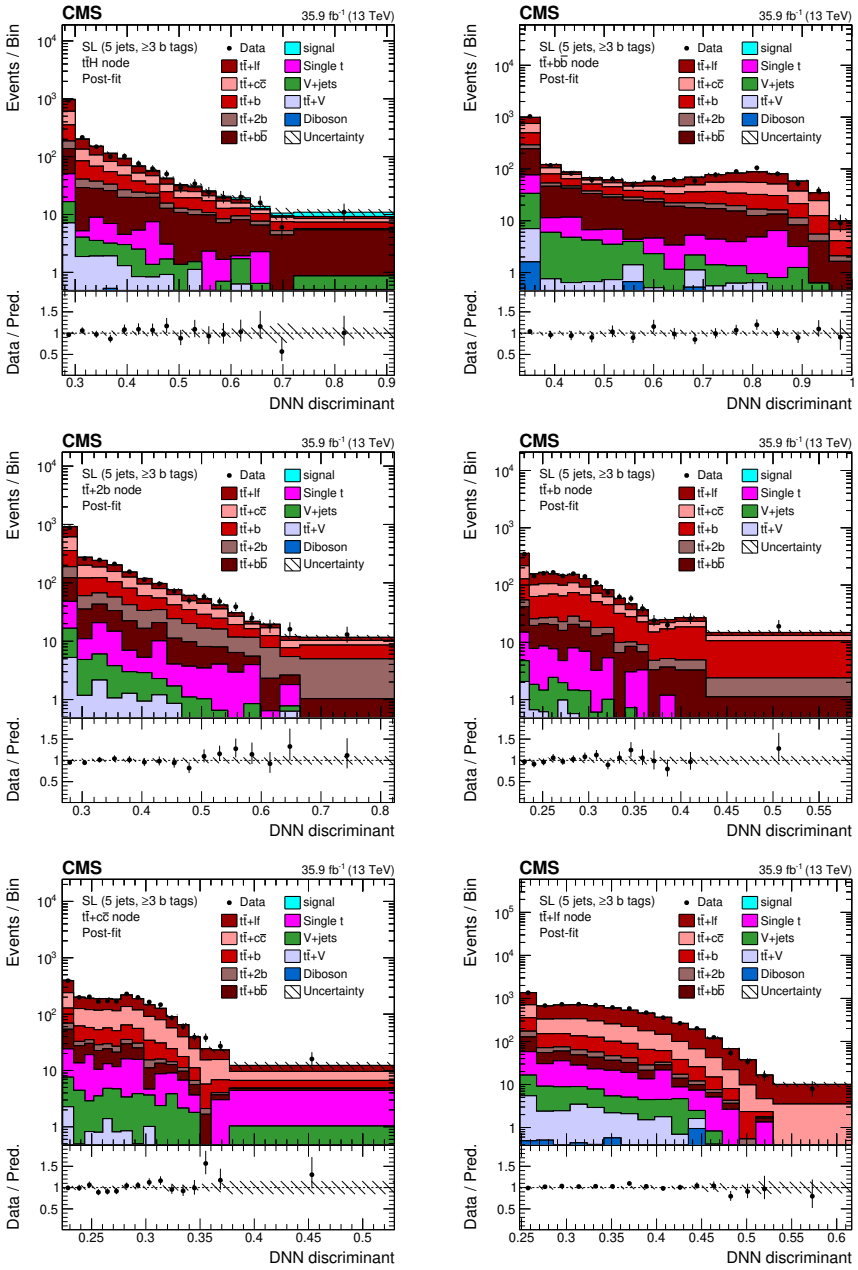

Figure 16. Final discriminant (DNN) shapes in the single-lepton (SL) channel after the fit to data, in the jet-process categories with (5 jets, $\geq$ 3 b tags) and (from upper left to lower right) $t\bar{t}H$, $t\bar{t}+b\bar{b}$, $t\bar{t}+2b$, $t\bar{t}+b$, $t\bar{t}+c\bar{c}$, and $t\bar{t}+lf$. The error bands include the total uncertainty after the fit to data. The first and the last bins include underflow and overflow events, respectively. The lower plots show the ratio of the data to the post-fit background plus signal distribution.

JHEP03(2019)026

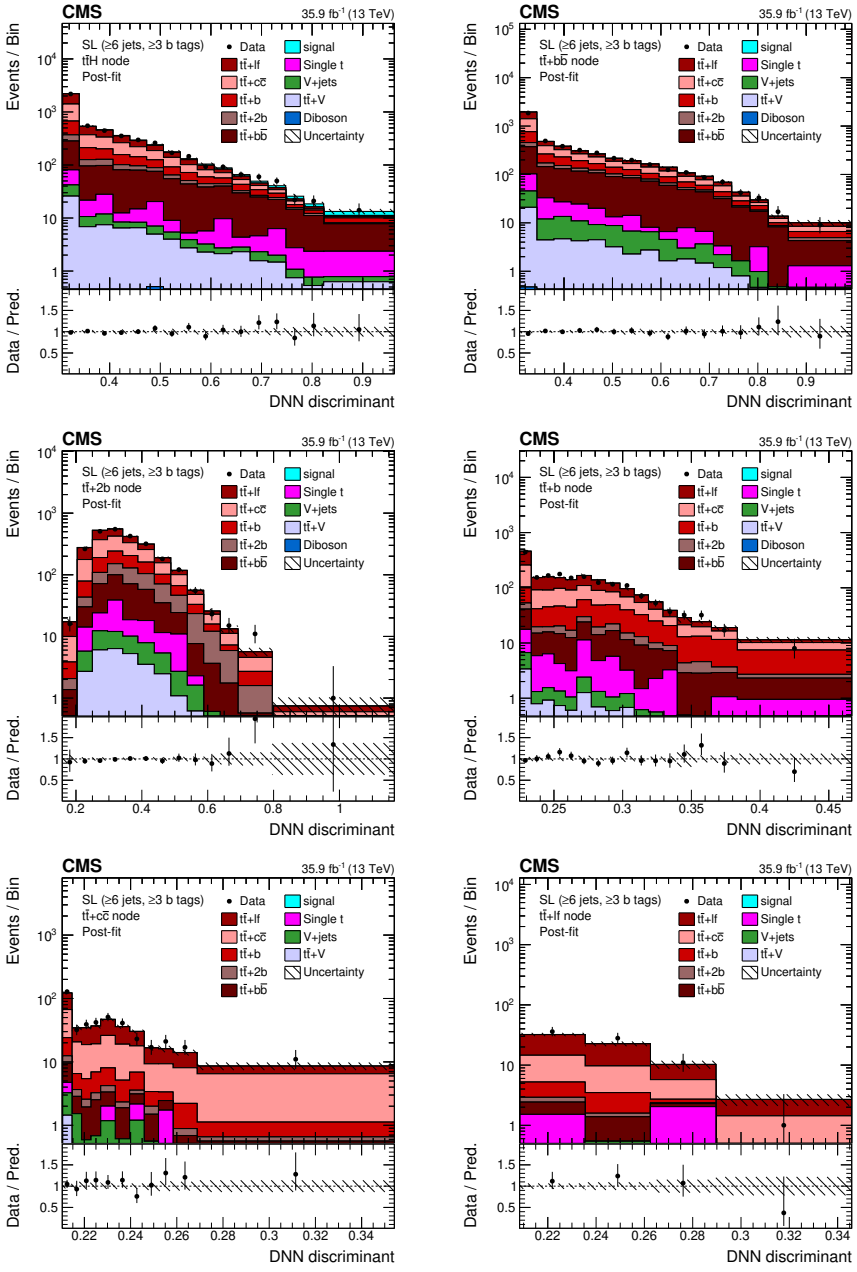

Figure 17. Final discriminant (DNN) shapes in the single-lepton (SL) channel after the fit to data, in the jet-process categories with (≥ 6 jets, ≥ 3 b tags) and (from upper left to lower right) $t\bar{t}H$, $t\bar{t}+b\bar{b}$, $t\bar{t}+2b$, $t\bar{t}+b$, $t\bar{t}+c\bar{c}$, and $t\bar{t}+lf$. The error bands include the total uncertainty after the fit to data. The first and the last bins include underflow and overflow events, respectively. The lower plots show the ratio of the data to the post-fit background plus signal distribution.

JHEP03(2019)026

References

[1] ATLAS collaboration, *Observation of a new particle in the search for the Standard Model Higgs boson with the ATLAS detector at the LHC*, *Phys. Lett.* **B 716** (2012) 1 [arXiv:1207.7214] [INSPIRE].

[2] CMS collaboration, *Observation of a new boson at a mass of* 125 *GeV with the CMS experiment at the LHC*, *Phys. Lett.* **B 716** (2012) 30 [arXiv:1207.7235] [INSPIRE].

[3] CMS collaboration, *A new boson with a mass of* 125 *GeV observed with the CMS experiment at the Large Hadron Collider*, *Science* **338** (2012) 1569 [INSPIRE].

[4] ATLAS and CMS collaborations, *Combined measurement of the Higgs boson mass in pp collisions at* $\sqrt{s} = 7$ *and* 8 *TeV with the ATLAS and CMS experiments*, *Phys. Rev. Lett.* **114** (2015) 191803 [arXiv:1503.07589] [INSPIRE].

[5] CMS collaboration, *Measurements of properties of the Higgs boson decaying into the four-lepton final state in pp collisions at* $\sqrt{s} = 13$ *TeV*, *JHEP* **11** (2017) 047 [arXiv:1706.09936] [INSPIRE].

[6] CMS collaboration, *Evidence for the direct decay of the* 125 *GeV Higgs boson to fermions*, *Nature Phys.* **10** (2014) 557 [arXiv:1401.6527] [INSPIRE].

[7] ATLAS collaboration, *Evidence for the Higgs-boson Yukawa coupling to tau leptons with the ATLAS detector*, *JHEP* **04** (2015) 117 [arXiv:1501.04943] [INSPIRE].

[8] CMS collaboration, *Observation of the Higgs boson decay to a pair of* τ *leptons with the CMS detector*, *Phys. Lett.* **B 779** (2018) 283 [arXiv:1708.00373] [INSPIRE].

[9] ATLAS collaboration, *Evidence for the* $H \to b\bar{b}$ *decay with the ATLAS detector*, *JHEP* **12** (2017) 024 [arXiv:1708.03299] [INSPIRE].

[10] CMS collaboration, *Evidence for the Higgs boson decay to a bottom quark-antiquark pair*, *Phys. Lett.* **B 780** (2018) 501 [arXiv:1709.07497] [INSPIRE].

[11] ATLAS collaboration, *Measurements of Higgs boson production and couplings in diboson final states with the ATLAS detector at the LHC*, *Phys. Lett.* **B 726** (2013) 88 [*Erratum ibid.* **B 734** (2014) 406] [arXiv:1307.1427] [INSPIRE].

[12] CMS collaboration, *Precise determination of the mass of the Higgs boson and tests of compatibility of its couplings with the Standard Model predictions using proton collisions at* 7 *and* 8 *TeV*, *Eur. Phys. J.* **C 75** (2015) 212 [arXiv:1412.8662] [INSPIRE].

[13] ATLAS collaboration, *Evidence for the spin-*0 *nature of the Higgs boson using ATLAS data*, *Phys. Lett.* **B 726** (2013) 120 [arXiv:1307.1432] [INSPIRE].

[14] CMS collaboration, *Constraints on the spin-parity and anomalous HVV couplings of the Higgs boson in proton collisions at* 7 *and* 8 *TeV*, *Phys. Rev.* **D 92** (2015) 012004 [arXiv:1411.3441] [INSPIRE].

[15] CMS collaboration, *Search for Standard Model production of four top quarks with same-sign and multilepton final states in proton-proton collisions at* $\sqrt{s} = 13$ *TeV*, *Eur. Phys. J.* **C 78** (2018) 140 [arXiv:1710.10614] [INSPIRE].

[16] LHC Higgs Cross Section Working Group collaboration, *Handbook of LHC Higgs cross sections:* 4. *Deciphering the nature of the Higgs sector*, arXiv:1610.07922 [INSPIRE].

JHEP03(2019)026

[17] G. Burdman, M. Perelstein and A. Pierce, *Large Hadron Collider tests of a little Higgs model*, *Phys. Rev. Lett.* **90** (2003) 241802 [*Erratum ibid.* **92** (2004) 049903] [hep-ph/0212228] [INSPIRE].

[18] T. Han, H.E. Logan, B. McElrath and L.-T. Wang, *Phenomenology of the little Higgs model*, *Phys. Rev.* **D 67** (2003) 095004 [hep-ph/0301040] [INSPIRE].

[19] M. Perelstein, M.E. Peskin and A. Pierce, *Top quarks and electroweak symmetry breaking in little Higgs models*, *Phys. Rev.* **D 69** (2004) 075002 [hep-ph/0310039] [INSPIRE].

[20] H.-C. Cheng, I. Low and L.-T. Wang, *Top partners in little Higgs theories with T-parity*, *Phys. Rev.* **D 74** (2006) 055001 [hep-ph/0510225] [INSPIRE].

[21] H.-C. Cheng, B.A. Dobrescu and C.T. Hill, *Electroweak symmetry breaking and extra dimensions*, *Nucl. Phys.* **B 589** (2000) 249 [hep-ph/9912343] [INSPIRE].

[22] M. Carena, E. Ponton, J. Santiago and C.E.M. Wagner, *Light Kaluza Klein states in Randall-Sundrum models with custodial* SU(2), *Nucl. Phys.* **B 759** (2006) 202 [hep-ph/0607106] [INSPIRE].

[23] R. Contino, L. Da Rold and A. Pomarol, *Light custodians in natural composite Higgs models*, *Phys. Rev.* **D 75** (2007) 055014 [hep-ph/0612048] [INSPIRE].

[24] G. Burdman and L. Da Rold, *Electroweak symmetry breaking from a holographic fourth generation*, *JHEP* **12** (2007) 086 [arXiv:0710.0623] [INSPIRE].

[25] C.T. Hill, *Topcolor: top quark condensation in a gauge extension of the Standard Model*, *Phys. Lett.* **B 266** (1991) 419 [INSPIRE].

[26] A. Carmona, M. Chala and J. Santiago, *New Higgs production mechanism in composite Higgs models*, *JHEP* **07** (2012) 049 [arXiv:1205.2378] [INSPIRE].

[27] CMS collaboration, *Search for the associated production of the Higgs boson with a top-quark pair*, *JHEP* **09** (2014) 087 [*Erratum ibid.* **10** (2014) 106] [arXiv:1408.1682] [INSPIRE].

[28] ATLAS collaboration, *Search for the associated production of the Higgs boson with a top quark pair in multilepton final states with the ATLAS detector*, *Phys. Lett.* **B 749** (2015) 519 [arXiv:1506.05988] [INSPIRE].

[29] CMS collaboration, *Search for a Standard Model Higgs boson produced in association with a top-quark pair and decaying to bottom quarks using a matrix element method*, *Eur. Phys. J.* **C 75** (2015) 251 [arXiv:1502.02485] [INSPIRE].

[30] ATLAS collaboration, *Search for the Standard Model Higgs boson produced in association with top quarks and decaying into $b\bar{b}$ in pp collisions at $\sqrt{s} = 8$ TeV with the ATLAS detector*, *Eur. Phys. J.* **C 75** (2015) 349 [arXiv:1503.05066] [INSPIRE].

[31] LHC Higgs Cross Section Working Group collaboration, *Handbook of LHC Higgs cross sections:* 1. *Inclusive observables*, arXiv:1101.0593 [INSPIRE].

[32] CMS collaboration, *Search for $t\bar{t}H$ production in the all-jet final state in proton-proton collisions at $\sqrt{s} = 13$ TeV*, *JHEP* **06** (2018) 101 [arXiv:1803.06986] [INSPIRE].

[33] CMS collaboration, *Evidence for associated production of a Higgs boson with a top quark pair in final states with electrons, muons and hadronically decaying τ leptons at $\sqrt{s} = 13$ TeV*, *JHEP* **08** (2018) 066 [arXiv:1803.05485] [INSPIRE].

JHEP03(2019)026

[34] ATLAS collaboration, *Evidence for the associated production of the Higgs boson and a top quark pair with the ATLAS detector*, *Phys. Rev.* **D 97** (2018) 072003 [arXiv:1712.08891] [INSPIRE].

[35] ATLAS collaboration, *Search for the Standard Model Higgs boson produced in association with top quarks and decaying into a $b\bar{b}$ pair in pp collisions at $\sqrt{s} = 13$ TeV with the ATLAS detector*, *Phys. Rev.* **D 97** (2018) 072016 [arXiv:1712.08895] [INSPIRE].

[36] T.J. Hastie, R.J. Tibshirani and J.H. Friedman, *The elements of statistical learning: data mining, inference and prediction*, second edition, Springer series in statistics, Springer, New York, NY, U.S.A. (2013) [ISBN:978-0-387-84857-0].

[37] P.C. Bhat, *Multivariate analysis methods in particle physics*, *Ann. Rev. Nucl. Part. Sci.* **61** (2011) 281 [INSPIRE].

[38] A. Höcker et al., *TMVA — toolkit for multivariate data analysis*, PoS(ACAT)040 [physics/0703039] [INSPIRE].

[39] K. Kondo, *Dynamical likelihood method for reconstruction of events with missing momentum. 1: method and toy models*, *J. Phys. Soc. Jap.* **57** (1988) 4126 [INSPIRE].

[40] D0 collaboration, *A precision measurement of the mass of the top quark*, *Nature* **429** (2004) 638 [hep-ex/0406031] [INSPIRE].

[41] CMS collaboration, *The CMS experiment at the CERN LHC*, 2008 *JINST* **3** S08004 [INSPIRE].

[42] CMS collaboration, *The CMS trigger system*, 2017 *JINST* **12** P01020 [arXiv:1609.02366] [INSPIRE].

[43] GEANT4 collaboration, *GEANT4: a simulation toolkit*, *Nucl. Instrum. Meth.* **A 506** (2003) 250 [INSPIRE].

[44] P. Nason, *A new method for combining NLO QCD with shower Monte Carlo algorithms*, *JHEP* **11** (2004) 040 [hep-ph/0409146] [INSPIRE].

[45] S. Frixione, P. Nason and C. Oleari, *Matching NLO QCD computations with parton shower simulations: the POWHEG method*, *JHEP* **11** (2007) 070 [arXiv:0709.2092] [INSPIRE].

[46] S. Alioli, P. Nason, C. Oleari and E. Re, *A general framework for implementing NLO calculations in shower Monte Carlo programs: the POWHEG BOX*, *JHEP* **06** (2010) 043 [arXiv:1002.2581] [INSPIRE].

[47] H.B. Hartanto, B. Jager, L. Reina and D. Wackeroth, *Higgs boson production in association with top quarks in the POWHEG BOX*, *Phys. Rev.* **D 91** (2015) 094003 [arXiv:1501.04498] [INSPIRE].

[48] T. Sjöstrand et al., *An introduction to PYTHIA* 8.2, *Comput. Phys. Commun.* **191** (2015) 159 [arXiv:1410.3012] [INSPIRE].

[49] J. Alwall et al., *The automated computation of tree-level and next-to-leading order differential cross sections and their matching to parton shower simulations*, *JHEP* **07** (2014) 079 [arXiv:1405.0301] [INSPIRE].

[50] NNPDF collaboration, *Parton distributions for the LHC run II*, *JHEP* **04** (2015) 040 [arXiv:1410.8849] [INSPIRE].

JHEP03(2019)026

[51] S. Alioli, P. Nason, C. Oleari and E. Re, *NLO single-top production matched with shower in POWHEG: s- and t-channel contributions*, *JHEP* **09** (2009) 111 [*Erratum ibid.* **02** (2010) 011] [arXiv:0907.4076] [INSPIRE].

[52] E. Re, *Single-top Wt-channel production matched with parton showers using the POWHEG method*, *Eur. Phys. J.* **C 71** (2011) 1547 [arXiv:1009.2450] [INSPIRE].

[53] R. Frederix and S. Frixione, *Merging meets matching in MC@NLO*, *JHEP* **12** (2012) 061 [arXiv:1209.6215] [INSPIRE].

[54] CMS collaboration, *Investigations of the impact of the parton shower tuning in PYTHIA 8 in the modelling of $t\bar{t}$ at $\sqrt{s} = 8$ and 13 TeV*, CMS-PAS-TOP-16-021, CERN, Geneva, Switzerland (2016).

[55] CMS collaboration, *Event generator tunes obtained from underlying event and multiparton scattering measurements*, *Eur. Phys. J.* **C 76** (2016) 155 [arXiv:1512.00815] [INSPIRE].

[56] N. Kidonakis, *Two-loop soft anomalous dimensions for single top quark associated production with a W^- or H^-*, *Phys. Rev.* **D 82** (2010) 054018 [arXiv:1005.4451] [INSPIRE].

[57] M. Aliev, H. Lacker, U. Langenfeld, S. Moch, P. Uwer and M. Wiedermann, *HATHOR: HAdronic Top and Heavy quarks crOss section calculatoR*, *Comput. Phys. Commun.* **182** (2011) 1034 [arXiv:1007.1327] [INSPIRE].

[58] P. Kant et al., *HatHor for single top-quark production: updated predictions and uncertainty estimates for single top-quark production in hadronic collisions*, *Comput. Phys. Commun.* **191** (2015) 74 [arXiv:1406.4403] [INSPIRE].

[59] F. Maltoni, D. Pagani and I. Tsinikos, *Associated production of a top-quark pair with vector bosons at NLO in QCD: impact on $t\bar{t}H$ searches at the LHC*, *JHEP* **02** (2016) 113 [arXiv:1507.05640] [INSPIRE].

[60] J.M. Campbell, R.K. Ellis and C. Williams, *Vector boson pair production at the LHC*, *JHEP* **07** (2011) 018 [arXiv:1105.0020] [INSPIRE].

[61] M. Cacciari, M. Czakon, M. Mangano, A. Mitov and P. Nason, *Top-pair production at hadron colliders with next-to-next-to-leading logarithmic soft-gluon resummation*, *Phys. Lett.* **B 710** (2012) 612 [arXiv:1111.5869] [INSPIRE].

[62] P. Bärnreuther, M. Czakon and A. Mitov, *Percent level precision physics at the Tevatron: first genuine NNLO QCD corrections to $q\bar{q} \to t\bar{t} + X$*, *Phys. Rev. Lett.* **109** (2012) 132001 [arXiv:1204.5201] [INSPIRE].

[63] M. Czakon and A. Mitov, *NNLO corrections to top-pair production at hadron colliders: the all-fermionic scattering channels*, *JHEP* **12** (2012) 054 [arXiv:1207.0236] [INSPIRE].

[64] M. Czakon and A. Mitov, *NNLO corrections to top pair production at hadron colliders: the quark-gluon reaction*, *JHEP* **01** (2013) 080 [arXiv:1210.6832] [INSPIRE].

[65] M. Beneke, P. Falgari, S. Klein and C. Schwinn, *Hadronic top-quark pair production with NNLL threshold resummation*, *Nucl. Phys.* **B 855** (2012) 695 [arXiv:1109.1536] [INSPIRE].

[66] M. Czakon, P. Fiedler and A. Mitov, *Total top-quark pair-production cross section at hadron colliders through $O(\alpha_S^4)$*, *Phys. Rev. Lett.* **110** (2013) 252004 [arXiv:1303.6254] [INSPIRE].

JHEP03(2019)026

[67] M. Czakon and A. Mitov, *Top++: a program for the calculation of the top-pair cross-section at hadron colliders*, *Comput. Phys. Commun.* **185** (2014) 2930 [arXiv:1112.5675] [INSPIRE].

[68] CMS collaboration, *Identification of heavy-flavour jets with the CMS detector in pp collisions at* 13 *TeV*, 2018 *JINST* **13** P05011 [arXiv:1712.07158] [INSPIRE].

[69] CMS collaboration, *Particle-flow reconstruction and global event description with the CMS detector*, 2017 *JINST* **12** P10003 [arXiv:1706.04965] [INSPIRE].

[70] CMS collaboration, *Description and performance of track and primary-vertex reconstruction with the CMS tracker*, 2014 *JINST* **9** P10009 [arXiv:1405.6569] [INSPIRE].

[71] M. Cacciari, G.P. Salam and G. Soyez, *The anti-k_t jet clustering algorithm*, *JHEP* **04** (2008) 063 [arXiv:0802.1189] [INSPIRE].

[72] M. Cacciari, G.P. Salam and G. Soyez, *FastJet user manual*, *Eur. Phys. J.* **C 72** (2012) 1896 [arXiv:1111.6097] [INSPIRE].

[73] CMS collaboration, *Performance of electron reconstruction and selection with the CMS detector in proton-proton collisions at* $\sqrt{s} = 8$ *TeV*, 2015 *JINST* **10** P06005 [arXiv:1502.02701] [INSPIRE].

[74] CMS collaboration, *Performance of the CMS muon detector and muon reconstruction with proton-proton collisions at* $\sqrt{s} = 13$ *TeV*, 2018 *JINST* **13** P06015 [arXiv:1804.04528] [INSPIRE].

[75] M. Cacciari, G.P. Salam and G. Soyez, *The catchment area of jets*, *JHEP* **04** (2008) 005 [arXiv:0802.1188] [INSPIRE].

[76] CMS collaboration, *Jet energy scale and resolution in the CMS experiment in pp collisions at* 8 *TeV*, 2017 *JINST* **12** P02014 [arXiv:1607.03663] [INSPIRE].

[77] I. Goodfellow, Y. Bengio and A. Courville, *Deep learning*, http://www.deeplearningbook.org, MIT Press, U.S.A. (2016).

[78] J.H. Friedman, *Stochastic gradient boosting*, *Comput. Stat. Data Anal.* **38** (2002) 367.

[79] J. Kennedy and R. Eberhart, *Particle swarm optimization*, in *Proceedings of ICNN'95 — International Conference on Neural Networks*, volume 4, IEEE, (1995), pg. 1942.

[80] K. El Morabit, *A study of the multivariate analysis of Higgs boson production in association with a top quark-antiquark pair in the boosted regime at the CMS experiment*, master's thesis, EKP-2016-00035, Karlsruher Institut für Technologie (KIT), Germany (2015).

[81] CMS collaboration, *CMS luminosity measurements for the* 2016 *data taking period*, CMS-PAS-LUM-17-001, CERN, Geneva, Switzerland (2017).

[82] ATLAS collaboration, *Measurement of the inelastic proton-proton cross section at* $\sqrt{s} = 13$ *TeV with the ATLAS detector at the LHC*, *Phys. Rev. Lett.* **117** (2016) 182002 [arXiv:1606.02625] [INSPIRE].

[83] CMS collaboration, *Measurement of the cross section ratio* $\sigma_{t\bar{t}b\bar{b}}/\sigma_{t\bar{t}jj}$ *in pp collisions at* $\sqrt{s} = 8$ *TeV*, *Phys. Lett.* **B 746** (2015) 132 [arXiv:1411.5621] [INSPIRE].

[84] ATLAS collaboration, *Measurements of fiducial cross-sections for* $t\bar{t}$ *production with one or two additional b-jets in pp collisions at* $\sqrt{s} = 8$ *TeV using the ATLAS detector*, *Eur. Phys. J.* **C 76** (2016) 11 [arXiv:1508.06868] [INSPIRE].

JHEP03(2019)026

[85] CMS collaboration, *Measurement of $t\bar{t}$ production with additional jet activity, including b quark jets, in the dilepton decay channel using pp collisions at $\sqrt{s} = 8$ TeV*, *Eur. Phys. J.* **C 76** (2016) 379 [arXiv:1510.03072] [INSPIRE].

[86] CMS collaboration, *Measurements of $t\bar{t}$ cross sections in association with b jets and inclusive jets and their ratio using dilepton final states in pp collisions at $\sqrt{s} = 13$ TeV*, *Phys. Lett.* **B 776** (2018) 355 [arXiv:1705.10141] [INSPIRE].

[87] G. Bevilacqua, M.V. Garzelli and A. Kardos, *$t\bar{t}b\bar{b}$ hadroproduction with massive bottom quarks with PowHel*, arXiv:1709.06915 [INSPIRE].

[88] T. Ježo, J.M. Lindert, N. Moretti and S. Pozzorini, *New NLOPS predictions for $t\bar{t}$ + b-jet production at the LHC*, *Eur. Phys. J.* **C 78** (2018) 502 [arXiv:1802.00426] [INSPIRE].

[89] T. Gleisberg et al., *Event generation with SHERPA* 1.1, *JHEP* **02** (2009) 007 [arXiv:0811.4622] [INSPIRE].

[90] F. Cascioli, P. Maierhofer and S. Pozzorini, *Scattering amplitudes with open loops*, *Phys. Rev. Lett.* **108** (2012) 111601 [arXiv:1111.5206] [INSPIRE].

[91] P. Skands, S. Carrazza and J. Rojo, *Tuning PYTHIA* 8.1*: the Monash* 2013 *tune*, *Eur. Phys. J.* **C 74** (2014) 3024 [arXiv:1404.5630] [INSPIRE].

[92] CMS collaboration, *Measurement of differential cross sections for the production of top quark pairs and of additional jets in lepton+jets events from pp collisions at $\sqrt{s} = 13$ TeV*, *Phys. Rev.* **D 97** (2018) 112003 [arXiv:1803.08856] [INSPIRE].

[93] R.J. Barlow and C. Beeston, *Fitting using finite Monte Carlo samples*, *Comput. Phys. Commun.* **77** (1993) 219 [INSPIRE].

[94] J.S. Conway, *Incorporating nuisance parameters in likelihoods for multisource spectra*, in *Proceedings, PHYSTAT* 2011 *Workshop on statistical issues related to discovery claims in search experiments and unfolding*, CERN-2011-006, CERN, Geneva, Switzerland 17–20 January 2011, pg. 115 [arXiv:1103.0354] [INSPIRE].

[95] T. Junk, *Confidence level computation for combining searches with small statistics*, *Nucl. Instrum. Meth.* **A 434** (1999) 435 [hep-ex/9902006] [INSPIRE].

[96] A.L. Read, *Presentation of search results: the CL_s technique*, *J. Phys.* **G 28** (2002) 2693 [INSPIRE].

[97] G. Cowan, K. Cranmer, E. Gross and O. Vitells, *Asymptotic formulae for likelihood-based tests of new physics*, *Eur. Phys. J.* **C 71** (2011) 1554 [*Erratum ibid.* **C 73** (2013) 2501] [arXiv:1007.1727] [INSPIRE].

[98] B. Efron, *The jackknife, the bootstrap and other resampling plans*, Society for Industrial and Applied Mathematics, SIAM, U.S.A. (1982).

[99] J.D. Bjorken and S.J. Brodsky, *Statistical model for electron-positron annihilation into hadrons*, *Phys. Rev.* **D 1** (1970) 1416 [INSPIRE].

[100] G.C. Fox and S. Wolfram, *Event shapes in e^+e^- annihilation*, *Nucl. Phys.* **B 149** (1979) 413 [*Erratum ibid.* **B 157** (1979) 543] [INSPIRE].

JHEP03(2019)026

The CMS collaboration

Yerevan Physics Institute, Yerevan, Armenia

A.M. Sirunyan, A. Tumasyan

Institut für Hochenergiephysik, Wien, Austria

W. Adam, F. Ambrogi, E. Asilar, T. Bergauer, J. Brandstetter, M. Dragicevic, J. Erö, A. Escalante Del Valle, M. Flechl, R. Frühwirth[1], V.M. Ghete, J. Hrubec, M. Jeitler[1], N. Krammer, I. Krätschmer, D. Liko, T. Madlener, I. Mikulec, N. Rad, H. Rohringer, J. Schieck[1], R. Schöfbeck, M. Spanring, D. Spitzbart, A. Taurok, W. Waltenberger, J. Wittmann, C.-E. Wulz[1], M. Zarucki

Institute for Nuclear Problems, Minsk, Belarus

V. Chekhovsky, V. Mossolov, J. Suarez Gonzalez

Universiteit Antwerpen, Antwerpen, Belgium

E.A. De Wolf, D. Di Croce, X. Janssen, J. Lauwers, M. Pieters, M. Van De Klundert, H. Van Haevermaet, P. Van Mechelen, N. Van Remortel

Vrije Universiteit Brussel, Brussel, Belgium

S. Abu Zeid, F. Blekman, J. D'Hondt, I. De Bruyn, J. De Clercq, K. Deroover, G. Flouris, D. Lontkovskyi, S. Lowette, I. Marchesini, S. Moortgat, L. Moreels, Q. Python, K. Skovpen, S. Tavernier, W. Van Doninck, P. Van Mulders, I. Van Parijs

Université Libre de Bruxelles, Bruxelles, Belgium

D. Beghin, B. Bilin, H. Brun, B. Clerbaux, G. De Lentdecker, H. Delannoy, B. Dorney, G. Fasanella, L. Favart, R. Goldouzian, A. Grebenyuk, A.K. Kalsi, T. Lenzi, J. Luetic, N. Postiau, E. Starling, L. Thomas, C. Vander Velde, P. Vanlaer, D. Vannerom, Q. Wang

Ghent University, Ghent, Belgium

T. Cornelis, D. Dobur, A. Fagot, M. Gul, I. Khvastunov[2], D. Poyraz, C. Roskas, D. Trocino, M. Tytgat, W. Verbeke, B. Vermassen, M. Vit, N. Zaganidis

Université Catholique de Louvain, Louvain-la-Neuve, Belgium

H. Bakhshiansohi, O. Bondu, S. Brochet, G. Bruno, C. Caputo, P. David, C. Delaere, M. Delcourt, B. Francois, A. Giammanco, G. Krintiras, V. Lemaitre, A. Magitteri, A. Mertens, M. Musich, K. Piotrzkowski, A. Saggio, M. Vidal Marono, S. Wertz, J. Zobec

Centro Brasileiro de Pesquisas Fisicas, Rio de Janeiro, Brazil

F.L. Alves, G.A. Alves, L. Brito, M. Correa Martins Junior, G. Correia Silva, C. Hensel, A. Moraes, M.E. Pol, P. Rebello Teles

Universidade do Estado do Rio de Janeiro, Rio de Janeiro, Brazil

E. Belchior Batista Das Chagas, W. Carvalho, J. Chinellato[3], E. Coelho, E.M. Da Costa, G.G. Da Silveira[4], D. De Jesus Damiao, C. De Oliveira Martins, S. Fonseca De Souza, H. Malbouisson, D. Matos Figueiredo, M. Melo De Almeida, C. Mora Herrera, L. Mundim, H. Nogima, W.L. Prado Da Silva, L.J. Sanchez Rosas, A. Santoro, A. Sznajder, M. Thiel, E.J. Tonelli Manganote[3], F. Torres Da Silva De Araujo, A. Vilela Pereira

JHEP03(2019)026

Universidade Estadual Paulista [a], Universidade Federal do ABC [b], São Paulo, Brazil

S. Ahuja[a], C.A. Bernardes[a], L. Calligaris[a], T.R. Fernandez Perez Tomei[a], E.M. Gregores[b], P.G. Mercadante[b], S.F. Novaes[a], Sandra S. Padula[a], D. Romero Abad[b]

Institute for Nuclear Research and Nuclear Energy, Bulgarian Academy of Sciences, Sofia, Bulgaria

A. Aleksandrov, R. Hadjiiska, P. Iaydjiev, A. Marinov, M. Misheva, M. Rodozov, M. Shopova, G. Sultanov

University of Sofia, Sofia, Bulgaria

A. Dimitrov, L. Litov, B. Pavlov, P. Petkov

Beihang University, Beijing, China

W. Fang[5], X. Gao[5], L. Yuan

Institute of High Energy Physics, Beijing, China

M. Ahmad, J.G. Bian, G.M. Chen, H.S. Chen, M. Chen, Y. Chen, C.H. Jiang, D. Leggat, H. Liao, Z. Liu, F. Romeo, S.M. Shaheen[6], A. Spiezia, J. Tao, C. Wang, Z. Wang, E. Yazgan, H. Zhang, J. Zhao

State Key Laboratory of Nuclear Physics and Technology, Peking University, Beijing, China

Y. Ban, G. Chen, A. Levin, J. Li, L. Li, Q. Li, Y. Mao, S.J. Qian, D. Wang, Z. Xu

Tsinghua University, Beijing, China

Y. Wang

Universidad de Los Andes, Bogota, Colombia

C. Avila, A. Cabrera, C.A. Carrillo Montoya, L.F. Chaparro Sierra, C. Florez, C.F. González Hernández, M.A. Segura Delgado

University of Split, Faculty of Electrical Engineering, Mechanical Engineering and Naval Architecture, Split, Croatia

B. Courbon, N. Godinovic, D. Lelas, I. Puljak, T. Sculac

University of Split, Faculty of Science, Split, Croatia

Z. Antunovic, M. Kovac

Institute Rudjer Boskovic, Zagreb, Croatia

V. Brigljevic, D. Ferencek, K. Kadija, B. Mesic, A. Starodumov[7], T. Susa

University of Cyprus, Nicosia, Cyprus

M.W. Ather, A. Attikis, M. Kolosova, G. Mavromanolakis, J. Mousa, C. Nicolaou, F. Ptochos, P.A. Razis, H. Rykaczewski

Charles University, Prague, Czech Republic

M. Finger[8], M. Finger Jr.[8]

JHEP03(2019)026

Escuela Politecnica Nacional, Quito, Ecuador

E. Ayala

Universidad San Francisco de Quito, Quito, Ecuador

E. Carrera Jarrin

Academy of Scientific Research and Technology of the Arab Republic of Egypt, Egyptian Network of High Energy Physics, Cairo, Egypt

H. Abdalla[9], A.A. Abdelalim[10,11], A. Mohamed[11]

National Institute of Chemical Physics and Biophysics, Tallinn, Estonia

S. Bhowmik, A. Carvalho Antunes De Oliveira, R.K. Dewanjee, K. Ehataht, M. Kadastik, M. Raidal, C. Veelken

Department of Physics, University of Helsinki, Helsinki, Finland

P. Eerola, H. Kirschenmann, J. Pekkanen, M. Voutilainen

Helsinki Institute of Physics, Helsinki, Finland

J. Havukainen, J.K. Heikkilä, T. Järvinen, V. Karimäki, R. Kinnunen, T. Lampén, K. Lassila-Perini, S. Laurila, S. Lehti, T. Lindén, P. Luukka, T. Mäenpää, H. Siikonen, E. Tuominen, J. Tuominiemi

Lappeenranta University of Technology, Lappeenranta, Finland

T. Tuuva

IRFU, CEA, Université Paris-Saclay, Gif-sur-Yvette, France

M. Besancon, F. Couderc, M. Dejardin, D. Denegri, J.L. Faure, F. Ferri, S. Ganjour, A. Givernaud, P. Gras, G. Hamel de Monchenault, P. Jarry, C. Leloup, E. Locci, J. Malcles, G. Negro, J. Rander, A. Rosowsky, M.Ö. Sahin, M. Titov

Laboratoire Leprince-Ringuet, Ecole polytechnique, CNRS/IN2P3, Université Paris-Saclay, Palaiseau, France

A. Abdulsalam[12], C. Amendola, I. Antropov, F. Beaudette, P. Busson, C. Charlot, R. Granier de Cassagnac, I. Kucher, S. Lisniak, A. Lobanov, J. Martin Blanco, M. Nguyen, C. Ochando, G. Ortona, P. Pigard, R. Salerno, J.B. Sauvan, Y. Sirois, A.G. Stahl Leiton, A. Zabi, A. Zghiche

Université de Strasbourg, CNRS, IPHC UMR 7178, F-67000 Strasbourg, France

J.-L. Agram[13], J. Andrea, D. Bloch, J.-M. Brom, E.C. Chabert, V. Cherepanov, C. Collard, E. Conte[13], J.-C. Fontaine[13], D. Gelé, U. Goerlach, M. Jansová, A.-C. Le Bihan, N. Tonon, P. Van Hove

Centre de Calcul de l'Institut National de Physique Nucleaire et de Physique des Particules, CNRS/IN2P3, Villeurbanne, France

S. Gadrat

JHEP03(2019)026

Université de Lyon, Université Claude Bernard Lyon 1, CNRS-IN2P3, Institut de Physique Nucléaire de Lyon, Villeurbanne, France

S. Beauceron, C. Bernet, G. Boudoul, N. Chanon, R. Chierici, D. Contardo, P. Depasse, H. El Mamouni, J. Fay, L. Finco, S. Gascon, M. Gouzevitch, G. Grenier, B. Ille, F. Lagarde, I.B. Laktineh, H. Lattaud, M. Lethuillier, L. Mirabito, A.L. Pequegnot, S. Perries, A. Popov[14], V. Sordini, M. Vander Donckt, S. Viret, S. Zhang

Georgian Technical University, Tbilisi, Georgia

A. Khvedelidze[8]

Tbilisi State University, Tbilisi, Georgia

Z. Tsamalaidze[8]

RWTH Aachen University, I. Physikalisches Institut, Aachen, Germany

C. Autermann, L. Feld, M.K. Kiesel, K. Klein, M. Lipinski, M. Preuten, M.P. Rauch, C. Schomakers, J. Schulz, M. Teroerde, B. Wittmer, V. Zhukov[14]

RWTH Aachen University, III. Physikalisches Institut A, Aachen, Germany

A. Albert, D. Duchardt, M. Endres, M. Erdmann, T. Esch, R. Fischer, S. Ghosh, A. Güth, T. Hebbeker, C. Heidemann, K. Hoepfner, H. Keller, S. Knutzen, L. Mastrolorenzo, M. Merschmeyer, A. Meyer, P. Millet, S. Mukherjee, T. Pook, M. Radziej, Y. Rath, H. Reithler, M. Rieger, F. Scheuch, A. Schmidt, D. Teyssier

RWTH Aachen University, III. Physikalisches Institut B, Aachen, Germany

G. Flügge, O. Hlushchenko, B. Kargoll, T. Kress, A. Künsken, T. Müller, A. Nehrkorn, A. Nowack, C. Pistone, O. Pooth, H. Sert, A. Stahl[15]

Deutsches Elektronen-Synchrotron, Hamburg, Germany

M. Aldaya Martin, T. Arndt, C. Asawatangtrakuldee, I. Babounikau, K. Beernaert, O. Behnke, U. Behrens, A. Bermúdez Martínez, D. Bertsche, A.A. Bin Anuar, K. Borras[16], V. Botta, A. Campbell, P. Connor, C. Contreras-Campana, F. Costanza, V. Danilov, A. De Wit, M.M. Defranchis, C. Diez Pardos, D. Domínguez Damiani, G. Eckerlin, T. Eichhorn, A. Elwood, E. Eren, E. Gallo[17], A. Geiser, J.M. Grados Luyando, A. Grohsjean, P. Gunnellini, M. Guthoff, M. Haranko, A. Harb, J. Hauk, H. Jung, M. Kasemann, J. Keaveney, C. Kleinwort, J. Knolle, D. Krücker, W. Lange, A. Lelek, T. Lenz, K. Lipka, W. Lohmann[18], R. Mankel, I.-A. Melzer-Pellmann, A.B. Meyer, M. Meyer, M. Missiroli, G. Mittag, J. Mnich, V. Myronenko, S.K. Pflitsch, D. Pitzl, A. Raspereza, A. Saibel, M. Savitskyi, P. Saxena, P. Schütze, C. Schwanenberger, R. Shevchenko, A. Singh, N. Stefaniuk, H. Tholen, O. Turkot, A. Vagnerini, G.P. Van Onsem, R. Walsh, Y. Wen, K. Wichmann, C. Wissing, O. Zenaiev

University of Hamburg, Hamburg, Germany

R. Aggleton, S. Bein, L. Benato, A. Benecke, V. Blobel, M. Centis Vignali, T. Dreyer, E. Garutti, D. Gonzalez, J. Haller, A. Hinzmann, A. Karavdina, G. Kasieczka, R. Klanner, R. Kogler, N. Kovalchuk, S. Kurz, V. Kutzner, J. Lange, D. Marconi, J. Multhaup, M. Niedziela, D. Nowatschin, A. Perieanu, A. Reimers, O. Rieger, C. Scharf, P. Schleper,

JHEP03(2019)026

S. Schumann, J. Schwandt, J. Sonneveld, H. Stadie, G. Steinbrück, F.M. Stober, M. Stöver, D. Troendle, A. Vanhoefer, B. Vormwald

Institut für Experimentelle Teilchenphysik, Karlsruhe, Germany

M. Akbiyik, C. Barth, M. Baselga, S. Baur, E. Butz, R. Caspart, T. Chwalek, F. Colombo, W. De Boer, A. Dierlamm, K. El Morabit, N. Faltermann, B. Freund, M. Giffels, M.A. Harrendorf, F. Hartmann[15], S.M. Heindl, U. Husemann, F. Kassel[15], I. Katkov[14], P. Keicher, S. Kudella, H. Mildner, S. Mitra, M.U. Mozer, Th. Müller, M. Plagge, G. Quast, K. Rabbertz, M. Schröder, I. Shvetsov, G. Sieber, H.J. Simonis, R. Ulrich, M. Waßmer, S. Wayand, M. Weber, T. Weiler, S. Williamson, C. Wöhrmann, R. Wolf

Institute of Nuclear and Particle Physics (INPP), NCSR Demokritos, Aghia Paraskevi, Greece

G. Anagnostou, G. Daskalakis, T. Geralis, A. Kyriakis, D. Loukas, G. Paspalaki, I. Topsis-Giotis

National and Kapodistrian University of Athens, Athens, Greece

G. Karathanasis, S. Kesisoglou, P. Kontaxakis, A. Panagiotou, N. Saoulidou, E. Tziaferi, K. Vellidis

National Technical University of Athens, Athens, Greece

K. Kousouris, I. Papakrivopoulos, G. Tsipolitis

University of Ioánnina, Ioánnina, Greece

I. Evangelou, C. Foudas, P. Gianneios, P. Katsoulis, P. Kokkas, S. Mallios, N. Manthos, I. Papadopoulos, E. Paradas, J. Strologas, F.A. Triantis, D. Tsitsonis

MTA-ELTE Lendület CMS Particle and Nuclear Physics Group, Eötvös Loránd University, Budapest, Hungary

M. Bartók[19], M. Csanad, N. Filipovic, P. Major, M.I. Nagy, G. Pasztor, O. Surányi, G.I. Veres

Wigner Research Centre for Physics, Budapest, Hungary

G. Bencze, C. Hajdu, D. Horvath[20], Á. Hunyadi, F. Sikler, T.Á. Vámi, V. Veszpremi, G. Vesztergombi[†]

Institute of Nuclear Research ATOMKI, Debrecen, Hungary

N. Beni, S. Czellar, J. Karancsi[21], A. Makovec, J. Molnar, Z. Szillasi

Institute of Physics, University of Debrecen, Debrecen, Hungary

P. Raics, Z.L. Trocsanyi, B. Ujvari

Indian Institute of Science (IISc), Bangalore, India

S. Choudhury, J.R. Komaragiri, P.C. Tiwari

National Institute of Science Education and Research, Bhubaneswar, India

S. Bahinipati[22], C. Kar, P. Mal, K. Mandal, A. Nayak[23], D.K. Sahoo[22], S.K. Swain

JHEP03(2019)026

Panjab University, Chandigarh, India
S. Bansal, S.B. Beri, V. Bhatnagar, S. Chauhan, R. Chawla, N. Dhingra, R. Gupta, A. Kaur, A. Kaur, M. Kaur, S. Kaur, R. Kumar, P. Kumari, M. Lohan, A. Mehta, K. Sandeep, S. Sharma, J.B. Singh, G. Walia

University of Delhi, Delhi, India
A. Bhardwaj, B.C. Choudhary, R.B. Garg, M. Gola, S. Keshri, Ashok Kumar, S. Malhotra, M. Naimuddin, P. Priyanka, K. Ranjan, Aashaq Shah, R. Sharma

Saha Institute of Nuclear Physics, HBNI, Kolkata, India
R. Bhardwaj[24], M. Bharti, R. Bhattacharya, S. Bhattacharya, U. Bhawandeep[24], D. Bhowmik, S. Dey, S. Dutt[24], S. Dutta, S. Ghosh, K. Mondal, S. Nandan, A. Purohit, P.K. Rout, A. Roy, S. Roy Chowdhury, S. Sarkar, M. Sharan, B. Singh, S. Thakur[24]

Indian Institute of Technology Madras, Madras, India
P.K. Behera

Bhabha Atomic Research Centre, Mumbai, India
R. Chudasama, D. Dutta, V. Jha, V. Kumar, P.K. Netrakanti, L.M. Pant, P. Shukla

Tata Institute of Fundamental Research-A, Mumbai, India
T. Aziz, M.A. Bhat, S. Dugad, G.B. Mohanty, N. Sur, B. Sutar, Ravindra Kumar Verma

Tata Institute of Fundamental Research-B, Mumbai, India
S. Banerjee, S. Bhattacharya, S. Chatterjee, P. Das, M. Guchait, Sa. Jain, S. Karmakar, S. Kumar, M. Maity[25], G. Majumder, K. Mazumdar, N. Sahoo, T. Sarkar[25]

Indian Institute of Science Education and Research (IISER), Pune, India
S. Chauhan, S. Dube, V. Hegde, A. Kapoor, K. Kothekar, S. Pandey, A. Rane, S. Sharma

Institute for Research in Fundamental Sciences (IPM), Tehran, Iran
S. Chenarani[26], E. Eskandari Tadavani, S.M. Etesami[26], M. Khakzad, M. Mohammadi Najafabadi, M. Naseri, F. Rezaei Hosseinabadi, B. Safarzadeh[27], M. Zeinali

University College Dublin, Dublin, Ireland
M. Felcini, M. Grunewald

INFN Sezione di Bari (a, Università di Bari (b, Politecnico di Bari [c], Bari, Italy
M. Abbrescia[a,b], C. Calabria[a,b], A. Colaleo[a], D. Creanza[a,c], L. Cristella[a,b], N. De Filippis[a,c], M. De Palma[a,b], A. Di Florio[a,b], F. Errico[a,b], L. Fiore[a], A. Gelmi[a,b], G. Iaselli[a,c], M. Ince[a,b], S. Lezki[a,b], G. Maggi[a,c], M. Maggi[a], G. Miniello[a,b], S. My[a,b], S. Nuzzo[a,b], A. Pompili[a,b], G. Pugliese[a,c], R. Radogna[a], A. Ranieri[a], G. Selvaggi[a,b], A. Sharma[a], L. Silvestris[a], R. Venditti[a], P. Verwilligen[a], G. Zito[a]

INFN Sezione di Bologna (a, Università di Bologna [b], Bologna, Italy
G. Abbiendi[a], C. Battilana[a,b], D. Bonacorsi[a,b], L. Borgonovi[a,b], S. Braibant-Giacomelli[a,b], R. Campanini[a,b], P. Capiluppi[a,b], A. Castro[a,b], F.R. Cavallo[a], S.S. Chhibra[a,b], C. Ciocca[a], G. Codispoti[a,b], M. Cuffiani[a,b], G.M. Dallavalle[a], F. Fabbri[a], A. Fanfani[a,b], P. Giacomelli[a],

JHEP03(2019)026

C. Grandi[a], L. Guiducci[a,b], F. Iemmi[a,b], S. Marcellini[a], G. Masetti[a], A. Montanari[a], F.L. Navarria[a,b], A. Perrotta[a], F. Primavera[a,b,15], A.M. Rossi[a,b], T. Rovelli[a,b], G.P. Siroli[a,b], N. Tosi[a]

INFN Sezione di Catania (a, Università di Catania [b], Catania, Italy

S. Albergo[a,b], A. Di Mattia[a], R. Potenza[a,b], A. Tricomi[a,b], C. Tuve[a,b]

INFN Sezione di Firenze (a, Università di Firenze [b], Firenze, Italy

G. Barbagli[a], K. Chatterjee[a,b], V. Ciulli[a,b], C. Civinini[a], R. D'Alessandro[a,b], E. Focardi[a,b], G. Latino, P. Lenzi[a,b], M. Meschini[a], S. Paoletti[a], L. Russo[a,28], G. Sguazzoni[a], D. Strom[a], L. Viliani[a]

INFN Laboratori Nazionali di Frascati, Frascati, Italy

L. Benussi, S. Bianco, F. Fabbri, D. Piccolo

INFN Sezione di Genova (a, Università di Genova [b], Genova, Italy

F. Ferro[a], F. Ravera[a,b], E. Robutti[a], S. Tosi[a,b]

INFN Sezione di Milano-Bicocca (a, Università di Milano-Bicocca [b], Milano, Italy

A. Benaglia[a], A. Beschi[b], L. Brianza[a,b], F. Brivio[a,b], V. Ciriolo[a,b,15], S. Di Guida[a,d,15], M.E. Dinardo[a,b], S. Fiorendi[a,b], S. Gennai[a], A. Ghezzi[a,b], P. Govoni[a,b], M. Malberti[a,b], S. Malvezzi[a], A. Massironi[a,b], D. Menasce[a], L. Moroni[a], M. Paganoni[a,b], D. Pedrini[a], S. Ragazzi[a,b], T. Tabarelli de Fatis[a,b]

INFN Sezione di Napoli (a, Università di Napoli 'Federico II' (b, Napoli, Italy, Università della Basilicata (c, Potenza, Italy, Università G. Marconi (d, Roma, Italy

S. Buontempo, N. Cavallo, A. Di Crescenzo, F. Fabozzi, F. Fienga, G. Galati, A.O.M. Iorio, W.A. Khan, L. Lista, S. Meola[15], P. Paolucci[15], C. Sciacca, E. Voevodina

INFN Sezione di Padova (a, Università di Padova (b, Padova, Italy, Università di Trento (c, Trento, Italy

P. Azzi, N. Bacchetta, M. Benettoni, A. Boletti, A. Bragagnolo, R. Carlin, P. Checchia, P. De Castro Manzano, T. Dorigo, U. Dosselli, F. Gasparini, U. Gasparini, A. Gozzelino, S. Lacaprara, P. Lujan, M. Margoni, A.T. Meneguzzo, J. Pazzini, N. Pozzobon, P. Ronchese, R. Rossin, F. Simonetto, A. Tiko, E. Torassa, M. Zanetti, P. Zotto, G. Zumerle

INFN Sezione di Pavia (a, Università di Pavia [b], Pavia, Italy

A. Braghieri[a], A. Magnani[a], P. Montagna[a,b], S.P. Ratti[a,b], V. Re[a], M. Ressegotti[a,b], C. Riccardi[a,b], P. Salvini[a], I. Vai[a,b], P. Vitulo[a,b]

INFN Sezione di Perugia (a, Università di Perugia [b], Perugia, Italy

L. Alunni Solestizi[a,b], M. Biasini[a,b], G.M. Bilei[a], C. Cecchi[a,b], D. Ciangottini[a,b], L. Fanò[a,b], P. Lariccia[a,b], R. Leonardi[a,b], E. Manoni[a], G. Mantovani[a,b], V. Mariani[a,b], M. Menichelli[a], A. Rossi[a,b], A. Santocchia[a,b], D. Spiga[a]

JHEP03(2019)026

INFN Sezione di Pisa (a, Università di Pisa (b, Scuola Normale Superiore di Pisa [c], Pisa, Italy

K. Androsov[a], P. Azzurri[a], G. Bagliesi[a], L. Bianchini[a], T. Boccali[a], L. Borrello, R. Castaldi[a], M.A. Ciocci[a,b], R. Dell'Orso[a], G. Fedi[a], F. Fiori[a,c], L. Giannini[a,c], A. Giassi[a], M.T. Grippo[a], F. Ligabue[a,c], E. Manca[a,c], G. Mandorli[a,c], A. Messineo[a,b], F. Palla[a], A. Rizzi[a,b], P. Spagnolo[a], R. Tenchini[a], G. Tonelli[a,b], A. Venturi[a], P.G. Verdini[a]

INFN Sezione di Roma (a, Sapienza Università di Roma [b], Rome, Italy

L. Barone[a,b], F. Cavallari[a], M. Cipriani[a,b], N. Daci[a], D. Del Re[a,b], E. Di Marco[a,b], M. Diemoz[a], S. Gelli[a,b], E. Longo[a,b], B. Marzocchi[a,b], P. Meridiani[a], G. Organtini[a,b], F. Pandolfi[a], R. Paramatti[a,b], F. Preiato[a,b], S. Rahatlou[a,b], C. Rovelli[a], F. Santanastasio[a,b]

INFN Sezione di Torino (a, Università di Torino (b, Torino, Italy, Università del Piemonte Orientale (c, Novara, Italy

N. Amapane, R. Arcidiacono, S. Argiro, M. Arneodo, N. Bartosik, R. Bellan, C. Biino, N. Cartiglia, F. Cenna, S. Cometti, M. Costa, R. Covarelli, N. Demaria, B. Kiani, C. Mariotti, S. Maselli, E. Migliore, V. Monaco, E. Monteil, M. Monteno, M.M. Obertino, L. Pacher, N. Pastrone, M. Pelliccioni, G.L. Pinna Angioni, A. Romero, M. Ruspa, R. Sacchi, K. Shchelina, V. Sola, A. Solano, D. Soldi, A. Staiano

INFN Sezione di Trieste (a, Università di Trieste [b], Trieste, Italy

S. Belforte[a], V. Candelise[a,b], M. Casarsa[a], F. Cossutti[a], G. Della Ricca[a,b], F. Vazzoler[a,b], A. Zanetti[a]

Kyungpook National University

D.H. Kim, G.N. Kim, M.S. Kim, J. Lee, S. Lee, S.W. Lee, C.S. Moon, Y.D. Oh, S. Sekmen, D.C. Son, Y.C. Yang

Chonnam National University, Institute for Universe and Elementary Particles, Kwangju, Korea

H. Kim, D.H. Moon, G. Oh

Hanyang University, Seoul, Korea

J. Goh[29], T.J. Kim

Korea University, Seoul, Korea

S. Cho, S. Choi, Y. Go, D. Gyun, S. Ha, B. Hong, Y. Jo, K. Lee, K.S. Lee, S. Lee, J. Lim, S.K. Park, Y. Roh

Sejong University, Seoul, Korea

H. S. Kim

Seoul National University, Seoul, Korea

J. Almond, J. Kim, J.S. Kim, H. Lee, K. Lee, K. Nam, S.B. Oh, B.C. Radburn-Smith, S.h. Seo, U.K. Yang, H.D. Yoo, G.B. Yu

University of Seoul, Seoul, Korea

D. Jeon, H. Kim, J.H. Kim, J.S.H. Lee, I.C. Park

JHEP03(2019)026

Sungkyunkwan University, Suwon, Korea

Y. Choi, C. Hwang, J. Lee, I. Yu

Vilnius University, Vilnius, Lithuania

V. Dudenas, A. Juodagalvis, J. Vaitkus

National Centre for Particle Physics, Universiti Malaya, Kuala Lumpur, Malaysia

I. Ahmed, Z.A. Ibrahim, M.A.B. Md Ali[30], F. Mohamad Idris[31], W.A.T. Wan Abdullah, M.N. Yusli, Z. Zolkapli

Universidad de Sonora (UNISON), Hermosillo, Mexico

A. Castaneda Hernandez, J.A. Murillo Quijada

Centro de Investigacion y de Estudios Avanzados del IPN, Mexico City, Mexico

Duran-Osuna, M. C., H. Castilla-Valdez, E. De La Cruz-Burelo, Ramirez-Sanchez, G., I. Heredia-De La Cruz[32], Rabadan-Trejo, R. I., R. Lopez-Fernandez, J. Mejia Guisao, Reyes-Almanza, R, M. Ramirez-Garcia, A. Sanchez-Hernandez

Universidad Iberoamericana, Mexico City, Mexico

S. Carrillo Moreno, C. Oropeza Barrera, F. Vazquez Valencia

Benemerita Universidad Autonoma de Puebla, Puebla, Mexico

J. Eysermans, I. Pedraza, H.A. Salazar Ibarguen, C. Uribe Estrada

Universidad Autónoma de San Luis Potosí, San Luis Potosí, Mexico

A. Morelos Pineda

University of Auckland, Auckland, New Zealand

D. Krofcheck

University of Canterbury, Christchurch, New Zealand

S. Bheesette, P.H. Butler

National Centre for Physics, Quaid-I-Azam University, Islamabad, Pakistan

A. Ahmad, M. Ahmad, M.I. Asghar, Q. Hassan, H.R. Hoorani, A. Saddique, M.A. Shah, M. Shoaib, M. Waqas

National Centre for Nuclear Research, Swierk, Poland

H. Bialkowska, M. Bluj, B. Boimska, T. Frueboes, M. Górski, M. Kazana, K. Nawrocki, M. Szleper, P. Traczyk, P. Zalewski

Institute of Experimental Physics, Faculty of Physics, University of Warsaw, Warsaw, Poland

K. Bunkowski, A. Byszuk[33], K. Doroba, A. Kalinowski, M. Konecki, J. Krolikowski, M. Misiura, M. Olszewski, A. Pyskir, M. Walczak

JHEP03(2019)026

Laboratório de Instrumentação e Física Experimental de Partículas, Lisboa, Portugal

P. Bargassa, C. Beirão Da Cruz E Silva, A. Di Francesco, P. Faccioli, B. Galinhas, M. Gallinaro, J. Hollar, N. Leonardo, L. Lloret Iglesias, M.V. Nemallapudi, J. Seixas, G. Strong, O. Toldaiev, D. Vadruccio, J. Varela

Joint Institute for Nuclear Research, Dubna, Russia

S. Afanasiev, V. Alexakhin, P. Bunin, M. Gavrilenko, A. Golunov, I. Golutvin, N. Gorbounov, V. Karjavin, A. Lanev, A. Malakhov, V. Matveev[34,35], P. Moisenz, V. Palichik, V. Perelygin, M. Savina, S. Shmatov, V. Smirnov, N. Voytishin, A. Zarubin

Petersburg Nuclear Physics Institute, Gatchina (St. Petersburg), Russia

V. Golovtsov, Y. Ivanov, V. Kim[36], E. Kuznetsova[37], P. Levchenko, V. Murzin, V. Oreshkin, I. Smirnov, D. Sosnov, V. Sulimov, L. Uvarov, S. Vavilov, A. Vorobyev

Institute for Nuclear Research, Moscow, Russia

Yu. Andreev, A. Dermenev, S. Gninenko, N. Golubev, A. Karneyeu, M. Kirsanov, N. Krasnikov, A. Pashenkov, D. Tlisov, A. Toropin

Institute for Theoretical and Experimental Physics, Moscow, Russia

V. Epshteyn, V. Gavrilov, N. Lychkovskaya, V. Popov, I. Pozdnyakov, G. Safronov, A. Spiridonov, A. Stepennov, V. Stolin, M. Toms, E. Vlasov, A. Zhokin

Moscow Institute of Physics and Technology, Moscow, Russia

T. Aushev

National Research Nuclear University 'Moscow Engineering Physics Institute' (MEPhI), Moscow, Russia

R. Chistov[38], M. Danilov[38], P. Parygin, D. Philippov, S. Polikarpov[38], E. Tarkovskii

P.N. Lebedev Physical Institute, Moscow, Russia

V. Andreev, M. Azarkin[35], I. Dremin[35], M. Kirakosyan[35], S.V. Rusakov, A. Terkulov

Skobeltsyn Institute of Nuclear Physics, Lomonosov Moscow State University, Moscow, Russia

A. Baskakov, A. Belyaev, E. Boos, V. Bunichev, M. Dubinin[39], L. Dudko, A. Ershov, V. Klyukhin, O. Kodolova, I. Lokhtin, I. Miagkov, S. Obraztsov, S. Petrushanko, V. Savrin, A. Snigirev

Novosibirsk State University (NSU), Novosibirsk, Russia

V. Blinov[40], T. Dimova[40], L. Kardapoltsev[40], D. Shtol[40], Y. Skovpen[40]

State Research Center of Russian Federation, Institute for High Energy Physics of NRC 'Kurchatov Institute', Protvino, Russia

I. Azhgirey, I. Bayshev, S. Bitioukov, D. Elumakhov, A. Godizov, V. Kachanov, A. Kalinin, D. Konstantinov, P. Mandrik, V. Petrov, R. Ryutin, S. Slabospitskii, A. Sobol, S. Troshin, N. Tyurin, A. Uzunian, A. Volkov

JHEP03(2019)026

National Research Tomsk Polytechnic University, Tomsk, Russia

A. Babaev, S. Baidali, V. Okhotnikov

University of Belgrade, Faculty of Physics and Vinca Institute of Nuclear Sciences, Belgrade, Serbia

P. Adzic[41], P. Cirkovic, D. Devetak, M. Dordevic, J. Milosevic

Centro de Investigaciones Energéticas Medioambientales y Tecnológicas (CIEMAT), Madrid, Spain

J. Alcaraz Maestre, A. Álvarez Fernández, I. Bachiller, M. Barrio Luna, J.A. Brochero Cifuentes, M. Cerrada, N. Colino, B. De La Cruz, A. Delgado Peris, C. Fernandez Bedoya, J.P. Fernández Ramos, J. Flix, M.C. Fouz, O. Gonzalez Lopez, S. Goy Lopez, J.M. Hernandez, M.I. Josa, D. Moran, A. Pérez-Calero Yzquierdo, J. Puerta Pelayo, I. Redondo, L. Romero, M.S. Soares, A. Triossi

Universidad Autónoma de Madrid, Madrid, Spain

C. Albajar, J.F. de Trocóniz

Universidad de Oviedo, Oviedo, Spain

J. Cuevas, C. Erice, J. Fernandez Menendez, S. Folgueras, I. Gonzalez Caballero, J.R. González Fernández, E. Palencia Cortezon, V. Rodríguez Bouza, S. Sanchez Cruz, P. Vischia, J.M. Vizan Garcia

Instituto de Física de Cantabria (IFCA), CSIC-Universidad de Cantabria, Santander, Spain

I.J. Cabrillo, A. Calderon, B. Chazin Quero, J. Duarte Campderros, M. Fernandez, P.J. Fernández Manteca, A. García Alonso, J. Garcia-Ferrero, G. Gomez, A. Lopez Virto, J. Marco, C. Martinez Rivero, P. Martinez Ruiz del Arbol, F. Matorras, J. Piedra Gomez, C. Prieels, T. Rodrigo, A. Ruiz-Jimeno, L. Scodellaro, N. Trevisani, I. Vila, R. Vilar Cortabitarte

CERN, European Organization for Nuclear Research, Geneva, Switzerland

D. Abbaneo, B. Akgun, E. Auffray, P. Baillon, A.H. Ball, D. Barney, J. Bendavid, M. Bianco, A. Bocci, C. Botta, E. Brondolin, T. Camporesi, M. Cepeda, G. Cerminara, E. Chapon, Y. Chen, G. Cucciati, D. d'Enterria, A. Dabrowski, V. Daponte, A. David, A. De Roeck, N. Deelen, M. Dobson, M. Dünser, N. Dupont, A. Elliott-Peisert, P. Everaerts, F. Fallavollita[42], D. Fasanella, G. Franzoni, J. Fulcher, W. Funk, D. Gigi, A. Gilbert, K. Gill, F. Glege, M. Guilbaud, D. Gulhan, J. Hegeman, V. Innocente, A. Jafari, P. Janot, O. Karacheban[18], J. Kieseler, A. Kornmayer, M. Krammer[1], C. Lange, P. Lecoq, C. Lourenço, L. Malgeri, M. Mannelli, F. Meijers, J.A. Merlin, S. Mersi, E. Meschi, P. Milenovic[43], F. Moortgat, M. Mulders, J. Ngadiuba, S. Orfanelli, L. Orsini, F. Pantaleo[15], L. Pape, E. Perez, M. Peruzzi, A. Petrilli, G. Petrucciani, A. Pfeiffer, M. Pierini, F.M. Pitters, D. Rabady, A. Racz, T. Reis, G. Rolandi[44], M. Rovere, H. Sakulin, C. Schäfer, C. Schwick, M. Seidel, M. Selvaggi, A. Sharma, P. Silva, P. Sphicas[45], A. Stakia, J. Steggemann, M. Tosi, D. Treille, A. Tsirou, V. Veckalns[46], W.D. Zeuner

JHEP03(2019)026

Paul Scherrer Institut, Villigen, Switzerland

L. Caminada[47], K. Deiters, W. Erdmann, R. Horisberger, Q. Ingram, H.C. Kaestli, D. Kotlinski, U. Langenegger, T. Rohe, S.A. Wiederkehr

ETH Zurich - Institute for Particle Physics and Astrophysics (IPA), Zurich, Switzerland

M. Backhaus, L. Bäni, P. Berger, N. Chernyavskaya, G. Dissertori, M. Dittmar, M. Donegà, C. Dorfer, C. Grab, C. Heidegger, D. Hits, J. Hoss, T. Klijnsma, W. Lustermann, R.A. Manzoni, M. Marionneau, M.T. Meinhard, F. Micheli, P. Musella, F. Nessi-Tedaldi, J. Pata, F. Pauss, G. Perrin, L. Perrozzi, S. Pigazzini, M. Quittnat, D. Ruini, D.A. Sanz Becerra, M. Schönenberger, L. Shchutska, V.R. Tavolaro, K. Theofilatos, M.L. Vesterbacka Olsson, R. Wallny, D.H. Zhu

Universität Zürich, Zurich, Switzerland

T.K. Aarrestad, C. Amsler[48], D. Brzhechko, M.F. Canelli, A. De Cosa, R. Del Burgo, S. Donato, C. Galloni, T. Hreus, B. Kilminster, I. Neutelings, D. Pinna, G. Rauco, P. Robmann, D. Salerno, K. Schweiger, C. Seitz, Y. Takahashi, A. Zucchetta

National Central University, Chung-Li, Taiwan

Y.H. Chang, K.y. Cheng, T.H. Doan, Sh. Jain, R. Khurana, C.M. Kuo, W. Lin, A. Pozdnyakov, S.S. Yu

National Taiwan University (NTU), Taipei, Taiwan

P. Chang, Y. Chao, K.F. Chen, P.H. Chen, W.-S. Hou, Arun Kumar, Y.y. Li, Y.F. Liu, R.-S. Lu, E. Paganis, A. Psallidas, A. Steen, J.f. Tsai

Chulalongkorn University, Faculty of Science, Department of Physics, Bangkok, Thailand

B. Asavapibhop, N. Srimanobhas, N. Suwonjandee

Çukurova University, Physics Department, Science and Art Faculty, Adana, Turkey

A. Bat, F. Boran, S. Cerci[49], S. Damarseckin, Z.S. Demiroglu, F. Dolek, C. Dozen, I. Dumanoglu, S. Girgis, G. Gokbulut, Y. Guler, E. Gurpinar, I. Hos[50], C. Isik, E.E. Kangal[51], O. Kara, A. Kayis Topaksu, U. Kiminsu, M. Oglakci, G. Onengut, K. Ozdemir[52], S. Ozturk[53], D. Sunar Cerci[49], B. Tali[49], U.G. Tok, S. Turkcapar, I.S. Zorbakir, C. Zorbilmez

Middle East Technical University, Physics Department, Ankara, Turkey

B. Isildak[54], G. Karapinar[55], M. Yalvac, M. Zeyrek

Bogazici University, Istanbul, Turkey

I.O. Atakisi, E. Gülmez, M. Kaya[56], O. Kaya[57], S. Tekten, E.A. Yetkin[58]

Istanbul Technical University, Istanbul, Turkey

M.N. Agaras, S. Atay, A. Cakir, K. Cankocak, Y. Komurcu, S. Sen[59]

JHEP03(2019)026

Institute for Scintillation Materials of National Academy of Science of Ukraine, Kharkov, Ukraine

B. Grynyov

National Scientific Center, Kharkov Institute of Physics and Technology, Kharkov, Ukraine

L. Levchuk

University of Bristol, Bristol, United Kingdom

F. Ball, L. Beck, J.J. Brooke, D. Burns, E. Clement, D. Cussans, O. Davignon, H. Flacher, J. Goldstein, G.P. Heath, H.F. Heath, L. Kreczko, D.M. Newbold[60], S. Paramesvaran, B. Penning, T. Sakuma, D. Smith, V.J. Smith, J. Taylor, A. Titterton

Rutherford Appleton Laboratory, Didcot, United Kingdom

K.W. Bell, A. Belyaev[61], C. Brew, R.M. Brown, D. Cieri, D.J.A. Cockerill, J.A. Coughlan, K. Harder, S. Harper, J. Linacre, E. Olaiya, D. Petyt, C.H. Shepherd-Themistocleous, A. Thea, I.R. Tomalin, T. Williams, W.J. Womersley

Imperial College, London, United Kingdom

G. Auzinger, R. Bainbridge, P. Bloch, J. Borg, S. Breeze, O. Buchmuller, A. Bundock, S. Casasso, D. Colling, L. Corpe, P. Dauncey, G. Davies, M. Della Negra, R. Di Maria, Y. Haddad, G. Hall, G. Iles, T. James, M. Komm, C. Laner, L. Lyons, A.-M. Magnan, S. Malik, A. Martelli, J. Nash[62], A. Nikitenko[7], V. Palladino, M. Pesaresi, A. Richards, A. Rose, E. Scott, C. Seez, A. Shtipliyski, T. Strebler, S. Summers, A. Tapper, K. Uchida, T. Virdee[15], N. Wardle, D. Winterbottom, J. Wright, S.C. Zenz

Brunel University, Uxbridge, United Kingdom

J.E. Cole, P.R. Hobson, A. Khan, P. Kyberd, C.K. Mackay, A. Morton, I.D. Reid, L. Teodorescu, S. Zahid

Baylor University, Waco, U.S.A.

K. Call, J. Dittmann, K. Hatakeyama, H. Liu, C. Madrid, B. Mcmaster, N. Pastika, C. Smith

Catholic University of America, Washington DC, U.S.A.

R. Bartek, A. Dominguez

The University of Alabama, Tuscaloosa, U.S.A.

A. Buccilli, S.I. Cooper, C. Henderson, P. Rumerio, C. West

Boston University, Boston, U.S.A.

D. Arcaro, T. Bose, D. Gastler, D. Rankin, C. Richardson, J. Rohlf, L. Sulak, D. Zou

Brown University, Providence, U.S.A.

G. Benelli, X. Coubez, D. Cutts, M. Hadley, J. Hakala, U. Heintz, J.M. Hogan[63], K.H.M. Kwok, E. Laird, G. Landsberg, J. Lee, Z. Mao, M. Narain, S. Piperov, S. Sagir[64], R. Syarif, E. Usai, D. Yu

JHEP03(2019)026

University of California, Davis, Davis, U.S.A.

R. Band, C. Brainerd, R. Breedon, D. Burns, M. Calderon De La Barca Sanchez, M. Chertok, J. Conway, R. Conway, P.T. Cox, R. Erbacher, C. Flores, G. Funk, W. Ko, O. Kukral, R. Lander, C. Mclean, M. Mulhearn, D. Pellett, J. Pilot, S. Shalhout, M. Shi, D. Stolp, D. Taylor, K. Tos, M. Tripathi, Z. Wang, F. Zhang

University of California, Los Angeles, U.S.A.

M. Bachtis, C. Bravo, R. Cousins, A. Dasgupta, A. Florent, J. Hauser, M. Ignatenko, N. Mccoll, S. Regnard, D. Saltzberg, C. Schnaible, V. Valuev

University of California, Riverside, Riverside, U.S.A.

E. Bouvier, K. Burt, R. Clare, J.W. Gary, S.M.A. Ghiasi Shirazi, G. Hanson, G. Karapostoli, E. Kennedy, F. Lacroix, O.R. Long, M. Olmedo Negrete, M.I. Paneva, W. Si, L. Wang, H. Wei, S. Wimpenny, B. R. Yates

University of California, San Diego, La Jolla, U.S.A.

J.G. Branson, S. Cittolin, M. Derdzinski, R. Gerosa, D. Gilbert, B. Hashemi, A. Holzner, D. Klein, G. Kole, V. Krutelyov, J. Letts, M. Masciovecchio, D. Olivito, S. Padhi, M. Pieri, M. Sani, V. Sharma, S. Simon, M. Tadel, A. Vartak, S. Wasserbaech[65], J. Wood, F. Würthwein, A. Yagil, G. Zevi Della Porta

University of California, Santa Barbara - Department of Physics, Santa Barbara, U.S.A.

N. Amin, R. Bhandari, J. Bradmiller-Feld, C. Campagnari, M. Citron, A. Dishaw, V. Dutta, M. Franco Sevilla, L. Gouskos, R. Heller, J. Incandela, A. Ovcharova, H. Qu, J. Richman, D. Stuart, I. Suarez, S. Wang, J. Yoo

California Institute of Technology, Pasadena, U.S.A.

D. Anderson, A. Bornheim, J.M. Lawhorn, H.B. Newman, T. Q. Nguyen, M. Spiropulu, J.R. Vlimant, R. Wilkinson, S. Xie, Z. Zhang, R.Y. Zhu

Carnegie Mellon University, Pittsburgh, U.S.A.

M.B. Andrews, T. Ferguson, T. Mudholkar, M. Paulini, M. Sun, I. Vorobiev, M. Weinberg

University of Colorado Boulder, Boulder, U.S.A.

J.P. Cumalat, W.T. Ford, F. Jensen, A. Johnson, M. Krohn, S. Leontsinis, E. MacDonald, T. Mulholland, K. Stenson, K.A. Ulmer, S.R. Wagner

Cornell University, Ithaca, U.S.A.

J. Alexander, J. Chaves, Y. Cheng, J. Chu, A. Datta, K. Mcdermott, N. Mirman, J.R. Patterson, D. Quach, A. Rinkevicius, A. Ryd, L. Skinnari, L. Soffi, S.M. Tan, Z. Tao, J. Thom, J. Tucker, P. Wittich, M. Zientek

Fermi National Accelerator Laboratory, Batavia, U.S.A.

S. Abdullin, M. Albrow, M. Alyari, G. Apollinari, A. Apresyan, A. Apyan, S. Banerjee, L.A.T. Bauerdick, A. Beretvas, J. Berryhill, P.C. Bhat, G. Bolla†, K. Burkett, J.N. Butler, A. Canepa, G.B. Cerati, H.W.K. Cheung, F. Chlebana, M. Cremonesi, J. Duarte, V.D. Elvira, J. Freeman, Z. Gecse, E. Gottschalk, L. Gray, D. Green, S. Grünendahl,

JHEP03(2019)026

O. Gutsche, J. Hanlon, R.M. Harris, S. Hasegawa, J. Hirschauer, Z. Hu, B. Jayatilaka, S. Jindariani, M. Johnson, U. Joshi, B. Klima, M.J. Kortelainen, B. Kreis, S. Lammel, D. Lincoln, R. Lipton, M. Liu, T. Liu, J. Lykken, K. Maeshima, J.M. Marraffino, D. Mason, P. McBride, P. Merkel, S. Mrenna, S. Nahn, V. O'Dell, K. Pedro, O. Prokofyev, G. Rakness, L. Ristori, A. Savoy-Navarro[66], B. Schneider, E. Sexton-Kennedy, A. Soha, W.J. Spalding, L. Spiegel, S. Stoynev, J. Strait, N. Strobbe, L. Taylor, S. Tkaczyk, N.V. Tran, L. Uplegger, E.W. Vaandering, C. Vernieri, M. Verzocchi, R. Vidal, M. Wang, H.A. Weber, A. Whitbeck

University of Florida, Gainesville, U.S.A.

D. Acosta, P. Avery, P. Bortignon, D. Bourilkov, A. Brinkerhoff, L. Cadamuro, A. Carnes, M. Carver, D. Curry, R.D. Field, S.V. Gleyzer, B.M. Joshi, J. Konigsberg, A. Korytov, P. Ma, K. Matchev, H. Mei, G. Mitselmakher, K. Shi, D. Sperka, J. Wang, S. Wang

Florida International University, Miami, U.S.A.

Y.R. Joshi, S. Linn

Florida State University, Tallahassee, U.S.A.

A. Ackert, T. Adams, A. Askew, S. Hagopian, V. Hagopian, K.F. Johnson, T. Kolberg, G. Martinez, T. Perry, H. Prosper, A. Saha, V. Sharma, R. Yohay

Florida Institute of Technology, Melbourne, U.S.A.

M.M. Baarmand, V. Bhopatkar, S. Colafranceschi, M. Hohlmann, D. Noonan, M. Rahmani, T. Roy, F. Yumiceva

University of Illinois at Chicago (UIC), Chicago, U.S.A.

M.R. Adams, L. Apanasevich, D. Berry, R.R. Betts, R. Cavanaugh, X. Chen, S. Dittmer, O. Evdokimov, C.E. Gerber, D.A. Hangal, D.J. Hofman, K. Jung, J. Kamin, C. Mills, I.D. Sandoval Gonzalez, M.B. Tonjes, N. Varelas, H. Wang, X. Wang, Z. Wu, J. Zhang

The University of Iowa, Iowa City, U.S.A.

M. Alhusseini, B. Bilki[67], W. Clarida, K. Dilsiz[68], S. Durgut, R.P. Gandrajula, M. Haytmyradov, V. Khristenko, J.-P. Merlo, A. Mestvirishvili, A. Moeller, J. Nachtman, H. Ogul[69], Y. Onel, F. Ozok[70], A. Penzo, C. Snyder, E. Tiras, J. Wetzel

Johns Hopkins University, Baltimore, U.S.A.

B. Blumenfeld, A. Cocoros, N. Eminizer, D. Fehling, L. Feng, A.V. Gritsan, W.T. Hung, P. Maksimovic, J. Roskes, U. Sarica, M. Swartz, M. Xiao, C. You

The University of Kansas, Lawrence, U.S.A.

A. Al-bataineh, P. Baringer, A. Bean, S. Boren, J. Bowen, A. Bylinkin, J. Castle, S. Khalil, A. Kropivnitskaya, D. Majumder, W. Mcbrayer, M. Murray, C. Rogan, S. Sanders, E. Schmitz, J.D. Tapia Takaki, Q. Wang

Kansas State University, Manhattan, U.S.A.

S. Duric, A. Ivanov, K. Kaadze, D. Kim, Y. Maravin, D.R. Mendis, T. Mitchell, A. Modak, A. Mohammadi, L.K. Saini, N. Skhirtladze

Lawrence Livermore National Laboratory, Livermore, U.S.A.

F. Rebassoo, D. Wright

JHEP03(2019)026

University of Maryland, College Park, U.S.A.

A. Baden, O. Baron, A. Belloni, S.C. Eno, Y. Feng, C. Ferraioli, N.J. Hadley, S. Jabeen, G.Y. Jeng, R.G. Kellogg, J. Kunkle, A.C. Mignerey, F. Ricci-Tam, Y.H. Shin, A. Skuja, S.C. Tonwar, K. Wong

Massachusetts Institute of Technology, Cambridge, U.S.A.

D. Abercrombie, B. Allen, V. Azzolini, A. Baty, G. Bauer, R. Bi, S. Brandt, W. Busza, I.A. Cali, M. D'Alfonso, Z. Demiragli, G. Gomez Ceballos, M. Goncharov, P. Harris, D. Hsu, M. Hu, Y. Iiyama, G.M. Innocenti, M. Klute, D. Kovalskyi, Y.-J. Lee, P.D. Luckey, B. Maier, A.C. Marini, C. Mcginn, C. Mironov, S. Narayanan, X. Niu, C. Paus, C. Roland, G. Roland, G.S.F. Stephans, K. Sumorok, K. Tatar, D. Velicanu, J. Wang, T.W. Wang, B. Wyslouch, S. Zhaozhong

University of Minnesota, Minneapolis, U.S.A.

A.C. Benvenuti, R.M. Chatterjee, A. Evans, P. Hansen, S. Kalafut, Y. Kubota, Z. Lesko, J. Mans, S. Nourbakhsh, N. Ruckstuhl, R. Rusack, J. Turkewitz, M.A. Wadud

University of Mississippi, Oxford, U.S.A.

J.G. Acosta, S. Oliveros

University of Nebraska-Lincoln, Lincoln, U.S.A.

E. Avdeeva, K. Bloom, D.R. Claes, C. Fangmeier, F. Golf, R. Gonzalez Suarez, R. Kamalieddin, I. Kravchenko, J. Monroy, J.E. Siado, G.R. Snow, B. Stieger

State University of New York at Buffalo, Buffalo, U.S.A.

A. Godshalk, C. Harrington, I. Iashvili, A. Kharchilava, D. Nguyen, A. Parker, S. Rappoccio, B. Roozbahani

Northeastern University, Boston, U.S.A.

E. Barberis, C. Freer, A. Hortiangtham, D.M. Morse, T. Orimoto, R. Teixeira De Lima, T. Wamorkar, B. Wang, A. Wisecarver, D. Wood

Northwestern University, Evanston, U.S.A.

S. Bhattacharya, O. Charaf, K.A. Hahn, N. Mucia, N. Odell, M.H. Schmitt, K. Sung, M. Trovato, M. Velasco

University of Notre Dame, Notre Dame, U.S.A.

R. Bucci, N. Dev, M. Hildreth, K. Hurtado Anampa, C. Jessop, D.J. Karmgard, N. Kellams, K. Lannon, W. Li, N. Loukas, N. Marinelli, F. Meng, C. Mueller, Y. Musienko[34], M. Planer, A. Reinsvold, R. Ruchti, P. Siddireddy, G. Smith, S. Taroni, M. Wayne, A. Wightman, M. Wolf, A. Woodard

The Ohio State University, Columbus, U.S.A.

J. Alimena, L. Antonelli, B. Bylsma, L.S. Durkin, S. Flowers, B. Francis, A. Hart, C. Hill, W. Ji, T.Y. Ling, W. Luo, B.L. Winer, H.W. Wulsin

JHEP03(2019)026

Princeton University, Princeton, U.S.A.

S. Cooperstein, P. Elmer, J. Hardenbrook, P. Hebda, S. Higginbotham, A. Kalogeropoulos, D. Lange, M.T. Lucchini, J. Luo, D. Marlow, K. Mei, I. Ojalvo, J. Olsen, C. Palmer, P. Piroué, J. Salfeld-Nebgen, D. Stickland, C. Tully

University of Puerto Rico, Mayaguez, U.S.A.

S. Malik, S. Norberg

Purdue University, West Lafayette, U.S.A.

A. Barker, V.E. Barnes, L. Gutay, M. Jones, A.W. Jung, A. Khatiwada, B. Mahakud, D.H. Miller, N. Neumeister, C.C. Peng, H. Qiu, J.F. Schulte, J. Sun, F. Wang, R. Xiao, W. Xie

Purdue University Northwest, Hammond, U.S.A.

T. Cheng, J. Dolen, N. Parashar

Rice University, Houston, U.S.A.

Z. Chen, K.M. Ecklund, S. Freed, F.J.M. Geurts, M. Kilpatrick, W. Li, B. Michlin, B.P. Padley, J. Roberts, J. Rorie, W. Shi, Z. Tu, J. Zabel, A. Zhang

University of Rochester, Rochester, U.S.A.

A. Bodek, P. de Barbaro, R. Demina, Y.t. Duh, J.L. Dulemba, C. Fallon, T. Ferbel, M. Galanti, A. Garcia-Bellido, J. Han, O. Hindrichs, A. Khukhunaishvili, K.H. Lo, P. Tan, R. Taus, M. Verzetti

Rutgers, The State University of New Jersey, Piscataway, U.S.A.

A. Agapitos, J.P. Chou, Y. Gershtein, T.A. Gómez Espinosa, E. Halkiadakis, M. Heindl, E. Hughes, S. Kaplan, R. Kunnawalkam Elayavalli, S. Kyriacou, A. Lath, R. Montalvo, K. Nash, M. Osherson, H. Saka, S. Salur, S. Schnetzer, D. Sheffield, S. Somalwar, R. Stone, S. Thomas, P. Thomassen, M. Walker

University of Tennessee, Knoxville, U.S.A.

A.G. Delannoy, J. Heideman, G. Riley, S. Spanier, K. Thapa

Texas A&M University, College Station, U.S.A.

O. Bouhali[71], A. Celik, M. Dalchenko, M. De Mattia, A. Delgado, S. Dildick, R. Eusebi, J. Gilmore, T. Huang, T. Kamon[72], S. Luo, R. Mueller, R. Patel, A. Perloff, L. Perniè, D. Rathjens, A. Safonov

Texas Tech University, Lubbock, U.S.A.

N. Akchurin, J. Damgov, F. De Guio, P.R. Dudero, S. Kunori, K. Lamichhane, S.W. Lee, T. Mengke, S. Muthumuni, T. Peltola, S. Undleeb, I. Volobouev, Z. Wang

Vanderbilt University, Nashville, U.S.A.

S. Greene, A. Gurrola, R. Janjam, W. Johns, C. Maguire, A. Melo, H. Ni, K. Padeken, J.D. Ruiz Alvarez, P. Sheldon, S. Tuo, J. Velkovska, M. Verweij, Q. Xu

JHEP03(2019)026

University of Virginia, Charlottesville, U.S.A.

M.W. Arenton, P. Barria, B. Cox, R. Hirosky, M. Joyce, A. Ledovskoy, H. Li, C. Neu, T. Sinthuprasith, Y. Wang, E. Wolfe, F. Xia

Wayne State University, Detroit, U.S.A.

R. Harr, P.E. Karchin, N. Poudyal, J. Sturdy, P. Thapa, S. Zaleski

University of Wisconsin - Madison, Madison, WI, U.S.A.

M. Brodski, J. Buchanan, C. Caillol, D. Carlsmith, S. Dasu, L. Dodd, B. Gomber, M. Grothe, M. Herndon, A. Hervé, U. Hussain, P. Klabbers, A. Lanaro, A. Levine, K. Long, R. Loveless, T. Ruggles, A. Savin, N. Smith, W.H. Smith, N. Woods

†: Deceased
1: Also at Vienna University of Technology, Vienna, Austria
2: Also at IRFU; CEA; Université Paris-Saclay, Gif-sur-Yvette, France
3: Also at Universidade Estadual de Campinas, Campinas, Brazil
4: Also at Federal University of Rio Grande do Sul, Porto Alegre, Brazil
5: Also at Université Libre de Bruxelles, Bruxelles, Belgium
6: Also at University of Chinese Academy of Sciences, Beijing, China
7: Also at Institute for Theoretical and Experimental Physics, Moscow, Russia
8: Also at Joint Institute for Nuclear Research, Dubna, Russia
9: Also at Cairo University, Cairo, Egypt
10: Also at Helwan University, Cairo, Egypt
11: Now at Zewail City of Science and Technology, Zewail, Egypt
12: Also at Department of Physics; King Abdulaziz University, Jeddah, Saudi Arabia
13: Also at Université de Haute Alsace, Mulhouse, France
14: Also at Skobeltsyn Institute of Nuclear Physics; Lomonosov Moscow State University, Moscow, Russia
15: Also at CERN; European Organization for Nuclear Research, Geneva, Switzerland
16: Also at RWTH Aachen University; III. Physikalisches Institut A, Aachen, Germany
17: Also at University of Hamburg, Hamburg, Germany
18: Also at Brandenburg University of Technology, Cottbus, Germany
19: Also at MTA-ELTE Lendület CMS Particle and Nuclear Physics Group; Eötvös Loránd University, Budapest, Hungary
20: Also at Institute of Nuclear Research ATOMKI, Debrecen, Hungary
21: Also at Institute of Physics; University of Debrecen, Debrecen, Hungary
22: Also at Indian Institute of Technology Bhubaneswar, Bhubaneswar, India
23: Also at Institute of Physics, Bhubaneswar, India
24: Also at Shoolini University, Solan, India
25: Also at University of Visva-Bharati, Santiniketan, India
26: Also at Isfahan University of Technology, Isfahan, Iran
27: Also at Plasma Physics Research Center; Science and Research Branch; Islamic Azad University, Tehran, Iran
28: Also at Università degli Studi di Siena, Siena, Italy
29: Also at Kyunghee University, Seoul, Korea
30: Also at International Islamic University of Malaysia, Kuala Lumpur, Malaysia
31: Also at Malaysian Nuclear Agency; MOSTI, Kajang, Malaysia
32: Also at Consejo Nacional de Ciencia y Tecnología, Mexico city, Mexico

JHEP03(2019)026

33: Also at Warsaw University of Technology; Institute of Electronic Systems, Warsaw, Poland
34: Also at Institute for Nuclear Research, Moscow, Russia
35: Now at National Research Nuclear University 'Moscow Engineering Physics Institute' (MEPhI), Moscow, Russia
36: Also at St. Petersburg State Polytechnical University, St. Petersburg, Russia
37: Also at University of Florida, Gainesville, U.S.A.
38: Also at P.N. Lebedev Physical Institute, Moscow, Russia
39: Also at California Institute of Technology, Pasadena, U.S.A.
40: Also at Budker Institute of Nuclear Physics, Novosibirsk, Russia
41: Also at Faculty of Physics; University of Belgrade, Belgrade, Serbia
42: Also at INFN Sezione di Pavia (a; Università di Pavia, Pavia, Italy
43: Also at University of Belgrade; Faculty of Physics and Vinca Institute of Nuclear Sciences, Belgrade, Serbia
44: Also at Scuola Normale e Sezione dell'INFN, Pisa, Italy
45: Also at National and Kapodistrian University of Athens, Athens, Greece
46: Also at Riga Technical University, Riga, Latvia
47: Also at Universität Zürich, Zurich, Switzerland
48: Also at Stefan Meyer Institute for Subatomic Physics (SMI), Vienna, Austria
49: Also at Adiyaman University, Adiyaman, Turkey
50: Also at Istanbul Aydin University, Istanbul, Turkey
51: Also at Mersin University, Mersin, Turkey
52: Also at Piri Reis University, Istanbul, Turkey
53: Also at Gaziosmanpasa University, Tokat, Turkey
54: Also at Ozyegin University, Istanbul, Turkey
55: Also at Izmir Institute of Technology, Izmir, Turkey
56: Also at Marmara University, Istanbul, Turkey
57: Also at Kafkas University, Kars, Turkey
58: Also at Istanbul Bilgi University, Istanbul, Turkey
59: Also at Hacettepe University, Ankara, Turkey
60: Also at Rutherford Appleton Laboratory, Didcot, United Kingdom
61: Also at School of Physics and Astronomy; University of Southampton, Southampton, United Kingdom
62: Also at Monash University; Faculty of Science, Clayton, Australia
63: Also at Bethel University, St. Paul, U.S.A.
64: Also at Karamanoğlu Mehmetbey University, Karaman, Turkey
65: Also at Utah Valley University, Orem, U.S.A.
66: Also at Purdue University, West Lafayette, U.S.A.
67: Also at Beykent University, Istanbul, Turkey
68: Also at Bingol University, Bingol, Turkey
69: Also at Sinop University, Sinop, Turkey
70: Also at Mimar Sinan University; Istanbul, Istanbul, Turkey
71: Also at Texas A&M University at Qatar, Doha, Qatar
72: Also at Kyungpook National University, Daegu, Korea

JHEP03(2019)026